Exploring Winter Rainfall in Western South Africa: Connections, Influences and the Potential for Statistical Seasonal Forecasting

Brandon Wolding

Department of Oceanography, University of Cape Town, Private Bag X3,

Rondebosch 7701, Cape Town, South Africa

Dissertation submitted to the Faculty of Science, University of Cape Town, in fulfillment of the requirements for the Applied Marine Science Masters degree, 2010.

Contents

Abstract:

The development and underlying physical connections of relationships between SWC rainfall and the Southern Annular Mode (SAM), South Atlantic sea surface temperature (SST), Antarctic sea ice concentration (SIC), and the El Nino-Southern Oscillation (ENSO) were explored using spatial and temporal correlations. Insight gained from the correlation analysis was used to develop statistical forecast models for SWC seasonal rainfall, which served as an initial assessment of the potential for statistical seasonal forecasting of SWC rainfall.

SST in several regions of the South Atlantic appears to influence rainfall, primarily on seasonal timescales. Both the SAM and ENSO contribute to the variability of SST within these regions. Antarctic SIC also has a strong relationship with SWC rainfall, though it remains unclear if rainfall is directly influenced by SIC or the two are related through larger modes of variability. The SAM appears to influence SWC rainfall directly through its affects on atmospheric circulation, and indirectly through its persisting affects on SST. ENSO appears to influence SWC rainfall directly through its affects on atmospheric circulation during the year of onset, and indirectly through lagged affects on SST during its mature phase.

A statistical forecast model of SWC late-winter rainfall was able to produce an estimated 60% reduction of variance from a forecast based on climatological average values, as estimated with cross-validation techniques. The potential practical application of this forecast is overshadowed by the instability of the predictor-predictand relationships. This instability is observed in the relationships between SWC rainfall and South Atlantic SST, SAM indices, and ENSO.

Chapter 1

Introduction

1.1 Introduction

The western, coastal region of South Africa, or Southwestern Cape (SWC), is unique to the country in receiving most of its rainfall during the austral winter (May-September). Home to the country's second most populace city and substantial agricultural resources, the ever-increasing demand placed on water resources by a growing population, and the dependence of the local economy on the appropriate management of these resources makes an understanding of SWC rainfall variability, and the mechanisms that affect it, essential. Most of South Africa receives primarily summer rainfall, the variability of which has been the subject of numerous studies as well as attempts at seasonal forecasting (e.g. Hastenrath et al. 1995). While several studies have highlighted the potential predictability of seasonal rainfall in the SWC (e.g. Blamey and Reason 2007, Reason and Rouault 2005, Reason et. al 2002), no such forecast has yet been attempted.

Rainfall in the SWC is characterized by significant inter-annual and inter-decadal variability (Reason et. al. 2002, Reason and Rouault 2002). The SWC receives most of its rainfall via temperate disturbances in the westerlies, in particular cold fronts and associated extra-tropical cyclones (Blamey and Reason 2007). Other westerly disturbances such as cut off lows, whose frequency shows a semi-annual oscillation with

peaks in March to May and September to November (Tyson and White 2000), occasionally produce significant rainfall (Singleton and Reason, 2006).

Several variables have been identified as having significant correlations with anomalously wet/dry SWC winters, including sea surface temperatures (SST) in various parts of the South Atlantic Ocean (Reason and Jagadheesha 2005), sea ice concentration (SIC) in different regions of the Antarctic (Blamey and Reason, 2007), and the Southern Annular Mode (SAM) (Reason and Rouault 2005). In some cases these relationships may remain strong given a several month lead and have potential use as a prognostic forecasting tool. Though potential mechanisms for influencing SWC rainfall have been identified for some variables, the relationships with other variables remains less clear. This study aims to further investigate variables with established relationships to SWC rainfall, and to use these relationships to provide an initial assessment of the potential for forecasting SWC rainfall. This situation, with multiple variables of various locations, lead times and uncertain physical connections lends itself well to a stepwise regression procedure that will assess the relative contributions of each variable.

Chapter 2 will examine the basis for statistical seasonal forecasting, review features of the general circulation and primary modes of variability in the Southern Hemisphere, discuss how they may potentially influence SWC rainfall, and provide a literature review of related topics. Chapter 3 explores relationships between variables and SWC rainfall, their underlying physical connections, and the predictability that they may offer. Chapter 4 uses stepwise regression to further explore relationships between variables and SWC rainfall, and assess the potential for statistical seasonal rainfall forecasting. Conclusions and a summary will be offered in Chapter 5.

Chapter 2

Background and Literature Review

2.1 Statistical forecasting theory and methods

While the chaotic nature of internal atmospheric dynamics imposes inherent limits on the ability to forecast individual weather systems, significantly longer predictability of atmospheric development can be gained from certain large-scale components of atmospheric circulation and lower-boundary forcings that evolve on slower time scales than that of weather (Palmer and Anderson, 1994). This imparted predictability is utilized in seasonal forecasting not to predict the timing of individual weather systems, but instead to assess the probable occurrence of weather regimes over a season. The variables that offer predictability over longer time scales, and themselves evolve with time, determine what weather is possible and how likely it is to occur (Stockdale, 2000). Seasonal forecasting can thus be viewed as attempting to predict shifts and changes in the probability distribution function (pdf) of weather based on changes in these variables (Palmer, 1993 as in Stockdale, 2000). Consequently, variables that lead to intensified frontal activity over the SWC must first be identified, and then the predictability offered by such variables must be assessed.

In general, slowly evolving lower-boundary forcings (e.g. SST, land surface characteristics, etc.) serve as the primary source of predictability on seasonal time scales (Goddard et. al. 2001). This is particularly true for the tropics, where large scale seasonal

circulation and rainfall patterns are so strongly influenced by boundary conditions of SST that they show little sensitivity to changes in the initial conditions of the atmosphere (Shukla, 1998). Such a case provides considerable seasonal predictability. In contrast, much of the variability of the extratropics is associated with internal instability and non-linearity (Tyson and Preston-Whyte, 2000) and the potential for seasonal predictability is less clear.

As previously stated, a relationship between SWC rainfall and various oceanic/atmospheric variables is thought to exist. Some variables may directly influence SWC rainfall through some physical process or mechanism. In other cases a variable may exert no tangible physical influence on SWC rainfall, but may still play an important role as a "predictor". In either case, the functional relationship between SWC rainfall and the various predictor variables is too complicated to be fully understood and described in simple terms. As such, an approximation of these functional relationships over some limited period of time, in the form of simple mathematical models, must be made. In addition to their potential application as predictive tools, these models can provide information on the underlying true relationships of the predictor and response variables and illuminate the separate and joint effects produced by changes in these variables.

In this study, the mathematical model used to approximate the predictor/predictand relationship is the product of a method called regression analysis. This is a process whose foundations rest on certain assumptions that, in reality, may only be true to varying degrees. Each model must undergo a critical examination of these underlying assumptions to assess its real value. Implicit is the idea that random

variations in any predictor variable are small compared to the range of the predictor variable observed.

The small number of observations available in this study makes the potential hazards of constructing a model forecast more concerning. Changes in lurking variables (variables which influence SWC rainfall not included in the model) could introduce non-random error and cause the model equation to become unreliable. Even in the event that the model developed successfully describes the data set, it must be remembered that this data set is but a small sample of the "population" of potential SWC winters. Thus, two sources of uncertainty exist: uncertainty within the model (in how well the model describes the observed winters) as well as uncertainty of how well the sample represents the true population. Considering the strong changes in regional climates now being observed, a particular concern of any study of this nature at present would be the stability of the predictor-predictand relationship and the duration a model may remain viable for. Many such changes are thought to originate from anthropogenic forcing and therefore are not part of the natural variability.

An honest assessment of SWC rainfall predictability depends on a thorough understanding of the factors that may influence SWC rainfall, the primary modes of SH atmospheric variability, and the influences these modes may have on the ocean and sea ice systems.

2.2 Atmospheric circulation

2.2.1 General circulation pertaining to South Africa

Atmospheric motion is driven by energy imbalances and is most conveniently

thought of as occurring on a variety of scales in both time and space. Although weather systems are typically characterized by their associated scales and circulation pattern, the weather at any specific point is a product of motions on all scales, which are interdependent and in reality indistinguishable from each other. Bearing this in mind, synoptic and smaller scale disturbances, which often determine the day-to-day weather in South Africa, originate in tropical, sub-tropical and temperate features of the general circulation (Tyson and Whyte 2000). In large part, this general atmospheric circulation constructs the climate of South Africa, yet it has little affect on the day-to-day weather observed.

Two Anticyclonic features, the South Atlantic Anticyclone and the South Indian Anticyclone, border South Africa and vary in both latitude and longitude seasonally. During the summer months the South Atlantic Anticyclone has a tendency to ridge south of South Africa, bringing generally dry conditions to the SWC (Tyson and Whyte, 2000). However, as both anticyclones move approximately six degrees north during the winter, they create a col region into which disturbances in the westerlies bring rainfall (Tyson and Whyte 2000). The austral winter climate of South Africa is dominated by the pressure gradient between these two anticyclones and the mid-latitude westerlies (Reason and Jagadheesha, 2005). Upstream of South Africa, SST patterns in the South Atlantic are thought to modify the intensity, track and amount of moisture present in such westerly disturbances (Reason and Jagadheesha, 2005). As the primary source of SWC rainfall, the origin and nature of the westerlies (and the associated jetstreams) deserves brief mention.

The mid-latitudes are a region of strong horizontal temperature gradients, owing

to the difference in radiation received between the Tropics and the Poles. These energy imbalances manifest themselves in the form of a strong geostrophic westerly wind that extends into the upper troposphere and strengthens with height. The dynamics of these enhanced upper level westerly winds, known as the jetstream, exert an important influence on surface weather and serve as a boundary across which heat, momentum and water vapor are transferred. High zonal velocities and large meridional temperature gradients promote baroclinic instability and the formation of transient eddies, which act to transfer this heat, momentum and water vapor. These transient eddies are a major source of variability, with the ability to be modified by, and feedback onto the mean flow (Limpasuvan and Hartmann (2000), Hartman and Low (1998), Kidson and Sinclair (1995)). Changes in the position and strength of the SH jetstream have been associated with anomalous rainfall over the SWC by numerous studies (Reason, Jagadheesha and Tadross (2003), Reason and Jagadheesha (2005), Reason et .al. (2002)).

The SH jetstream exhibits a dual structure, consisting of a single Polar Frontal Jet from approximately December to mid April, which then abruptly shifts north (from ~42°S to ~30°S) and splits into a dominant Sub-Tropical Jet and a weaker Polar Frontal Jet (Gallego et. al., 2005). The Polar Frontal Jet drifts south (from ~42°S to ~60°S) until October, at which time the Sub-Tropical Jet slowly begins to weaken while the Polar Frontal Jet gradually drifts back north (Gallego et. al., 2005). The system has typically transitioned back to a single Polar Frontal Jet by December (Gallego et. al., 2005).

Jet stream variability originating from both the tropics and mid to high latitudes has been recognized, identifying potential predictors of SWC rainfall. Gallego et. al. (2005) found that both the Southern Annular Mode (SAM) and the El-Nino Southern-

Oscillation (ENSO) significantly affect the position and strength of the jetstream(s). ENSO seems to primarily influence the Sub-Tropical Jet, with the most prominent affects being regionally restricted to the Pacific Ocean (Gallego et. al., 2005). The influence of the SAM appears strongest on the Polar Frontal Jet, which shifts poleward and strengthens in many regions during positive phases, while the Sub-Tropical Jet shows small regional shifts equatorward (Gallego et. al., 2005). Changes in the latitude and strength of the jetstream(s) induced by SAM/ENSO have a distinct regional and seasonal nature. Gallego et. al. (2005) found that in May the Sub-Tropical Jet over and upstream of South Africa shifted slightly equatorward in response to positive SAM events, but no significant changes were observed for the remainder of the winter. The Polar Frontal Jet in this region was found to shift poleward in response to SAM events in May, July, August and September (Gallego et. al. 2005). In June, the Sub-Tropical Jet over South Africa was found to shift slightly equatorward in response to positive ENSO events, but remains unaffected along with the Polar Frontal Jet for other winter months (Gallego et. al. 2005).

The relative zonal uniformity of SH geography, whereby the surface area is dominated by ocean and interrupted by relatively little landmass, plays an important role in determining the character of jetstream variability and how its affects propagate through the ocean-atmosphere system. This zonal uniformity reinforces the zonal symmetry of the mid latitude jet stream and leads to a more even distribution of eddy activity, which is reflected in the zonal symmetry of the annular mode (Thompson and Wallace, 2000). This contrasts its NH jetstream counterpart, whose wave pattern and associated storm tracks are thought to originate substantially from orography (Broccoli and Manabe, 1992 as in Hall and Visbeck, 2002). Such geography also allows a coherent, zonally

symmetric ocean response to atmospheric forcing (whose greatest variability has an annular structure), establishing ocean-atmosphere covariability (Sen Gupta and England, 2006 Hall and Visbeck, 2002). This will be dealt with further in following sections.

2.2.2 Primary modes of mid-high southern latitude variability

A number of distinct mid-high latitude climate modes, including the SAM, Semi-Annual Oscillation, Pacific South America Pattern (PSA), and the Stationary Wave-3 pattern, exist at intraseasonal to decadal time scales in the Southern Hemisphere (Yuan and Li, 2008). These modes actively interact within the climate system, impacting the ocean/sea-ice system in regions of interest for this study. The collective influence these climate modes exert is particularly strong and intricate within the sea ice system around Antarctica. As with previous studies of SWC rainfall, this study only provides a limited investigation and will not deal with all these primary modes of variability. Not accounting for these other modes of variability will limit the ability of this study to speculate about the relationship between the ocean/sea ice systems, modes of SH variability and SWC rainfall.

2.2.3 Circulation anomalies during anomalous wet/dry SWC winters

Several studies (Reason et. al. 2002, Reason and Rouault 2005, Blamey and Reason, 2007) have composited wet and dry winters using NCEP/NCAR re-analysis data in order to identify anomalies in atmospheric circulation corresponding with anomalously wet/dry SWC winters. NCEP/NCAR re-analysis uses a state of the art analysis/forecast system to perform data assimilation using past data from 1948 to present (Kalnay et. al.,

1996). Anomalies in atmospheric circulation present during anomalous wet/dry SWC winters include shifts in the position and strength of the Sub-Tropical Jet, changes in low-level moisture flux over the region, local uplift, low-level convergence and relative vorticity.

Wet winters appear to be associated with weaker South Atlantic and South Indian subtropical anticyclones and a robust low-pressure anomaly that stretches from the SW Atlantic across the central Atlantic and SA to the SW Indian Ocean (Reason et. al. 2002, Reason and Rouault 2005, Blamey and Reason, 2007). There is a stronger (~15%) and northward shifted Sub-Tropical Jet (Reason et. al. 2002, Reason and Rouault 2005, Blamey and Reason, 2007), and shifts in the position of the wave 3-4 pattern are thought to influence cyclonic/anticyclonic anomalies upstream of the SWC (Reason and Rouault, 2005). There is increased moisture flux from the South Atlantic (Reason and Rouault, 2005) and a region of reduced 1000-500hPa thickness over SA and upstream in the South Atlantic (Reason and Rouault 2005, Blamey and Reason 2007). This layer of reduced thickness implies a colder lower atmosphere less able to hold water vapour, leading to increased precipitation over and upstream of the SWC (Reason and Rouault, 2005). Regionally enhanced uplift at 850 hPa implies decreased subsidence and conditions favorable for the strengthening of approaching fronts (Blamey and Reason 2007, Reason and Rouault 2005). Approximately opposite circulation anomalies are present during anomalously dry winters.

2.3 South Atlantic SST patterns

The ocean-atmosphere system in the mid-latitudes is coupled to a lesser degree

than in the tropics, where convection is particularly sensitive to underlying SST (Shukla, 1998). Despite this, baroclinic theory (Trenberth, 1991), model analysis (Reason and Jagadheesha 2005, Reason and Murray 2001) and observational relationships (Reason et. al. (2002), Reason (2002)) indicate that South Atlantic SST patterns are an important modulator of cyclogenesis and the location and intensity of midlatitude storm tracks. Consequently, South Atlantic SST patterns are of particular interest given the frontal nature of SWC rainfall.

Reason et. al. (2002) found that of the nine wettest winters in the SWC over the last 50 years (i.e. normalized anomalies exceeding one standard deviation), eight showed warm SST anomalies in the SW Atlantic, seven showed warm SST anomalies in the SE Atlantic (part of the Agulhas retroflection area), and six showed cool SST anomalies in the central Atlantic. In a composite analysis of anomalous wet minus dry SWC winters (Fig. 2.6) performed by Blamey and Reason (2007), the warm-cold-warm SST pattern is evident.

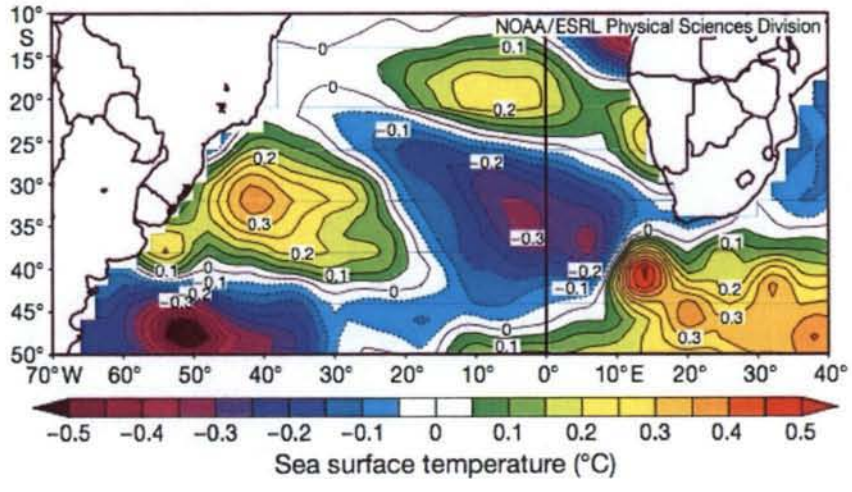

Figure 2.1: Composite of SST derived for wet minus dry years, after Blamey and Reason (2007)

The SW Atlantic has been identified as an important region of cyclogenesis for the SH (Fig 2.2) (Simmonds and Keay, 2000). Reason et. al. (2002) proposed that warm SST anomalies in the SW Atlantic would lead to additional and stronger depressions occurring there, which are then advected in the mid-latitude westerly flow across the South Atlantic. Reason and Jagadheesha (2005) argued that cool SST anomalies in the central South Atlantic would increase the near surface meridional temperature gradient, enhancing baroclinicity between the tropics and the mid-latitudes of the storm track approaching South Africa. SH storm tracks tend to be associated with areas of largest meridional temperature gradients in the lower troposphere (Trenberth, 1991). Reason et. al. (2002) also suggested that cool SST anomalies in the central Atlantic would act to shift the westerly flow north to conserve potential vorticity (acting like increased orography), leading to a northward shifted storm track upstream of the SWC. In the SE Atlantic, warm anomalies are thought to intensify parent depressions tracking south of the SWC, acting to strengthen the fronts that cross it (Reason, 2001). Both model response (Reason and Jagadheesha, 2005) and observational analysis (Reason et. al., 2002) indicate that South Atlantic SST anomalies modulate the wavenumber-3 pattern over the mid-latitude SH.

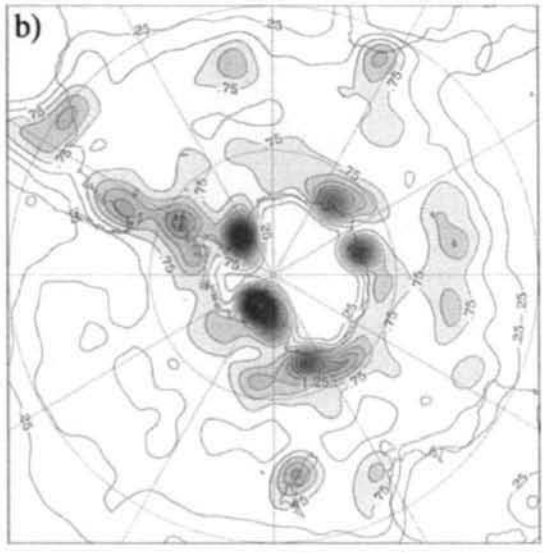

Figure 2.2: Cyclogenesis density in JJA, with contour interval of 0.25×10^{-3} cyclones (deg lat)$^{-2}$ day^{-1}, after Simmonds and Keay (2000)

Reason , Jagadheesha, and Tadross (2003) used the HadAM3 atmospheric general circulation model, forced by SST, to create wet minus dry composites of circulation patterns in order to identify mechanisms potentially related to anomalously wet winters. The results suggested that wet SWC winters are associated with enhanced inflow of moisture from low-latitude South America and the South Atlantic Convergence Zone, a strengthening of the Sub-Tropical Jet over the mid-latitude Atlantic, increased evaporation over the SW Atlantic warm SST anomaly, as well as increased low level convergence and eddy activity just upstream of the SWC (Reason, Jagadheesha and Tadross, 2003). This supports observational analysis mentioned in the previous section.

Using the HadAM3 general circulation model, Reason and Jagadheesha (2005) assessed the affects of SST anomalies on regional atmospheric circulation by imposing idealized SST anomalies similar to (but of ~ 2 times larger magnitude) those observed in

anomalously wet SWC winters. The model response was consistent with the observations of Reason et. al. (2002), including a low pressure anomaly over the SW Atlantic, a strengthened Sub-Tropical Jet that was shifted northward, and increased surface latent heat flux over the SW Atlantic. When similar SST anomalies were imposed, but a region of anomalously high SST centered at ~20°S was added (as observed in 2003, a dry winter), the model reproduced a dry winter with a circulation response suggestive of a positive SAM (Reason and Jagadheesha, 2005). When the warm/cold anomalies used in the first model run were moved farther north and oriented in a more meridional fashion, increased rainfall of a larger magnitude was observed, suggesting that the atmospheric response over South Africa and the neighboring ocean is sensitive to the distribution and spatial extent of warm and cold SST forcing in the central and western South Atlantic (Reason and Jagadheesha, 2005). In all cases, net surface heat fluxes acted to dampen the SST anomaly while Ekman transport re-enforced the anomaly, suggesting a mechanism for the observed tendency of anomalies to maintain their distribution and magnitude throughout the winter, if such opposing dynamic-thermodynamic effects exist in the real world (Reason and Jagadheesha, 2005).

The origins of such South Atlantic SST anomalies remain unclear. Although the scale of the anomalies appears to be too small to be associated with the SAM or the Antarctic Circumpolar Wave, the possibility remains that both SST patterns and SWC rainfall anomalies result from a regional response to other large-scale forcings (Reason and Jagadheesha, 2005). This possibility will be looked at in greater detail in the following section.

2.4 The Southern Annular Mode

2.4.1 Description and system influences

The Southern Annular Mode (SAM), otherwise known as the Antarctica Oscillation or High Latitude Mode (Reason and Rouault 2005) is the leading mode of Southern Hemisphere atmospheric circulation variability (Rashid and Simmonds, 2005). It is a deep, barotropic, zonally symmetric structure with geopotential height perturbations of opposite sign over the polar cap region and centered near 45°S (Thompson and Wallace, 2000). The SAM represents a large-scale exchange of atmospheric mass between mid and high latitudes, acting like a zonally symmetric seesaw of Sea Level Pressure (SLP). It is an internal mode of atmospheric variability that would exist in the absence of external forcing. While boundary conditions (i.e. solar forcing) may modulate the SAM, it does not require interactions with boundary conditions to exist.

It is found as the leading Empirical Orthogonal Function (EOF) in numerous variables including SLP (Gong and Wang 1999), 500 hPa height (Rogers and Van Loon 1982), 300 hPa height (Karoly, 1990), the SH zonally averaged geopotential height field at 1000 hPa (Shiotani, 1990), the zonally averaged zonal wind at 500 hPa height (Roger and Van Loon, 1982) and in the 1000-100 hPa layer (Yoden et. al., 1987).

A positive phase, or high index polarity, is indicative of positive pressure anomalies over mid-latitudes and negative pressure anomalies over Antarctica, while a negative phase, or low index polarity, exhibits the opposite. During positive phases the shifting of atmospheric mass away from the pole leads to a region of anomalously low pressure over Antarctica extending to ~ 55°S, with a corresponding area of high pressure

centered over ~ 45°S (Sen Gupta and England, 2006). The westerlies are thus enhanced poleward of ~45°S and weakened equatorward, while the poleward limit of the Hadley cell and the entire Ferrell cell are displaced poleward (Thompson and Wallace, 2000). Sen Gupta and England (2006) created both observational and model constructions, using the National Center for Atmospheric Research Community Coupled Climate Model (version 2), of the SLP signal and surface wind response to a positive SAM anomaly. The changes in westerly wind strength contribute to anomalous poleward (equatorward) flow south(north) of ~ 45°S within the surface boundary layer, where frictional forces act (Hall and Visbeck (2002), Sen Gupta and England (2006)). The redistribution of atmospheric mass associated with the SAM leads to areas of relative ascent extending from ~ 55°S to 90°S and relative subsidence extending from ~ 35°S to 50°S. The rising(subsiding) air is thought to result in the colder(warmer) temperature observed throughout the troposphere centered over the respective regions (Thompson and Wallace, 2000). An exception to this is the Antarctic Peninsula, which will be discussed later.

Changes in atmospheric circulation associated with SAM induce dynamic and thermodynamic responses in the ocean and sea ice system. The ocean quickly responds to changes in momentum transfer at the air-sea interface with Ekman-driven transport at shallow depth (Sen Gupta and England, 2006). A generalized response to a positive SAM is westerly zonal and equatorward meridional surface transports enhanced south of ~45°S and reduced north of ~45°S (Sen Gupta and England, 2006). The meridional transports results in increased upwelling along the Antarctic coast and downwelling centered at ~45°S (Hall and Visbeck, 2002). Changes in wind speed, surface layer temperature and surface layer salinity alter the mixed layer depth, causing a shoaling equatorward of

~45°S and a deepening poleward of ~45°S (at maximum between ~45°S and ~60°S) (Lefebvre and Goosse, 2005), thereby modifying the mixed layers response to surface heat fluxes (Sen Gupta and England, 2006). The oceanic/atmospheric responses to a positive SAM phase are illustrated in Figure 2.3.

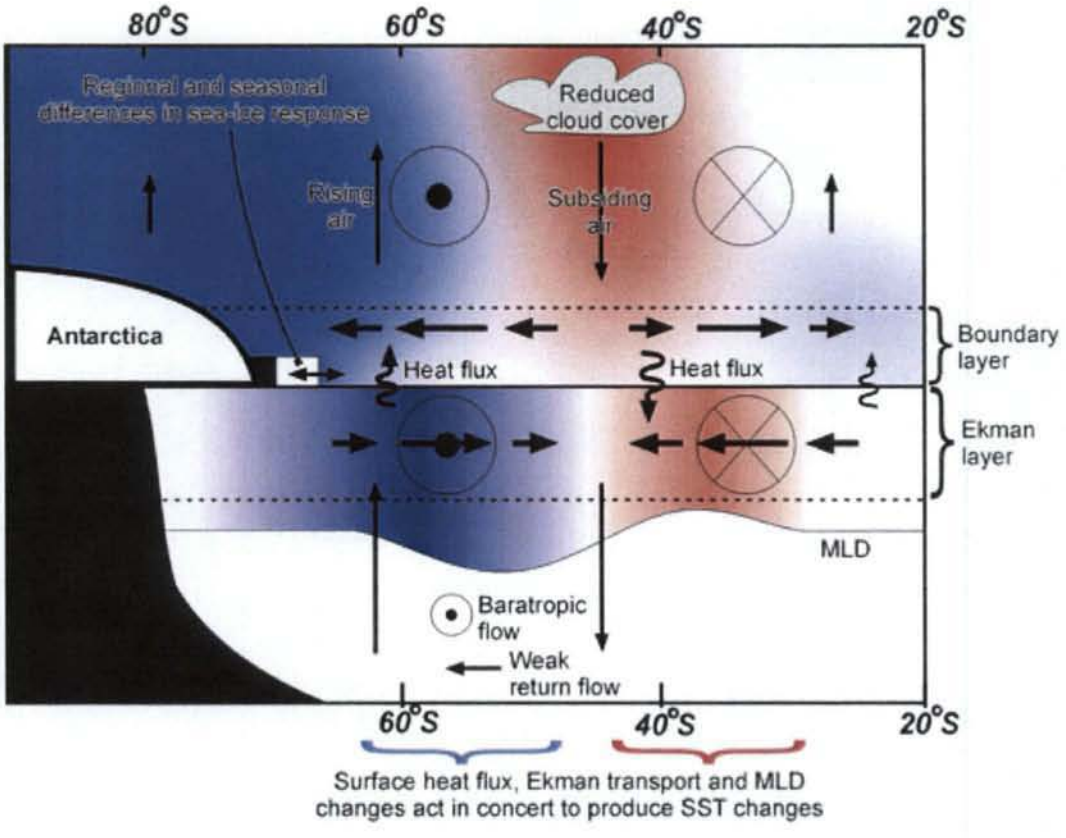

Figure 2.3: Schematic representation of affects of a positive SAM on the oceanic/atmospheric systems. Red(blue) shading indicates warming(cooling), and arrow tails(heads) indicate anomalous flow into(out of) the page. A schematic representation of a negative SAM phase would be the same as above, but with an opposite direction of circulation anomalies and opposite signs for anomalies and fluxes, after Sen Gupta and England (2006)

Sen Gupta and England (2006) used the National Center for Atmospheric

Research Community Coupled Climate Model (version 2) to perform an analysis of the ocean mixed layer heat budget and identified air-sea heat flux and meridional advection as the dominant terms, with zonal and vertical advection playing minor roles. Sen Gupta and England (2006) suggest that, in response to an annular wind forcing, model responses of SST (Fig 2.4a), zonal flow and meridional flow also exhibit an annular structure. Observational analysis of SST responses shows a less annular response with distinct regional differences (Fig. 2.4b). While changes in zonal and meridional flow respond quickly to SAM induced changes in wind, the large heat capacity of the mixed layer causes a ~ 1-month lag in the largest SST response (Sen Gupta and England, 2006). The high thermal inertia of the mixed layer allows the SST response to persist away from the Antarctic margin for several months, re-imprinting its annular form on the surface air temperature in a feedback response (Sen Gupta and England, 2006). Of course, within such a generalized view of SAM responses exist regional discrepancies. One such discrepancy of particular importance is a non-annular component occurring west of the Antarctic Peninsula, a pressure anomaly centered over the Bellingshausen Sea. This will be discussed in detail in following sections.

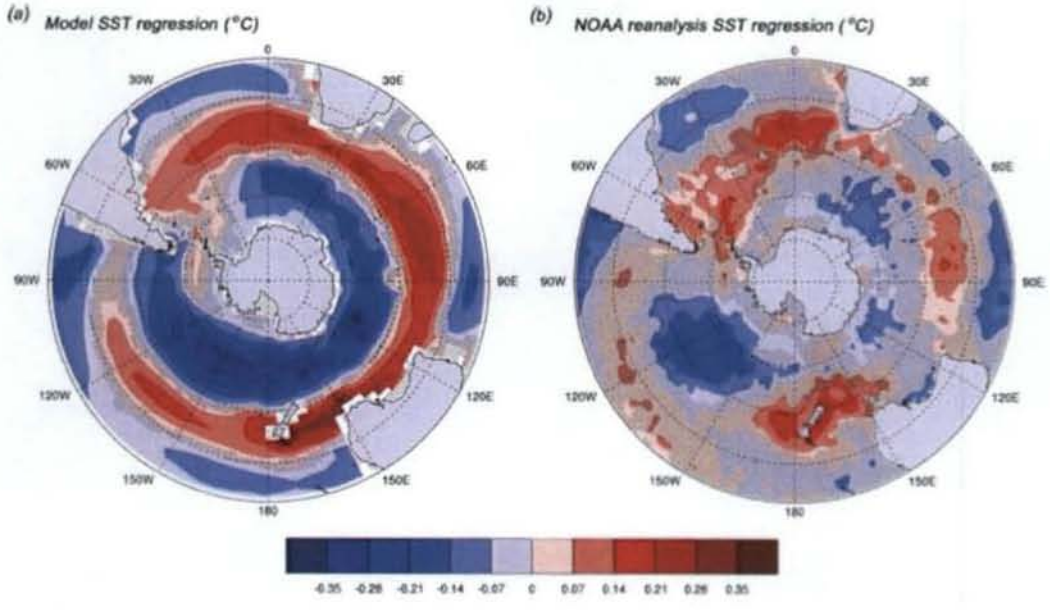

Figure 2.4: SST response at 1 month lag to a positive SAM phase as constructed from a.) model analysis and b.) observational analysis. Values are given in degrees C. After Sen Gupta and England (2006)

2.4.2 Variability and trends

The SAM shows significant variability on a variety of time scales ranging from weeks to decades. It should be noted that SAM events occur on sub-monthly time scales, with a maximum variability at the 10-day period (Thompson and Wallace, 2000), so any monthly or seasonal comparison will be considering a mean of several SAM events, and changes on these timescales reflect changes in the frequency and/or amplitude of specific SAM events averaged over this time.

A significant trend towards high index polarity has been observed over the past several decades and is present in all seasons (Thompson, Wallace and Hegerl (2000),

Thompson and Solomon (2002), Marshall (2003)), though largest in the summer and fall (Marshall, 2003). This trend towards positive phases is believed to have an anthropogenic forcing, and can only be accounted for when stratospheric ozone depletion and increased atmospheric greenhouse-gas concentration are taken into consideration (Thompson and Solomon 2002, Arblaster and Meehl 2006). Thus it is not part of the natural variability. Since the SAM acts as the leading mode of variability in so many components of SH circulation, there is an implication of a shift in the general climate of the SH with such a trend (Marshall, 2003).

2.4.3 Relationship to SWC rainfall

To date, research aimed at identifying the relationship between the SAM and SWC rainfall has been very limited. Reason and Rouault (2005) found that 6 (6) of the 7 (8) wettest (driest) winters (JJA) during 1948-2004 occurred during negative (positive) SAM phases. The authors observed that the wet winter not corresponding to a (-) SAM still showed low pressure anomalies over and stretching west from SA and noted the reason this year was not classified as (-) SAM was a lack of sufficient positive height anomaly over Antarctica. A correlation of 0.4 was found between rainfall and the SAM index (JJA) for 1964-2004 at 0 lag and of 0.6 if a 7 point (7 winters) running mean was applied, increasing slightly when SAM index was given a 2 year lead. During dry winters corresponding to a (-) SAM phase, shifts in the ridges of the wave 3 pattern were identified (Reason and Rouault, 2005). The mechanism(s) by which the SAM influences SWC rainfall have yet to be identified.

2.5 El Nino Southern Oscillation

2.5.1 Affects on mid and high latitude atmospheric circulation

While influences of ENSO are communicated across the world through its various teleconnections, those of particular importance to this study are the ones that affect the mid and high southern latitudes, particularly upstream of the SWC. Details of known teleconnections can be obtained from Tyson and Preston-Whyte (2000), Mo and Paegle (2001), Rind et. al. (2001), Liu et. al. (2002), Colberg et. al. (2004) and Yuan (2004), but a general description of atmospheric circulation changes related to ENSO events will suffice for this study.

GISS general circulation model results of Rind et. al. (2001) suggest that during an El Nino event, warm SST anomalies across the central and eastern Pacific increase regional tropical convection and equator to pole temperature gradients, strengthening and contracting the Pacific Hadley cell. The zonal circulation is shifted eastward and its descending branch is located over the tropical Atlantic, which counteracts the ascending branch of the Atlantic Hadley cell causing its relaxation and expansion (Rind et. al., 2001). In the South Pacific, the Sub-Tropical Jet is strengthened and the storm track is shifted equatorward, decreasing storm intensity as the distance from cold Antarctic air increases (Rind et. al. 2001). This shift in the strength and location of the Sub-Tropical Jet is supported by the observations of Gallego et. al. (2005). In the Atlantic, modeling results indicate the relaxed Hadley cell causes a poleward shift in the jet stream and the associated storm track, which intensifies as it is exposed to cold Antarctic air (Rind et. al., 2001). This shift in the Sub-Tropical Jet was not observed by Gallego et. al. (2005). The Ferrell cell is enhanced in the Pacific and weakened in the Atlantic, modifying low-level

poleward heat transport by the mean meridional circulation in each region (Liu et. al., 2002). An anomalous high-pressure center also sits over the Bellingshausen Sea (Yuan, 2004). La Nina affects atmospheric circulation in approximately the opposite way (Rind et. al. 2001).

ENSO also plays a large role in modulating the Pacific-South America (PSA) modes, two pervasive modes of variability in the southern hemisphere that experience considerable variance on intraseasonal to decadal timescales (Mo, 2000 and Mo and Paegle, 2001). The PSA modes exhibit wave 3 hemispheric patterns in the mid to high latitudes and a well-defined wave train with large amplitude in the Pacific-South America region (Mo and Peagle, 2001).

2.5.2 Connections to South Atlantic atmospheric circulation and SST

Colberg et. al. (2004) used the ORCA2 ocean general circulation model to investigate the South Atlantic response to ENSO. The authors suggest that during El Nino events, modified atmospheric convection in the Indo-Pacific region produces atmospheric rossby waves that provoke the PSA pattern, in turn creating a negative SLP anomaly over the South Atlantic that is strongest in AMJ and JAS, then weakening the following JFM. This SLP anomaly weakens the South Atlantic anticyclone and produces anomalous wind stress, with weakened southeasterly trades mainly during AMJ and JAS of the onset year, and strengthened westerlies from JAS to the following JFM of the mature phase. This anomalous wind stress leads to changes in net surface heat flux and Ekman heat transport. The authors suggest that changes in the wind driven surface flux plays a significant role in the evolution of upper ocean temperatures at approximately one

season lag.

Colberg et. al. (2004) further suggest that during El Nino events, surface waters of the tropical and subtropical South Atlantic warm, reaching their peak in OND. Mid-latitude surface waters grow significantly cooler in OND as well as JFM of the following year, and are still present in a weaker form during AMJ. This supports the findings of Lentini (2001), who found that warm phases of ENSO are connected with a northward expansion of cold water a year later in the western South Atlantic. Colberg et. al. (2004) suggest that La Nina events modify atmospheric circulation and ocean responses in the South Atlantic in approximately the opposite way.

2.5.3 Relationship with SWC rainfall

While these descriptions and schematics of ENSO influences provide a good conceptualization of how ENSO may modify atmospheric circulation and potentially influence SWC rainfall, there is much left to be understood about these links and the role initial conditions have in modulating the effects of ENSO on South Africa (Tyson and Preston-Whyte, 2000). The impacts of ENSO on SWC rainfall are neither coherent nor robust (Reason and Rouault 2005, Blamey and Reason 2007). The 10 wettest and 10 driest SWC winters are composed of El Nino, La Nina, and neutral years, and the El Nino and La Nina events since 1920 both include wet, dry and near average winters in the SWC (Blamey and Reason, 2007). Circulation composites of El Nino minus La Nina onset years and mature years from Blamey and Reason (2007) show similarities to those of wet minus dry SWC winter composites, but also show essential differences. Most notable are anticyclonic anomalies present over South Africa and the southeast Atlantic in

the El Nino minus La Nina composites.

2.6 Antarctic sea ice

2.6.1 Potential influences in mid latitudes

Sea ice brokers dynamic and thermodynamic interactions between the ocean and the atmosphere, inhibiting the transfer of heat, moisture and momentum. It also plays a substantial role in determining local, regional and global heat budgets through its high albedo. SH geography imparts no physical constraints to serve as Antarctic sea ice boundaries, allowing these ocean-ice-atmosphere interactions to take on a unique and dynamic nature. While atmospheric modes of variability originating in low (e.g. ENSO, see Stammerjohn et. al., 2008) and mid to high (e.g. SAM, see Sen Gupta and England, 2006 and Stammerjohn et. al. 2008) latitudes have demonstrated the ability to influence sea ice extent, and there is evidence of sea ice affecting atmospheric circulation near the sea ice margins (Watkins and Simmons, 1995), the extent to which sea ice extent anomalies influence atmospheric circulation of mid-latitudes remains less clear.

Considering the stated significance of sea ice in determining heat budgets and limiting ocean-atmosphere interactions, it seems plausible that such interactions could be propagated to lower latitudes where they may potentially influence climate. Simmonds and Budd (1991) suggested that anomalous sea-ice distribution could alter the position and strength of baroclinic zones in the high southern latitudes. Such a change may influence cyclogenesis or regionally affect the strength of existent systems propagating downstream, thereby potentially transmitting the effects to the mid-latitudes. Characterizing 40 years of re-analysis data, Simmonds and Keay (2000) note that in all

seasons the greatest numbers of cyclones are found between 50° and 70°S, and that the eastern flank of the Antarctic Peninsula is an important region of cyclogenesis.

Distinguishing between cause and effect poses a major obstacle for statistical studies of these interactions, as anomalies in sea ice are themselves a regionally specific response to atmospheric forcing (Sen Gupta and England 2006, Stammerjohn et. al 2008). In addition, sea ice extent does not always vary linearly with sea ice concentration (SIC), particularly in areas with anomalous zonal circulation, and the affect of SIC on atmospheric circulation may be as important as that of sea ice extent (Godfred-Spenning and Simmonds, 1996). Therefore, determining subsequent influences the sea ice may have on the atmosphere, and differentiating the regionally specific linkages they may form is difficult.

Godfred-Spenning and Simmonds (1996) attempted to discern the affect sea ice might have on cyclone activity. Their study supports the idea that influences of sea ice on cyclone activity are regionally specific, and furthermore found that they are often seasonally dependent. An exception to this is the Antarctic Peninsula, where sea ice on both sides shows a year round positive association with cyclone creation (Godfred-Spenning and Simmonds, 1996). Simmonds and Keay (2000) identified the Antarctic Peninsula and Weddell Sea as important regions of cyclogenesis. Godfred-Spenning and Simmonds (1996) concluded that in general, atmospheric processes and cyclone behavior modified sea ice to a greater extent than the reverse, though did not dismiss the ability of the latter, particularly at shorter time scales.

2.6.2 Variability and trends

The extent, concentration and timing of sea-ice around Antarctica experiences significant variability, both spatially and temporally, on various scales. Much of this variability is in response to regionally specific changes in atmospheric circulation and, as such, any description of a general sea ice response has limited descriptive value.

Stammerjohn et. al. (2008) found that, on average (1979-2004), sea ice retreat begins around September from the outer edges of the winter pack ice and proceeds poleward over the following 4 to 5 months. Sea ice advance typically begins in the most southerly coastal areas in February and continues for the following 7-8 months (Stammerjohn et. al., 2008). Sea-ice extent varies from a minimum of ~4 million km^2 in February to a maximum of ~20 km^2 in September (Godfred-Spenning and Simmonds, 1996). As sea ice extent does not behave as a single unit, and its variability results from a combination of regional sea ice changes, each region and its interactions must be discussed separately (Lefebvre and Goosse, 2008).

While sea ice extent integrated over the whole Southern Ocean does not show any significant trends (Smith and Stammerjohn, 2001), large contrasting decreasing/increasing trends in annual sea ice duration and monthly SIC exist in the western Antarctic Peninsula/southern Bellinghausen Sea (wAP/sBS) region and the western Ross Sea (wRS) region respectively (Liu et. al. 2004, Stammerjohn et. al. 2008). Stammerjohn et. al. (2008) found sea ice to be retreating 31+/- 10 days earlier and advancing 54 +/- 9 days later in the wAP/sBS region, contrasting the wRS region, where sea ice is retreating 29 +/- 6 days later and advancing 31+/- 6 days earlier. Stammerjohn et. al. (2008) note that changes in these regions (particularly those occurring during sea

ice advance) occurred in association with the decadal changes in the mean state of SAM (previously covered) and the high-latitude response to ENSO. The authors found the high latitude ice-atmosphere response to ENSO strongest when (–) SAM and El Nino coincided and when (+) SAM and La Nina coincided, particularly in the wAP/sBS region.

2.6.3 SAM influences on the sea ice system

The SAM induces a non-annular response in the sea ice system, namely a dipole response whereby a decrease(increase) in sea ice area occurs in the Weddell Sea and AP region while a increase(decrease) occurs in Ross and Amundsen Sea region during positive(negative) SAM index periods (Lefebvre et. al. 2004). The regional responses to SAM are thought to be the result of both thermal and mechanical components (Lefebvre and Goosse, 2005).

The surface air temperature response to SAM is non-annular, exhibiting warming in the Weddell and Bellinghausen Sea and cooling in the Indian, Pacific, Ross Sea and Amundsen Sea regions during a positive phase (Lefebvre and Goosse 2005, Sen Gupta and England 2006). This results in less/more sea ice respectively. (Lefebvre and Goosse, 2005). This non-annular component of SAM emerges from a significant pressure anomaly generated in the Amundsen Sea that imposes a meridional component to the otherwise zonally symmetric surface wind field (Hall and Visbeck 2002, Lefebvre et. al. 2004). During a (+) SAM a negative pressure anomaly is present in the Amundsen Sea, introducing warm northerly winds to the western Weddell Sea and Antarctic Peninsula region, while cold southerly winds blow over the Amundsen and Ross Sea regions.

A global sea ice-ocean model investigation performed by Lefebvre and Goosse (2005) indicates that the dynamic response of sea ice to SAM is most easily described as a composite of annular and non-annular components. The increased westerlies poleward of ~45° S (during + SAM) result in enhanced zonal flow as well as enhanced meridional flow due to Ekman transport (Sen Gupta and England, 2006). This induces upwelling along the Antarctic margin, bringing warm and salty water to the surface (Lefebvre and Goosse, 2005). Increased winds enhance mixing and promote upward transfer of warm and salty water, acting to re-enforce the warming effects of Ekman transfer and decrease SIC. Changes in ice drift occurred as a dynamical response to the annular and non-annular components of the wind stress: southerly winds causing an increase in ice area in the Ross Sea and northerly winds causing a small decrease in ice area in the Bellingshausen Sea, while areas away from the dipole region generally experienced an increase in sea ice area as northwesterly winds moved transport offshore (Lefebvre and Goosse, 2005). The sum model response of the sea ice to the dynamic and thermodynamic forcings was the observed dipole of increased/decreased sea ice (Lefebvre and Goosse, 2005). In the dipole region the dynamic and thermodynamic response re-enforced each other, while in sectors away from the dipole areas the dynamic and thermodynamic components induced opposite responses of a similar magnitude, leading to a smaller net response to SAM (Lefebvre and Goosse, 2005).

These findings generally agree with the model response of sea-ice to SAM observed by Sen Gupta and England (2006), although the later study found the advection of sea-ice to be more significant than the former, contributing to a stark seasonal character in the nature of the response. Looking at both model results and HadISST

reanalysis data, Sen Gupta and England (2006) found a relatively uniform increase in SIC away from the dipole region when (+) SAM phases occurred in the summer (Fig. 2.5a,c). Furthermore, the authors found that a positive ice-albedo feedback allowed these anomalies to persist for several months, with the greatest sea ice response occurring after the time of maximum external forcing. This ice-albedo feedback mechanism is stronger during periods of high insolation (i.e. summer), to the extent that a summer SAM event produces as large of a response the following winter as a winter SAM event can produce at short lags (Fig. 2.6) (Sen Gupta and England, 2006). During winter SAM events, the orientation of the sea ice edge relative to zonal advection establishes an alternating positive-negative-positive pattern in SIC anomalies (Fig. 2.5b,d) (Sen Gupta and England, 2006).

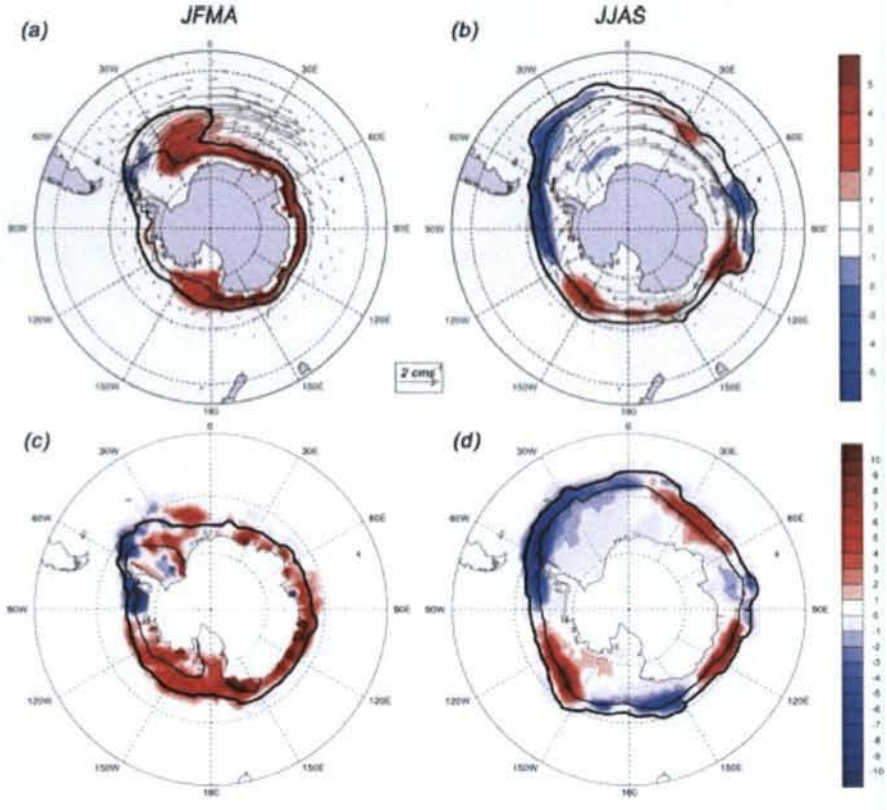

Figure 2.5: Model (a,b) and HadISST reanalysis (c,d) regressions of the SAM index on sea ice concentration lagged by one month for JFMA(left) and JJAS(right) seasons. Thick(thin) contour lines give the seasonally averaged 5%(50%) ice coverage extent. Model plots also show sea ice anomaly velocity vectors at 0-lag, and a 2 cm s^{-1} vector scale is shown. After Sen Gupta and England(2006)

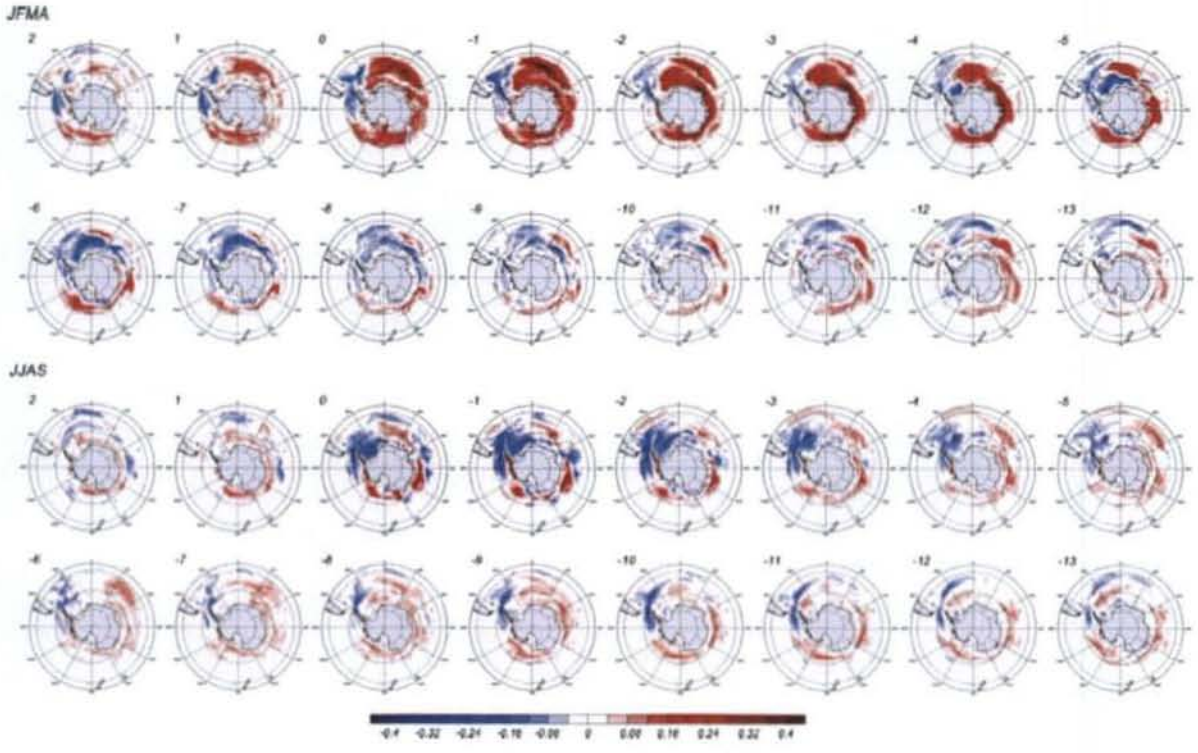

Figure 2.6: Model sea ice concentration correlation maps at various lags (negative lags imply SAM leading sea ice concentration), after Sen Gupta and England (2006).

2.6.4 ENSO influences on the sea ice system

An out of phase relationship in surface air temperature and sea ice anomalies, such as the aforementioned SAM dipole response, also occurs in response to ENSO events (Yuan and Martinson, 2001). This dipole, which sees warmer conditions and less sea ice in the southern Bellingshausen and western Weddell Seas and colder conditions with more sea ice in the Amundsen and Ross Seas, has been termed the Antarctic Dipole (Yuan and Martinson, 2001). The temperature anomalies of the Antarctic Dipole are the largest ENSO signal present outside the tropical Pacific (Liu et. al. 2002). A comprehensive mechanism description is provided in Yuan (2004), but for the purposes

rainfall. The authors found that sea-ice extent anomalies were highly positively correlated in the central South Atlantic sector (approx. 15W-35W) and west of the AP (approx. 75W-90W), while large negative correlations existed directly south of SA (approx. 10E-30E). In the central South Atlantic cool(warm) SST anomalies and increased(decreased) sea ice extent tend to be associated with wet(dry) SWC winters. Reason et. al. (2002) proposed that increased sea ice extent and negative SST anomalies act collectively in the central South Atlantic to re-enforce the meridional near-surface temperature gradient and thus bring about a equatorward shift in the storm track to conserve potential vorticity, leading to enhanced SWC rainfall. Opposite anomalies in sea ice extent and SST would have an opposite effect.

Blamey and Reason (2007) used Reynolds Optimally Interpolated sea ice data to examine potential relationships between SIC and winter-rainfall. Correlations were performed for the entire winter (MJJAS) as well as early (MJJ), mid(JJA) and late(JAS) winter. When correlations were performed between the two variables for the winter as a whole, a region of positive correlation was observed near the Antarctic Peninsula and Weddell Sea while a region of negative correlation was observed in the area of 0°-30° E. The Weddell Sea region of positive correlation remained significant with sea ice leading by up to two months, but weakened substantially more than the region of negative correlation due south of SA, which remained strong with sea ice leading by up to five months. Blamey and Reason (2007) found that the areas of strong contrast between the positive and negative correlation of sea ice to SWC rainfall were present even if only ENSO neutral years were used to make the wet-dry composite, suggesting that signal is robust and not merely a feature of ENSO. The area of positive correlation in the central

South Atlantic sector (approx. 15W-35W) found by Reason et. al. (2002) was not observed to be an area of significant positive correlation by Blamey and Reason (2007). Blamey and Reason (2007) also noted that mid-latitude SST anomalies appear to work in the same direction as the SIC anomalies, with cool(warm) sea ice anomalies north of positive(negative) sea ice correlations during wet winters.

2.7 Study objectives

Previous studies have identified relationships between numerous variables and SWC rainfall, some of which are known to be present several months before rainfall. The underlying physical connection between many of these variables and SWC rainfall is not well understood. The timescales over which these variables influence SWC rainfall have yet to be identified, and the seasonal nature of these influences has yet to be addressed. Potential application of the understanding of these relationships, in the form of a statistical forecast model, has yet to be explored. This study aims to further explore previously identified relationships between several variables and SWC rainfall. It will attempt to identify when these relationships initially develop, at what time they are strongest, the character of their relationship with different periods of winter rainfall, and their stability. Insight gained from this will be used to assess the potential for statistical seasonal forecasting of SWC rainfall.

Chapter 3

Exploring Connections To Southwestern Cape Rainfall

3.1 Introduction

This chapter further investigates established relationships between variables and SWC rainfall, identifies which of these variables may present predictability of SWC rainfall, and discusses possible co-interactions and co-variability. This is accomplished by exploring correlations with variables at various lead times to rainfall.

3.2 Data and Methods

3.2.1 Correlation maps

South African Weather Service (SAWS) gridded monthly rainfall data available from 1940 were used to form an index of district 4 winter rainfall (Fig. 3.1) for the entire season (May to September, MJJAS) as well as for early (May to July, MJJ), mid (June to August, JJA) and late (July to September, JAS) winter.

of this study a short synopsis will suffice. Via mechanisms described in the previous ENSO section, the mean meridional transport of heat by the Ferrell cell decreases in the Pacific and increases in the Atlantic (Yuan, 2004). The presence of a low-pressure anomaly in the Bellingshausen Sea, similar to that present in the (+) SAM phase, acts in combination with these anomalous poleward heat fluxes to produce the Antarctic Dipole (Yuan, 2004). Positive feedbacks between the jet stream and stationary eddies in the atmosphere, as well as feedbacks in the sea-ice-atmosphere system allow these anomalies in temperature and ice to persist for up to three seasons after the ENSO event occurs (Yuan, 2004). The regional mechanisms by which the Antarctic Dipole is created in response to ENSO events is remarkably similar to those responsible for the observed SAM dipole, and several authors have investigated the co-variability of the two (Fogt and Bromwich 2006, Stammerjohn et. al. 2008, Yuan and Li 2008, Lefebvre and Goosse, 2008). Fogt and Bromwich (2006) found that the high latitude ENSO response in the austral spring (SON) intensified from the 1980's to the 1990's in association with an increasingly in-phase relationship between ENSO and SAM. This in-phase relationship and increased high latitude response was also present in DJF of both the 1980's and 1990's (Fogt and Bromwich, 2006).

2.6.5 Relationships with SWC rainfall

Relatively little research has been done regarding the relationship between Antarctic sea ice and SWC rainfall. As part of a general investigation into large-scale ocean-atmosphere interactions and SWC rainfall, Reason et. al. (2002) used a global ice-ocean model to generate sea-ice data for the years 1982-1999 and compared it to SWC

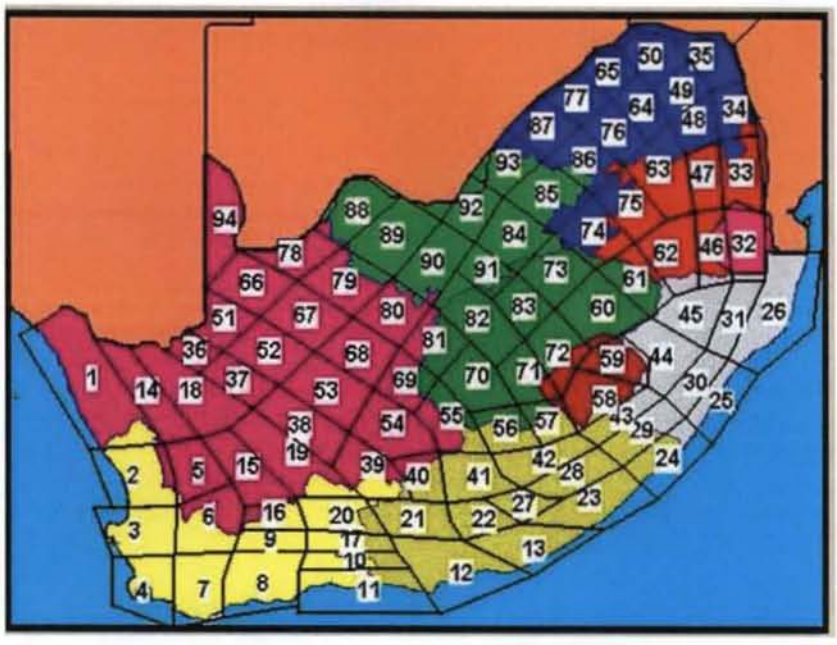

Figure 3.1: South Africa Weather Service rainfall districts, with district 4 located in the bottom-left hand corner of the image

NOAA optimum interpolation (OI) version 2 monthly (from weekly) SST data (Reynolds et. al. 2002) available from 1982 to 2009 were used to obtain SST and SIC values with 1° spatial resolution. For every month the SST or SIC in each 1° by 1° box was detrended and correlated with detrended rainfall of each season as well as each individual month to create correlation maps of various leads and lags. All correlations performed in this study were computed using the Pearson's correlation:

$$r_{xy} = \frac{Cov(x,y)}{s_x s_y} = \frac{\frac{1}{n-1}\sum_{i=1}^{n}[(x_i - \bar{x})(y_i - \bar{y})]}{[\frac{1}{n-1}\sum_{i=1}^{n}(x_i - \bar{x})^2]^{1/2}[\frac{1}{n-1}\sum_{i=1}^{n}(y_i - \bar{y})^2]^{1/2}} \qquad (3.1)$$

Where: x and y are variables of number n

It should be kept in mind that the Pearson's correlation is neither resistant nor robust, being sensitive to outliers and potentially unable to recognize nonlinear relationships. In order to investigate the stability of relationships between SST and rainfall found in the 1982-2009 time period, similar correlation maps for the period of 1959 to 1981 were created using the monthly Hadley Centre Sea Ice and Sea Surface Temperature (HadISST1) data set (Rayner et. al. 2003) with 1° spatial resolution.

Monthly mean U-wind and geopotential height values at the 1000-hPa, 500-hPa, and 200-hPa levels were obtained from the NCEP/NCAR reanalysis data set (Kalnay et. al., 1996) with 2.5° by 2.5° resolution. Correlation maps for the periods of 1940 to 1981 and from 1982 to 2009 were created using the method described above. Details of the data sets are in Table 3.1.

3.2.2 Southern Annular Mode Correlations

The role of the SAM as the leading mode of variability in many various fields, and its dominance throughout the tropopause, has led to numerous definitions of the SAM index. For the purposes of this study two measures of the SAM index will be used. The first, proposed by Gong and Wang (1999), is known as the Antarctic Oscillation Index (AAOI). It is calculated as the monthly mean difference between the sea level pressure (SLP) measured at 6 stations located near 65°S and 6 stations near 40°S according to the methodology of Marshall (2003),with data available from 1957 to 2009 at www.nerc-bas.ac.uk/icd/gjma/sam.html. The second index used index is created by projecting the monthly mean 700-hPa geopotential height anomaly onto the leading EOF

mode, as defined for the 1979-2000 period. It was obtained from the NOAA climate prediction center at www.cpc.ncep.noaa.gov/, and is available from 1979 to 2009. Details of the data sets are in Table 3.1. Both indices were detrended over various time periods and correlated with detrended monthly and seasonal rainfall.

3.2.3 El Nino Correlations

The Nino 3 index used in this study was derived from HadISST1 data spanning from 1870 to 2009, and is also available via the KNMI climate explorer. The index was detrended over various time periods and correlated with detrended monthly and seasonal rainfall. Details of the data set are in Table 3.1.

Property	Data Set	Description	Reference
Rainfall	South African Weather Service	Monthly gridded rainfall data from 1940	N/A
SST	NOAA optimum interpolation version 2 provided by the NOAA-CIRES climate diagnostic center from http://www.research.noaa.gov/	1° monthly data from 1982	Reynolds et. al. 2002
SST	HADISST 1.1 provided by the Met Office, Hadley Centre for Climate Research from their website (hadobs.metoffice.com/)	1° monthly data from 1890 [replaces the global sea ice and sea surface temperature (GISST)]	Rayner et. al. 2002
Sea Ice Concentration	NOAA optimum interpolation version 2 provided by the NOAA-CIRES climate diagnostic center from http://www.research.noaa.gov/	1° monthly data from 1982	
Geopotential Height	NCEP Reanalysis data provided by the NOAA/OAR/ESRL PSD, Boulder, Colorado, USA, from their Web site (http://www.esrl.noaa.gov/psd/)	2.5°×2.5° monthly data from 6 hourly records from 1948	Kalnay et. al. 1996
U Wind	NCEP Reanalysis data provided by the NOAA/OAR/ESRL PSD, Boulder, Colorado, USA, from their Web site (http://www.esrl.noaa.gov/psd/)	2.5°×2.5° monthly data from 6 hourly records from 1948	Kalnay et. al. 1996
SAM Index	Gareth Marshall SAM Index available at www.nerc-bas.ac.uk/icd/gjma/sam.html.	calculated as the monthly mean difference between the SLP measured at 6 stations located near 65°S and 6 stations near 40°S from 1957	Marshall 2003
SAM Index	provided by the NOAA climate prediction center from http://www.cpc.noaa.gov	calculated by projecting the monthly mean 700-hPa geopotential height anomaly onto the leading EOF mode, as defined for the 1979-2000 period	N/A
Nino3 Index	provided by the KNMI Climate explorer at http://climexp.knmi.nl/start.cgi?someone@somewhere	calculated from Hadley Centre SST data set HADISST available from 1870	Rayner et. al. 2002

Table 3.1: Details of data sets used

3.3 Results

3.3.1 SST Correlations

3.3.1.1 Seasonal Rainfall: 1982 to 2008

The evolution of the correlations between seasonal rainfall and SST throughout the year is displayed in Figures 3.2 – 3.19. When rainfall is partitioned into early, mid and late winter periods, its relationship to SST displays several characteristics common to all periods. In order to assist in the description of these features, six regions have been designated A1 to A6, as illustrated in Figure 3.2a.

Area A1 exhibits persistent, significant, negative correlations present off of the southeastern coast of South America stretching south to the Antarctic Peninsula. SST in this region is significantly correlated with rainfall of all winter periods, though the strength, spatial extent, and configuration vary. Early winter rainfall displays the weakest relationship in this area (Fig. 3.2a – 3.19a). Mid and late winter correlations are developed by March, strengthen and persist through July, finally weakening in August and September (Fig. 3.4b,c – 3.17b,c). In the case of late winter rainfall, this relationship is already present as early as January (not pictured).

To the north, corresponding with the positive SST anomaly Blamey and Reason (2007) identified in wet-dry composites, area A2 displays significant positive correlations that develop in April (Fig. 3.6,3.7). Both mid and later winter exhibit a much stronger relationship in this area than does early winter. This area of positive correlation persists through September, but decreases substantially in size and strength after April (Fig. 3.6 - 3.17). In May, late winter rainfall exhibits strong positive correlations in area A3, as do

all rainfall periods in area A4 (Fig. 3.8, 3.9). For late winter rainfall area A4 remains strongly correlated through August (Fig. 3.14, 3.15). Both early and mid winter also exhibit a negative correlation extending NW to SE between areas A2 and A3 in June (Fig. 3.10, 3.11).

Persistent negative correlations in area A5 develop in May (Fig. 3.8, 3.9). This area corresponds with the negative SST anomaly Blamey and Reason (2007) identified in wet-dry composites, and the relationship is present for early, mid, and late winter rainfall. While this relationship persists through September for both mid and late winter rainfall, mid winter rainfall shows its strongest correlations in June (Fig. 3.10, 3.11) whereas late winter rainfall does so in August and September (Fig. 3.14 - 3.17).

In area A6, persistent, significant, positive correlations are present for early, mid and late winter rainfall. This relationship is strongest for early winter, where it is present as early as March (Fig 3.4a, 3.5a), strengthens considerably in May and June (Fig. 3.7a – 3.10a), and persists through September (Fig. 3.16a, 3.17a). For mid and late winter this area of correlation does not develop until June and has a more limited spatial extent (Fig. 3.10b,c – 3.11b,c).

For each rainfall period, during the months of rainfall a robust pattern of negative correlation in areas A1 and A5, and positive correlation in areas A2 and A6 is present. This pattern is strongest in the first two months of the respective rainfall period. In addition, positive correlations in area A4 are present in the first month of each rainfall period (e.g. May for early winter rainfall)(Fig. 3.8a, 3.10b, 3.12c). When rainfall for the entire winter period is analyzed, the correlations and patterns described are even more persistent and robust (Fig. 3.2d-3.19d).

3.3.1.2 Monthly Rainfall: 1982 to 2008

The evolution of the correlations between monthly rainfall and SST throughout the year is displayed in Figures 3.20 – 3.28. While the relationship of monthly rainfall to SST similarly displays common features, such features are less robust, more incoherent in their timing, and show more variation in their location and spatial arrangement. Simply describing common features, and deviations from those common features, will not provide an adequate framework for understanding the origins of predictability on monthly and seasonal timescales offered by certain features. Instead, each month must be examined individually.

May rainfall (Fig. 3.20a - 3.28a) shows strong correlations in areas A2-A6 in January (Fig. 3.20a). The positive correlation in areas A2-A4 weakens after January, while the positive correlation in A6 seems to strengthen slightly in March, April and May (Fig. 3.22a – 3.24a). In February, the negative correlation in area A5 expands southwest down to the Antarctic Peninsula (Fig. 3.21a). The relationship remains strong through March (Fig. 3.22a) and then weakens until May (Fig. 3.24a), when it is present only in A5. Most notable is the large area of positive correlation present in the central pacific, more easily seen in Figures 3.29 – 3.33, which persists into September.

The relationship between June rainfall and SST displays characteristics much different than those of other rainfall months (Fig. 3.20b – 3.28b). Most notable is a negative correlation in June (Fig. 3.25b) that stretches from the northwest side of area A2 southeast, almost to South Africa. At the same time, a weaker positive correlation just to the south runs parallel the stronger negative one. The negative correlation is present several months prior to June, though in a weaker form. A strong positive correlation is

present in the northern part of area A6 during March (Fig. 3.22b), which persists in a weaker form until June (Fig. 3.25b).

July rainfall (Fig. 3.20c - 3.28c) exhibits its earliest strong correlations in April (Fig. 3.23c), with positive correlations stretching through areas A2, A3 and A4. Correlations in areas A2 and A3 weaken substantially thereafter, while area A4 strengthens significantly during May and June before diminishing in July (Fig. 3.24c - 3.26c). A6 also develops strong correlations in June (Fig. 3.25c) that persist for several months. During the months preceding rainfall area A1 generally shows weak to moderate negative correlations. The pattern of the positive correlations in areas A2, A4, A6 and negative correlation in area A5 is present in June and continues in a weaker form for several months (Fig. 3.25c – 3.27c).

August rainfall (Fig. 3.20e - 3.28e) shows a distinct pattern with particularly strong negative correlations stretching from area A1 east to A6, and particularly strong positive correlations in A2. These develop initially in February (Fig. 3.21d) and strengthen until April (Fig. 3.23d), then diminish significantly in May (Fig. 3.24d). In August, a pattern with negative correlation stretching from A5 southwest to the Antarctic Peninsula and positive correlation stretching from A2 to A4 is present (Fig. 3.27d). Additionally, very strong positive correlations bordering South Africa extend north along the west coast in August and persist for several months (Fig. 3.27d). The pattern of the positive correlations in areas A2, A4, A6 and negative correlation in area A5 is present in August (Fig. 3.27d).

September rainfall displays very persistent positive correlations in the region stretching from A2 to A4 that are present from January until August, and then diminish in

September (Fig. 3.20e -3.28e). Strong positive correlation in area A6 is present from June until September (Fig. 3.25e - 3.28e). In May a region of negative correlation stretching from area A5 southwest to the Antarctic Peninsula becomes apparent (Fig. 3.24e). This negative correlation persists, slowly consolidating into A5, where it becomes particularly strong in September (Fig. 3.25e - 3.28e). Also worth mention is a very strong negative correlation that occurs between the Antarctic Peninsula and South America in January and February (Fig. 3.20e – 3.21e). This feature is bordered by a region of strong positive correlation to the north, off of the west coast of South America.

The pattern of negative correlation in areas A1 and A5 and positive correlation in areas A2 and A6 appears to be present, though weakly so, in the respective month of rainfall for July rainfall (Fig. 3.26c) and August rainfall (Fig. 3.27d). May, June and September rainfall do not exhibit this pattern in the respective months of rainfall. The correlation pattern observed in the months leading up to June rainfall seems to be most dissimilar from those observed with seasonal rainfall, while those of May, July and August seem the most similar. The most robust features are found in areas A5 and A6, which are present in the respective month of rainfall for all but June rainfall, though the location of the A5 negative correlation varies moderately (Fig. 3.24a, 3.25b, 3.26c, 3.27d, 3.28e).

3.3.1.3 Seasonal and Monthly Rainfall: 1940 to 1981

Rainfall in the early, mid, late and entire winter periods shows no correlations with 1940-1981 SST similar to those observed with 1982-2008 SST. All rainfall periods show moderately strong positive correlations with SST, centered near 40°S and 20°W,

from January through April. In May to September, SST shows only weak correlations that do not persist in the same location. Of the five areas (A1-A5) described above, only area A5 has the semblance of persistent correlations, which are present and weakly positive for each rainfall period in the months leading up to rainfall. Similar to seasonal rainfall for this period, monthly rainfall for the period of 1940-1981 exhibits mostly weak, incoherent correlations with SST. Correlations patterns observed in the 1982-2008 period are not present.

3.3.2 SIC Correlations

3.3.2.1 Seasonal Rainfall

The evolution of the correlations between seasonal rainfall and SIC throughout the year is displayed in Figures 3.34 – 3.51. The relationship of SIC to each of the winter rainfall periods shows the development of a distinct dipole of positive-negative correlation, which was first observed by Blamey and Reason (2007). This dipole consists of a region of strong positive correlations extending eastward from the tip of the Antarctic Peninsula, and a region of strong negative correlation near the eastern Weddell Sea. While this dipole is observed with each of the winter rainfall periods, early winter rainfall exhibits a substantially stronger and more distinct dipole. The region of positive correlation develops strongly in May for all periods of rainfall (Fig. 3.43, 3.44), while the region of negative correlation does not seem to develop strongly until the first month of the respective rainfall period (Fig. 3.42a, 3.44b, 3.46c).

Significant positive correlations begin to develop in March near the tip of the Antarctic Peninsula (Fig. 3.38, 3.39), then strengthen and expand eastward considerably

in May (Fig. 3.42, 3.43). This eastward expansion continues through July (Fig. 3.46, 3.47) and then, in August, the main body of the correlation disconnects from the Antarctic Peninsula while continuing to expand and travel eastward (Fig. 3.48, 3.49). Of all the seasons, late winter rainfall shows the strongest correlations in late summer and early fall, but then displays distinctly weaker correlations throughout the winter than the other seasons.

The development of negative correlations along the sea ice edge in the eastern Weddell Sea can be seen as early as January/February for early winter rainfall (Fig. 3.34a - 3.37a). While this region is initially small, it grows in size and strengthens considerably in May, June and July (Fig. 3.42a – 3.47a). During this time it remains at the expanding sea ice edge, progressively moving eastward each month. Mid-winter rainfall displays a similar relationship, though the region of negative correlation does not initially appear until April/May (Fig. 3.40b – 3.43b). Late winter rainfall shows weak signs of correlation in June (Fig. 3.44b, 3.45b), which fully develop in July (Fig. 3.46b, 3.47b) and continue to move east through August (Fig. 3.48b, 3.49b), finally weakening in September (Fig. 3.50b, 3.51b).

3.3.2.2 Monthly Rainfall

The evolution of the correlations between monthly rainfall and SIC throughout the year is displayed in Figures 3.52 – 3.60. The SIC dipole that was clearly observed with seasonal rain is much less apparent with monthly rainfall. This dipole is most evident in June and July rainfall, while September rainfall displays an essentially

opposite dipole. While similarities are present, each month of rainfall displays a unique relationship with SIC.

May rainfall (Fig. 3.52a – 3.60a) exhibits weak and incoherent positive correlations near the Antarctic Peninsula, never showing a consolidated region of strong correlation. Weak early signs of the negative correlation, which persist and expands eastward each month, do not strengthen until May (Fig. 3.56a). This negative correlation is not restricted to the sea ice edge, but instead reaches into the Antarctic margin and extends along it westward to the Antarctic Peninsula.

June rainfall (Fig. 3.52b – 3.60b) shows moderate positive correlations near the Antarctic Peninsula in May (Fig. 3.56b), which then strengthen and expand in June (Fig. 3.57b) and persist until late in the year. The strongest positive correlations expand west of the Antarctic Peninsula in June, July and August (Fig. 3.57b - 3.59b). June also shows a moderate response in the negative dipole region that begins to develop in May (Fig. 3.56b).

July rainfall (Fig. 3.52c – 3.60c) displays the most distinct dipole, which is fully developed in July (Fig. 3.58c). Positive correlations observed near the tip of the Antarctic Peninsula strengthen and expand east in May, June and July (Fig. 3.56c - 3.58c). In August and September these correlations strengthen and expand even further, spanning along the Antarctic margin east of the negative dipole region (Fig. 3.59c, 3.60c). While weakly present earlier in the year, the negative correlation does not fully strengthen until June and July (Fig. 3.57c, 3.58c).

Generally weak and incoherent correlations are observed with August rainfall (Fig. 3.52d - 3.60d). No region, with perhaps the exception of a small area near the tip of

the Antarctic Peninsula, shows persistent strong correlations. A weak signal of the dipole can be observed in August (Fig. 3.59d), but is gone by September (Fig. 3.60d).

September rainfall (Fig. 3.52e – 3.60e) shows strong correlations stretching east from the tip of the Antarctic Peninsula in April (Fig. 3.55e). These correlations continue through September (Fig. 3.60e), with the core of the correlations continually moving east. In August, a region of negative correlation begins to develop near the tip of the Antarctic Peninsula, which then intensifies and expands in September (Fig. 3.59e, 3.60e). At this time, a dipole opposite that previously described is observed and persists in this location through November.

3.3.3 U Wind Correlations

Each winter month's rainfall shows especially strong positive correlations with zonal wind of the same month upstream and over southern Africa (Fig. 3.61 – 3.63). In most cases, these correlations are strongest at the 1000 hPa level and weaken slightly at 500 and 200 hPa. An exception to this is September rainfall, which shows correlations that not only remain strong at 200 hPa, but also extend west to South America at this level (Fig. 3.63e). May rainfall shows a weaker version of this correlation stretching to South America at the 200 hPa level (Fig. 3.63a). South of the region of strong positive correlation is a region of negative correlation, which is present in all rainfall periods. This correlation tends to be weaker, except in the cases of July and September rainfall (Fig. 3.61c,e - 3.63c,e). September rainfall also shows strong positive correlations at the 1000 and 500 hPa levels near the Antarctic Peninsula and extending east (Fig. 3.61e - 3.62e).

The regions of strong positive correlation described for May and September rainfall show similar patterns of positive correlation in the month leading up to rainfall (Fig. 3.64 - 3.65). These correlations are weaker and are present only at the 500 hPa and 200 hPa levels. In contrast, correlations in the month of rainfall are strongest at the 1000 hPa level and weaken at the 500 hPa and 200 hPa levels, suggesting the correlations present one month prior to rainfall may not be robust. Looking at U wind/rainfall correlations for the period of 1940 to 1981, patterns and strengths almost identical to those present for the 1982-2009 period were observed.

3.3.4 Geopotential Height Correlations

Each winter month's rainfall shows especially strong negative correlations with geopotential height of the same month over South Africa (Fig. 3.66 – 3.68). These regions of correlation are centered to the southwest of South Africa, and are observed at the 1000, 500 and 200 hPa levels. With the exception of July rainfall, negative correlations are also observed over South America. In most cases these are weaker than those in the South Africa region. September rainfall shows particularly strong negative correlations over South America, and also strong positive correlations in and to the north of the Weddell Sea (Fig. 3.66e – 3.68e).

3.3.5 SAM Correlations

3.3.5.1 Seasonal Rainfall 1982-2008

As previously mentioned, correlations of both seasonal and monthly rainfall were run with two different SAM indices. Significant correlations match closely in sign and

timing for both indices when examining seasonal rainfall, but the magnitudes of the correlations are larger for the GM SAM index in almost all cases (Table 3.2). In most cases, SAM indices in the fall to early winter (February to May) display the strongest correlations with seasonal rainfall. These correlations are more often found when a 2 to 4 month running mean is applied to the SAM index.

Early winter rainfall shows significant negative correlations in April with the GM SAM index at 0,1-month running mean, as well as May at 2-month running mean. The 700 EOF index shows similar but weaker correlations. Mid winter rainfall shows strong negative correlations in April and May with both indices at 2,3, and 4-month running means. Late winter rainfall shows significant negative correlations with the GM index in February, which progressively move to March, April and then May as the running mean of the index is increased from 0 to 4 months. The 700 EOF only shows significant correlations in April at 2,3 and 4 month running means.

3.3.5.2 Monthly Rainfall 1982-2008

For monthly rainfall, the sign and timing of significant correlations also match closely, with the GM index having a stronger relationship in some cases and the 700 EOF index in others (Table 3.3). Often only one index registers strong correlations while the other remains much weaker. Monthly rainfall shows little coherence in the timing of significant SAM events with relation to rainfall.

May rainfall shows no significant correlation with GM SAM events preceding rainfall, but shows negative correlation with 2,3-month running mean 700 EOF SAM events in January. June rainfall shows particularly strong negative correlations with 700

EOF SAM events in June at 0,2,3-month running lengths. The GM SAM index shows similar but weaker correlations. July rainfall shows no significant correlation with GM SAM events preceding rainfall, but shows a negative correlation with 2-month running mean 700 EOF SAM events in April. August rainfall shows particularly strong negative correlations with 0,2,3,4-month running mean GM SAM events in February and March. The 700 EOF SAM index shows similar but weaker correlations. September rainfall shows significant negative correlations with the 0,2,3-month running mean GM SAM index in September, and no significant correlations with the 700 EOF SAM index.

3.3.5.3 Seasonal Rainfall 1959-1981 (GM SAM index only)

Seasonal rainfall for both the 1959-1981 period and the 1982-2008 period show negative correlations, but correlations for the former period occur later in the year (June-August) than the later period (February to May) (Table 3.2). No significant correlations present in the 1982-2008 period are present in the 1959-1981 period.

Early winter rainfall shows no significant correlations. Mid winter rainfall shows significant negative correlations in June at 0-month running mean, and in August at 3,4-month running mean. Late winter rainfall also shows significant negative correlations in June with the SAM index at 0-month running mean, and in August at 3,4-month running mean.

3.3.5.4 Monthly Rainfall 1959-1981 (GM SAM index only)

Monthly rainfall for the period of 1959-1981 shows both positive and negative correlations of statistical significance (Table 3.3). The timing of these events in relation

to rainfall shows no coherent structure, although both positively correlated events occur in May (for June and September rainfall). No significant correlation present in the 1982-2008 period is observed in the 1959-1981 period.

May rainfall shows no significant correlations. June rainfall shows a significant positive correlation with the 2-month running mean SAM index in May. July rainfall shows a strong negative correlation with the 2-month running mean SAM index in June. August rainfall shows significant negative correlations with the SAM index at 0,2,3,4-running mean lengths in August. September rainfall shows a strong positive correlation with the 0 running mean SAM index in May.

3.3.6 El Nino Correlations

3.3.6.1 Seasonal Correlations

When the Nino3 index at 0-year lead is correlated with seasonal rainfall for the 1982-2009 period, early winter rainfall shows significant positive correlations in April and May (Table 3.4). These correlations are present in February, March and June as well, though weaker and not statistically significant. Mid, late, and entire winter rainfall show no statistically significant correlations in this time period, and no significant correlations are present for the 1940-1981 period.

When the Nino3 index at 1-year lead is correlated with seasonal rainfall for the 1982-2009 period (Table 3.5), early winter rainfall shows no significant correlations. Mid-winter rainfall shows significant negative correlations from January through July, with strongest correlations occurring in March. Late winter rainfall shows similar but weaker correlations, which are significant in March and May through July. Entire winter

rainfall shows significant negative correlation in March, with no other significant correlations occurring. No significant correlations are present for the 1941-1981 time period.

3.3.6.2 Monthly Correlations – 0 year lead

During the 1982-2009 period, May rainfall shows strong positive correlations with the Nino3 index at 0-year lead from January through May, with the strongest correlations being present in March and April (Table. 3.6). June rainfall also shows statistically significant positive correlations, but only in the month of rainfall. July, August and September rainfall show no statistically significant correlations for this time period. In the 1940-1981 time period July rainfall shows the strongest relationship to the Nino3 index at 0-year lead, with strong negative correlations in April, May and June. May rainfall, the month that showed strongest correlations in the 1982-2009 time period, also shows significant positive correlations in March.

When the Nino3 index at 1-year lead is correlated with monthly rainfall for the 1982-2009 period (Table 3.7), May rainfall shows strong, statistically significant positive correlations from May to October. August rainfall shows strong, statistically significant correlations from February to July, with strongest correlations occurring in May. July rainfall shows statistically significant correlations in March, and both June and September rainfall show no statistically significant correlations. No statistically significant correlations are present for the 1941-1981 time period.

3.4 Discussion

3.4.1 Origins of predictability: monthly and seasonal time scales

An examination of potential predictor variables has found significant correlations between these variables and SWC rainfall at monthly and seasonal timescales. Comparing the relative strengths of these correlations at monthly and seasonal timescales can give insight into the physical connection these variables have with SWC rainfall, and the timescales over which their influence is exerted. The SWC's location on the periphery of the itinerant westerlies ensures that the processes responsible for its rainfall are dynamic. Variables that hold influence one month may not be important the following month even if those variables persists in their original form, and any influence they have over seasonal rainfall may in fact originate primarily from their influence on a single months rainfall.

This seems to be the case with the Nino3 index at 0-year lead, where correlations with MJJ rainfall appear at similar timing, but in weaker form than those observed with May rainfall. June rainfall only shows correlation with the Nino3 index in June, and July rainfall shows no correlation at all.

Correlations between the SAM indices and seasonal rainfall do not reflect a dominant contribution from correlation with any single months rainfall. While August rainfall seems to contribute significantly to correlations observed in JAS rainfall, these same correlations are not present in JJA rainfall. Moreover, some strong correlations observed with monthly rainfall, for instance those between the GM SAM index in September and September rainfall, are not observed in seasonal rainfall periods that

incorporate those months. Correlations between rainfall and the Nino3 index at 1-year lead show similar characteristics. Much of the correlation observed in mid and late-winter rainfall appears to originate from the strong correlations observed with August rainfall. Yet May rainfall shows correlations just as strong as those observed in August, but these correlations are not projected onto early-winter rainfall.

Seasonal rainfall correlations with SST seem to display a few strong individual monthly relationships projected onto the seasonal timescale, but primarily consist of an amalgamation of similar or disparate weaker correlations. The pattern of correlation in areas A1, A2, A5 and A6, which is a robust feature present during all months of rainfall on the seasonal timescale, is only present during respective months of rainfall for July and August rainfall, and then only in a weaker form. This pattern that is common to all months during which rainfall occurs on the seasonal timescale is not produced from any single months relationship to SST, but is a pattern produced from the collective relationship of rainfall with SST over the rainfall period

Strong correlations between April SST and August rainfall in areas A1 and A2 are seen clearly in JJA and JAS rainfall correlations. Yet, for the most part, areas A1, A4, A5 and A6 show only weak to moderate, spatially limited correlations between SST and rainfall on the monthly scale. These correlations with rainfall on the monthly scale combine to produce the stronger, more persistent correlations observed with rainfall on the seasonal scale. In this view, the anomalous correlation patterns observed with June rainfall can be seen as the primary reason that the JAS rainfall period displays stronger, more persistent correlations than do the MJJ and JJA periods.

Similarly, correlations between SIC and seasonal rainfall do not originate from strong correlations with an individual months rainfall. Generally weaker correlations with monthly rainfall combine to form the stronger, more coherent correlations observed with seasonal rainfall periods. June, July and September rainfall does play a larger role in the later stage development of the region of positive correlation than May or August rainfall do. Also, the staggered timing in the development of the negative correlation region observed in monthly rainfall is projected onto the correlations with seasonal rainfall. Nevertheless, no single months rainfall plays a predominant role in shaping the correlations observed on the seasonal timescale.

3.4.2 Practical persistence of anomalies and their interpretation

The underlying rationalization in using correlations to explore phenomenon, such as SWC rainfall, is that strongly correlated variables may exhibit some physical connection to these phenomenon through which they transmit influence. In this study, several potential processes relating correlations at lead times of several months seem reasonable. Variables may affect the development of rainfall mechanisms at an early stage in such a way that changes remain apparent at the time of rainfall several months later. Variables in climatically sensitive regions, such as SIC near the Antarctic Peninsula, may serve as an index for the combined state of several broader modes of variability, some of which affect SWC rainfall. Anomalies in variables present several months before rainfall may have the tendency to develop and persist until the time of rainfall, when they can directly influence rainfall mechanisms. Any one, or a

combination of these physical processes may underlie the correlations observed in this study.

In the case of SST anomalies observed in this study, the latter seems likely given the dynamic nature of extratropical atmospheric circulation. The tendency of strong correlations observed months before rainfall to persist in the same region until the time of rainfall lends support to this idea. But if this is the case, then why are correlations in areas A1 and A2 stronger months before rainfall than those at the time of rainfall? Correlations within the remaining areas are typically stronger close to or during the rainfall period than they are several months before. This may indicate that SST anomalies present in areas A1 and A2 during periods of rainfall develop earlier in a stronger, more cohesive structure. As these anomalies persist, variability in their strength and spatial arrangement is introduced from their surroundings, until the time of rainfall when they exist in a less cohesive form.

Another potentially misleading attribute of correlations is the allusion that the time of occurrence of anomalies located with regions of correlation coincides. While there is a distinct pattern of correlation in areas A1, A2, A4, A5 and A6, this does not mean that anomalies within these areas occur at the same time, nor do they necessarily work in concert to create the anomalous rainfall conditions observed in the SWC. It is just as reasonable to assume that two separate influential SST patterns, working in different years influences SWC rainfall. Preliminary investigation suggests that anomalies within these areas work in concert, and their simultaneous occurrence plays an substantial role in influence SWC rainfall. For example, of the six years since 1982 when the entire SST pattern was observed in July, JAS rainfall was of the corresponding sign

during five years, and in four years was of greater than one standard deviation. During the eight years since 1982 that JAS rainfall has had larger than one standard deviation anomalies, the entire pattern was present in four years and in two of the remaining years only one area was missing from the pattern. The coincidence of anomalies in areas of high correlation needs to be looked at in great depth, and for other rainfall periods as well.

3.4.3 Possible direct effects of SAM and ENSO through atmospheric circulation

The mechanism(s) through which the SAM influences SWC rainfall have yet to be identified. It seems reasonable that the SAM may affect SWC rainfall directly through its impacts on atmospheric circulation. The findings of this study suggest that wet winters are associated with regionally decreased geopotential height and increased westerly wind over and upstream of the SWC. This agrees with the findings of Blamey and Reason (2006), who found that during wet winters the STJ upstream of SA is typically shifted equatorward and strengthened by around 15%. That this associated with the SAM phase is unsupported by the observations of Gallego et. al. 2005, who found relatively little modulation of the strength or position of the STJ just upstream of SA during winter months.

Model results of Sen Gupta and England (2006) suggest the impacts of the SAM on atmospheric circulation are largest at the time of an event and diminish significantly within a month. This suggests that if the SAM were in fact influencing SWC rainfall through its impacts on atmospheric circulation, it would be expected that correlations between the two were largest in the month(s) of, or one month prior to rainfall. Indeed,

both June and September rainfall show strong, significant, negative correlations with the SAM index in the corresponding month of rainfall. In contrast, May, July and August rainfall only show correlations with the SAM index several months prior to the month of rainfall. Yet rainfall of each month shows strong, statistically significant correlations with U-wind and geopotential height. While this certainly does not exclude the influence of the SAM in creating the U-wind and geopotential height anomalies observed in anomalous wet/dry winters, it suggests that the SAM is not the major mechanism responsible for this. This is also supported by the regional nature and non-annular structure of correlations with U-wind and geopotential height.

Seasonal rainfall has a more ambiguous relationship with the SAM. Both MJJ and JJA rainfall show moderate to strong correlations with the SAM index of 2 to 4 month running mean during months of rainfall, but the correlations tend to be stronger and more frequent a month before the rainfall season. The main body of these correlations happens far on the leading shoulder of the rainfall season, suggesting that their primary correlation does not occur through a strong direct atmospheric influence on SWC rainfall. JAS rainfall only shows correlations with the SAM index in the fall.

Colberg et. al. (2004) suggested that the atmospheric response to ENSO in the South Atlantic, transmitted via the PSA pattern, occurs primarily in AMJ, JAS and is weakened by JFM of the mature phase . El Nino events were said to results in a weakened South Atlantic anticyclone, weaker trade winds and intensified westerlies (Colberg et. al. 2004). Thus it would be expected that if ENSO were influencing SWC rainfall directly through modifications in atmospheric circulation, that rainfall would show a positive correlation with the Nino3 index at 0-year lead. May and June rainfall,

the only two months that do show significant correlations with the Nino3 index at 0-year lead, do indeed show positive correlations, as does MJJ rainfall. However, other periods of monthly and seasonal rainfall show no correlations with the Nino3 index at 0-year lead, suggesting that the atmospheric influence of ENSO on SWC rainfall is not a strong, consistent feature.

The overall structure of correlations between SAM indices and rainfall on both monthly and seasonal timescales suggests that both immediate and delayed responses to the SAM may be present. The correlations observed between the Nino3 index and rainfall, occurring at 0-lag and 1-year lag, similarly suggest both immediate and delayed affects of ENSO on SWC rainfall.

3.4.4 The SAM, ENSO, and their influence on rainfall through SST

Significant correlations between rainfall and the SAM index occurring more than a month before rainfall suggest that either the correlations are spurious, or that some aspect of the SAM persists for long enough to influence rainfall. Model results of Sen Gupta and England (2006) suggest that the maximum SST response to the SAM lags the atmospheric response by ~1 month, and that this response may persist for up to 6 months. The pattern of the SST response Sen Gupta and England (2006) obtained by regressing NOAA reanalysis SST on the SAM index (Fig. 2.11) closely matches the pattern of correlation exhibited by many periods of rainfall.

The SST pattern of positive correlation in areas A2 and A6 and negative correlation in areas A1 and A5 is a robust feature present during all months of rainfall for early, mid, and late winter rainfall periods. This suggests that this SST pattern creates

conditions favorable for rainfall in the SWC, and that rainfall would thus be correlated to this SST pattern independently of the SAM. The SAM can only account for a portion of the variability in SST that occurs in any of these areas, and anomalies in these areas occur independently of the SAM. However, as the SAM could potentially act as a substantial source of variability in these areas, it could be expected that rainfall periods that show a strong correlation with the SAM would also show stronger than normal relationships within areas A1, A2, A5 and A6 approximately one month after their correlations with SAM events. The results of this study do not provide clear evidence of this.

Another potentially significant source of SST variability in the areas correlated to rainfall is the ENSO mechanism identified by Colberg et. al. (2004). This study was limited to AMJ in the mature phase of ENSO events, but identified cold(warm) SST anomalies in areas A1 and A5 (A2, A3, and A4) at this time in response to El Nino. This suggests that rainfall would be positively correlated to the Nino3 index at 1-year lead. May rainfall is indeed positively correlated to the Nino3 index at 1-year lead, but in contrast July and August rainfall show strong negative correlations. In addition, seasonal rainfall only exhibits negative correlations, which are present for mid and late winter rainfall. This suggests that later in the mature phases SST anomalies reverse, or that there is a different mechanism of influence present.

3.4.5 Possible SAM links to SIC

The lagged nature of the sea ice response to the SAM, and its ability to persist, particularly in times of high insolation, provides a framework for understanding how SAM events occurring several months before periods of rainfall could set into motion

anomalies of sea ice which develop at the time of the rainfall. The findings of this study cannot support or reject this idea, especially considering the extent to which diverse modes of variability interact and influence the sea ice system, particularly near the Antarctic Peninsula.

The development of the negative region of correlation between SIC and rainfall typically coincides with the development of strong positive correlations with SST at the sea ice edge stretching north into area A6, particularly at seasonal rainfall timescales. While the two events could be independently related to SWC rainfall, this coincidence of timing suggests that these correlations are interconnected. The region of positive correlation with SST is often located as far north as 45°S and can extend west of 0° in some cases. The potential interconnection of the SIC and SST correlations suggests a more physical link to rainfall for the negative region of SIC correlation, which is itself so remote from the SWC that it seems unlikely to influence synoptic scale systems which bring the SWC its rainfall. These two regions of correlation may themselves be a combined response to larger modes of variability.

3.4.6 Southern hemisphere climate shifts and potential seasonal predictability

In the respective months leading up to rainfall, all periods of winter rainfall exhibit relationships with variables that could potentially be exploited for use in seasonal forecasting. In some cases these relationships appear to be strong, and the prospect of their use as forecasting tools seems promising. In other cases these relationships, while appearing robust and of sensible physical connection to SWC rainfall, exhibit only weak

correlations and their ability to create tangible probability shifts in SWC rainfall remains to be seen.

Early winter rainfall displays consistent relationships with SST in the months leading up to rainfall, but these relationships are weak. Rainfall in this period also shows moderate relationships with the GM SAM and Nino3 indices. Overall, early-winter rainfall seems to exhibit the least potential for seasonal predictability. Mid and late-winter rainfall show the most potential for seasonal predictability. Mid-winter rainfall shows moderately strong correlations with regions of SST and both the GM SAM and 700 EOF SAM indices in the months leading up to rainfall. Mid-winter rainfall also shows very strong correlations with the Nino 3 index the year before rainfall. Late winter rainfall shows the strongest, most persistent correlations with SST as well as moderate correlations with SAM indices in the months leading up to rainfall. Late-winter rainfall also has moderate correlations with the Nino 3 index the year before rainfall.

Seasonal and monthly rainfall correlations with SST, SAM indices (Table 3.1 i, j, k, l and Table 3.2 k, l, m, n, o respectively), and the Nino3 index (Table 3.3, 3.4 and Table 3.5, 3.6 respectively) in the corresponding time periods prior to 1982 do not show characteristics similar to those observed in the post 1982 time period. It is possible that this is in part an artifact of data quality prior to 1982, particularly with the HadISST data. Measurements of SST in regions of the mid to high southern latitudes are very limited, both spatially and temporally, prior to 1982. The coincidence of changed relationships of the SAM indices, SST, and the Nino3 index suggests that the perceived shift is more than an artifact of the data. This is supported by the findings of numerous studies. Yuan and Li (2008) found significant trends in the PSA pattern, stationary wave-3 index, SAM and

SAO from 1950 to 2003. Van Loon et. al. (1993) identified a sudden shift in SH circulation after 1976, whereby the zonal wave-3 intensified in the SH mid-latitudes while SLP fell over Antarctica. Mo (2000) examined long-term trends and interannual variations in circulation anomalies in the SH and found that changes in planetary circulation regimes are linked to global SST anomalies.

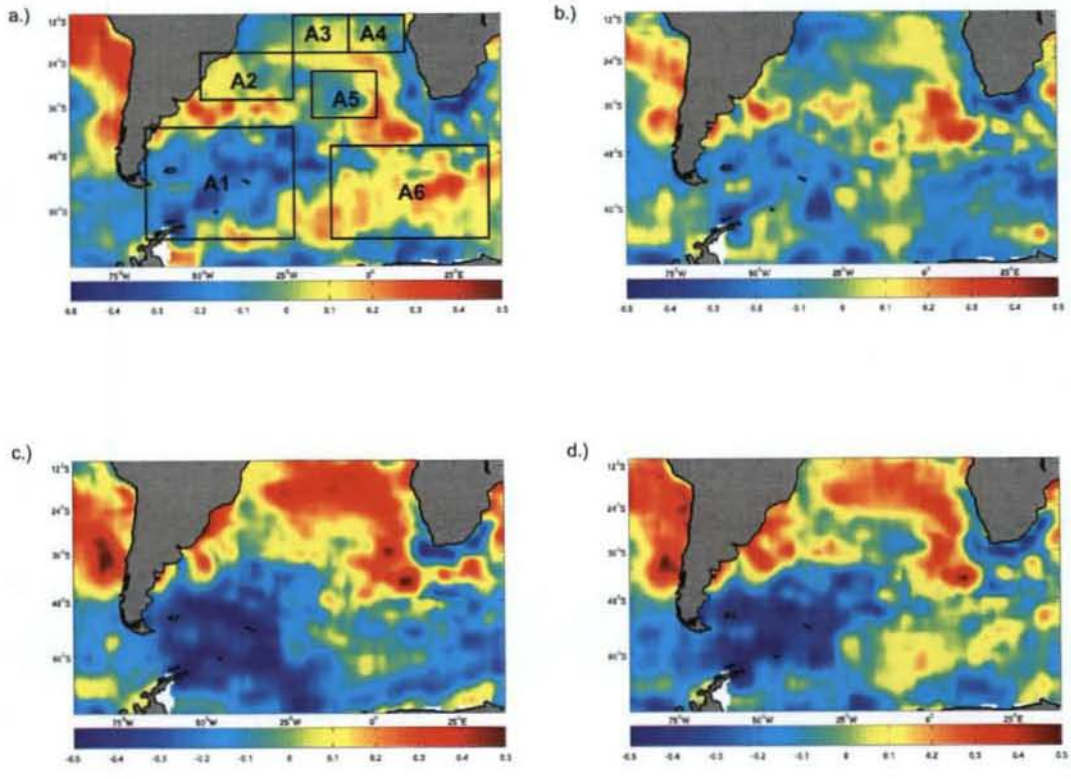

Figure 3.2: Spatial correlations between SWC rainfall in (a) MJJ, (b) JJA, (c) JAS, (d) MJJAS and sea surface temperatures in February for the period of 1982-2009. Correlation strength indicated by color shading ranging from -0.5 to 0.5. Black boxes in figure 4.1a indicate regions A1 to A6

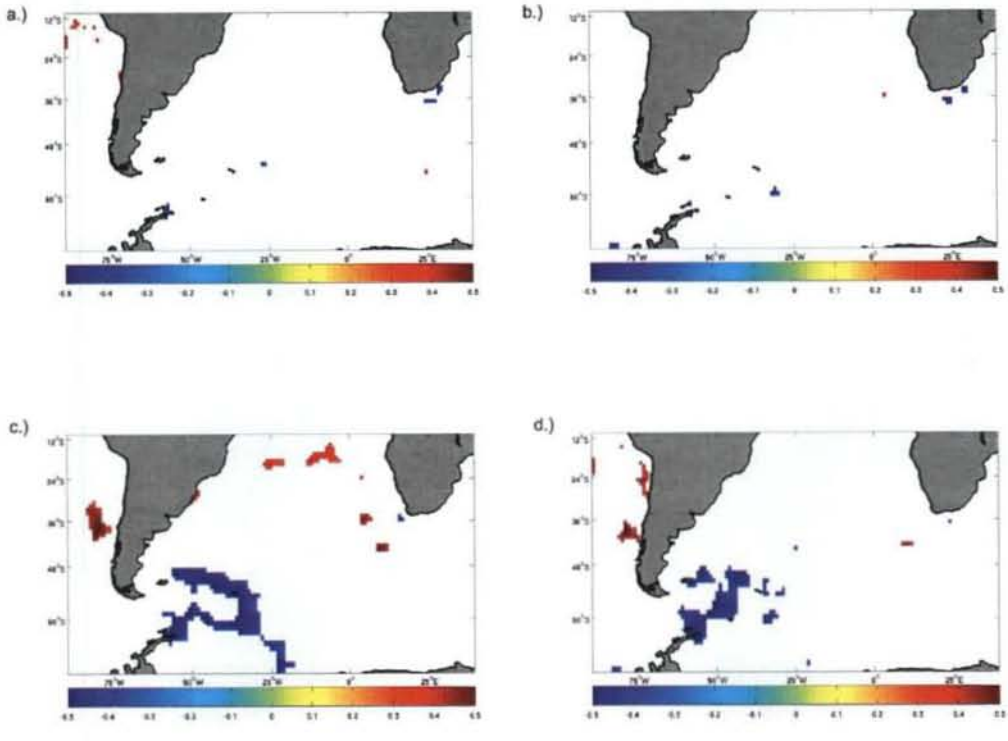

Figure 3.3: Spatial correlations of statistical significance (95%) between SWC rainfall in (a) MJJ, (b) JJA, (c) JAS, (d) MJJAS and sea surface temperatures in February for the period of 1982-2009. Correlation strength indicated by color shading ranging from -0.5 to 0.5

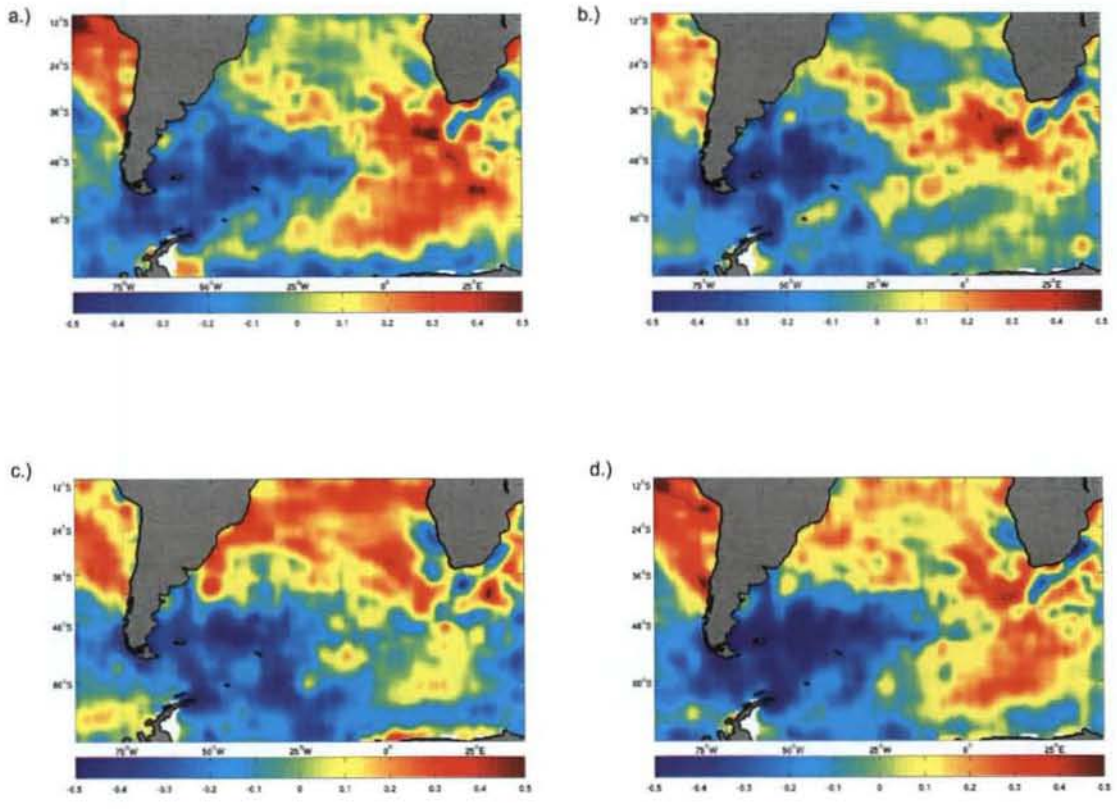

Figure 3.4: As for Figure 3.2 but for March sea surface temperature

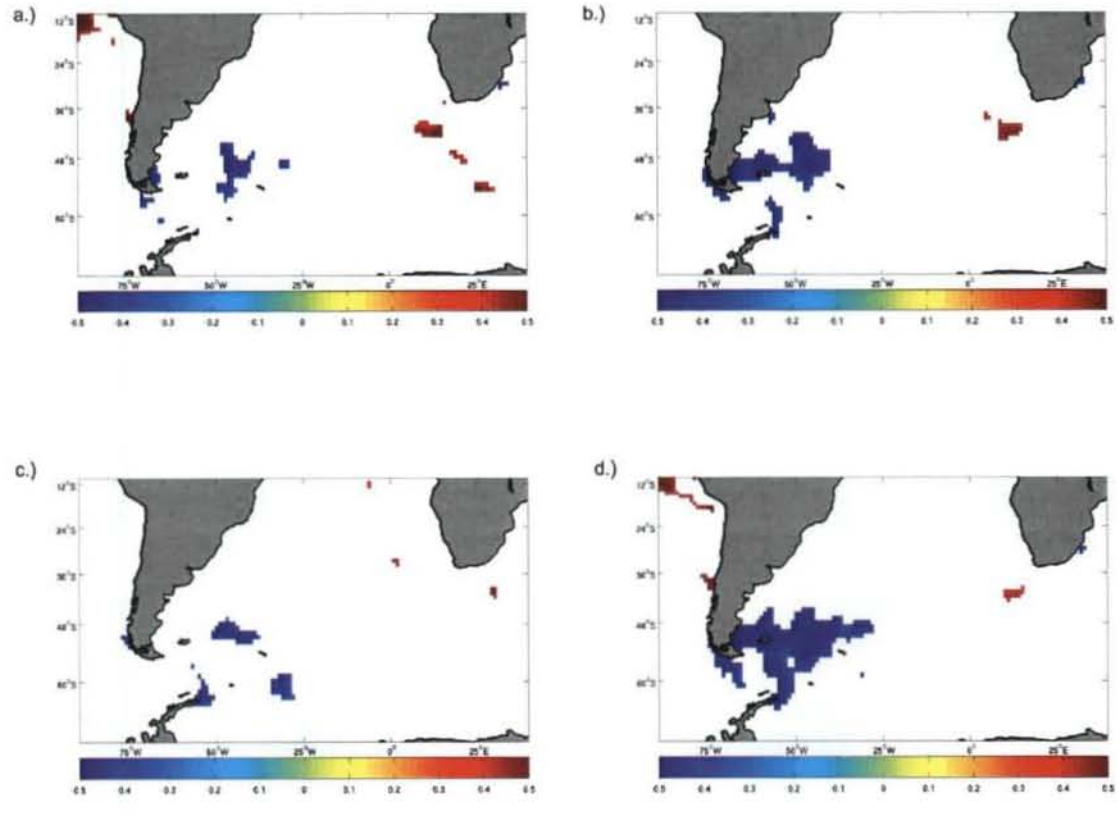

Figure 3.5: As for Figure 3.3 but for March sea surface temperature

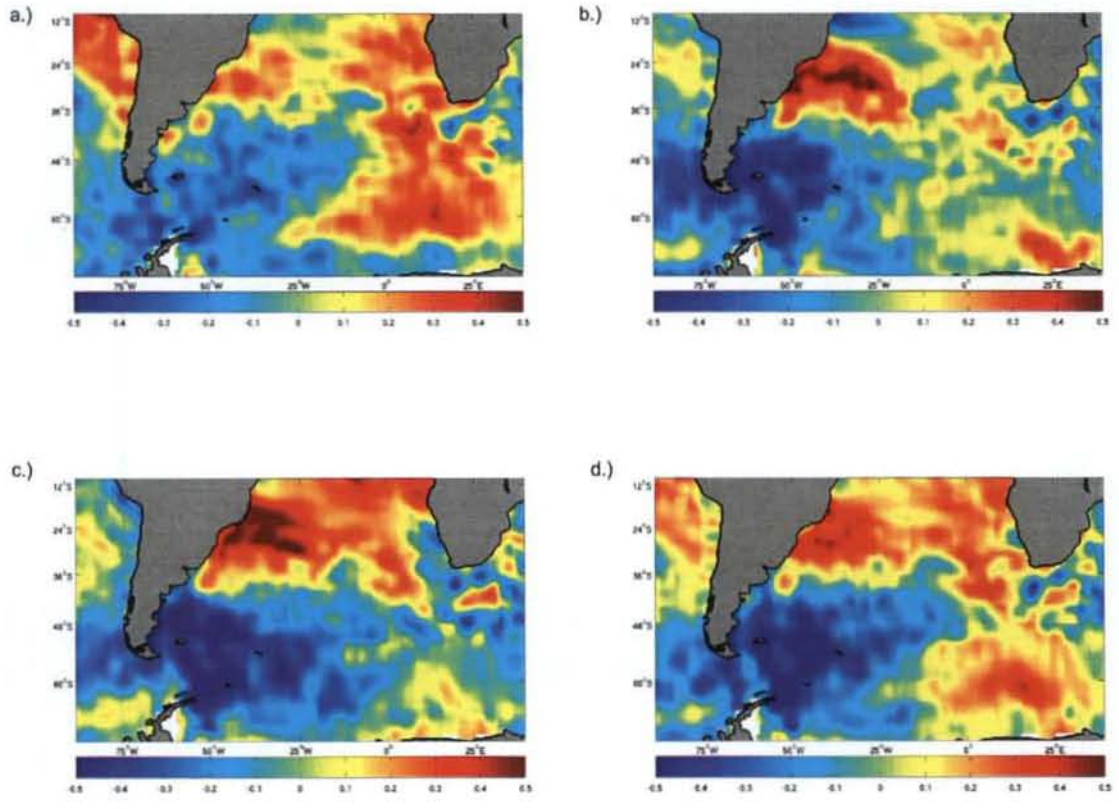

Figure 3.6: As for Figure 3.2 but for April sea surface temperature

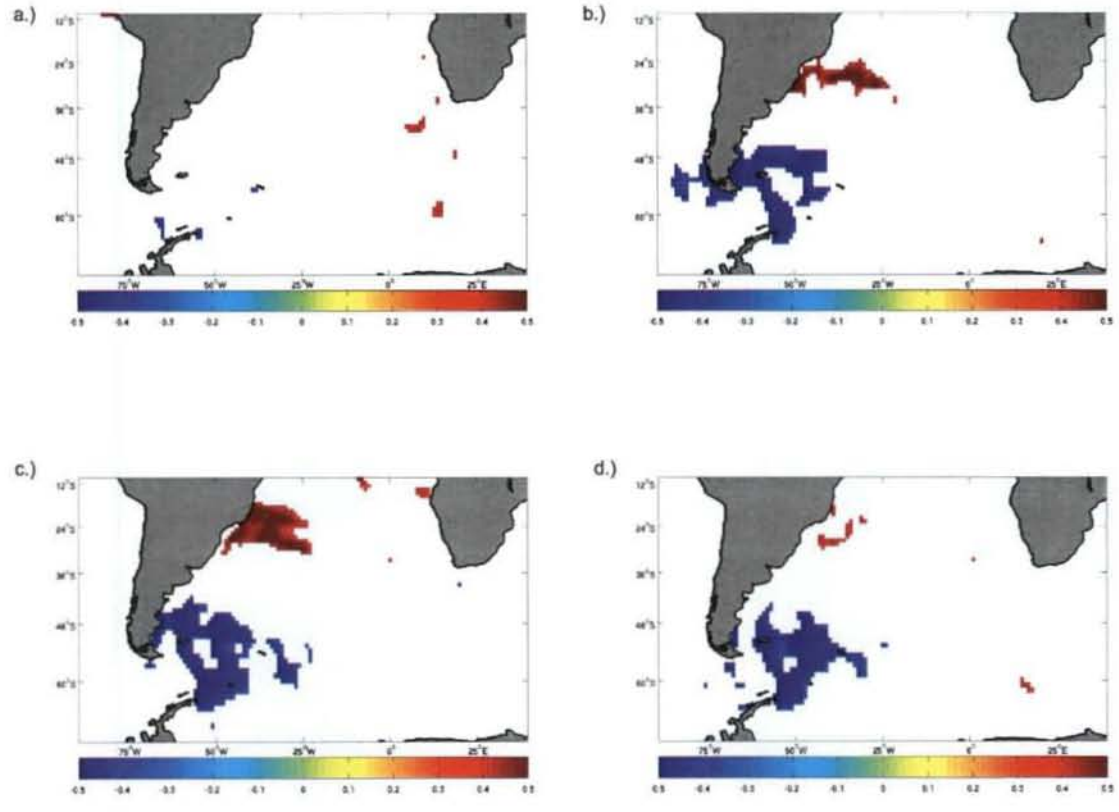

Figure 3.7: As for Figure 3.3 but for April sea surface temperature

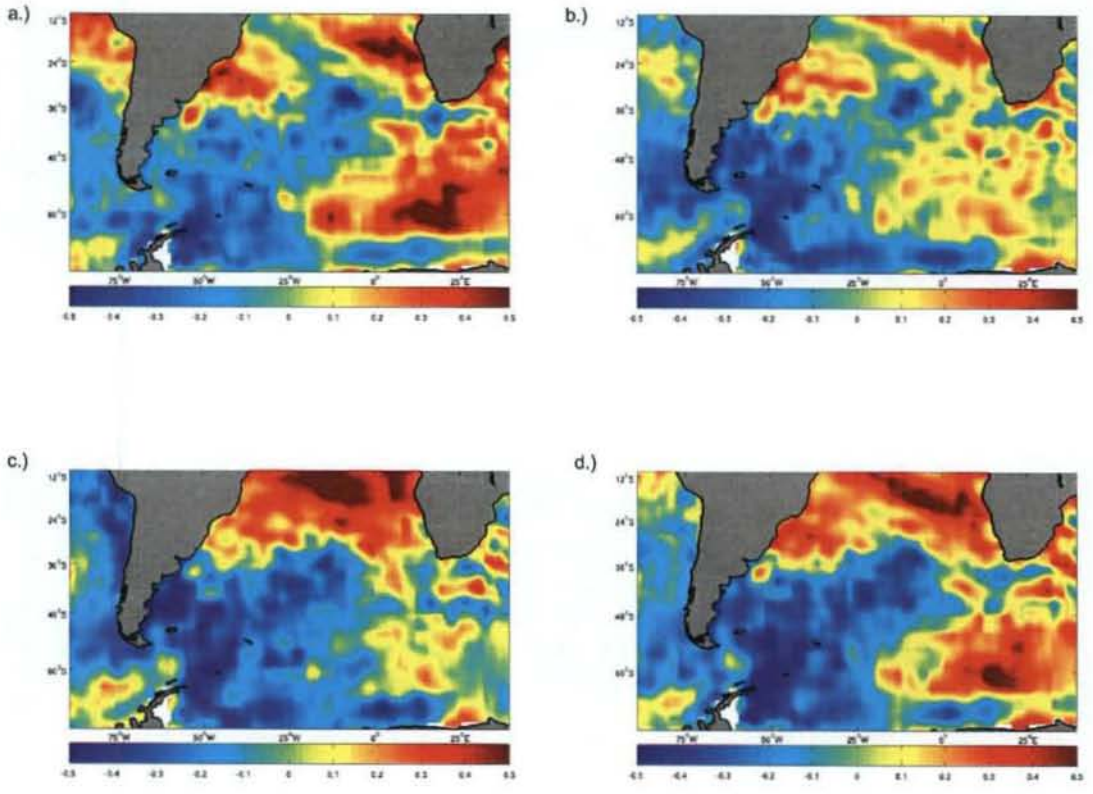

Figure 3.8: As for Figure 3.2 but for May sea surface temperature

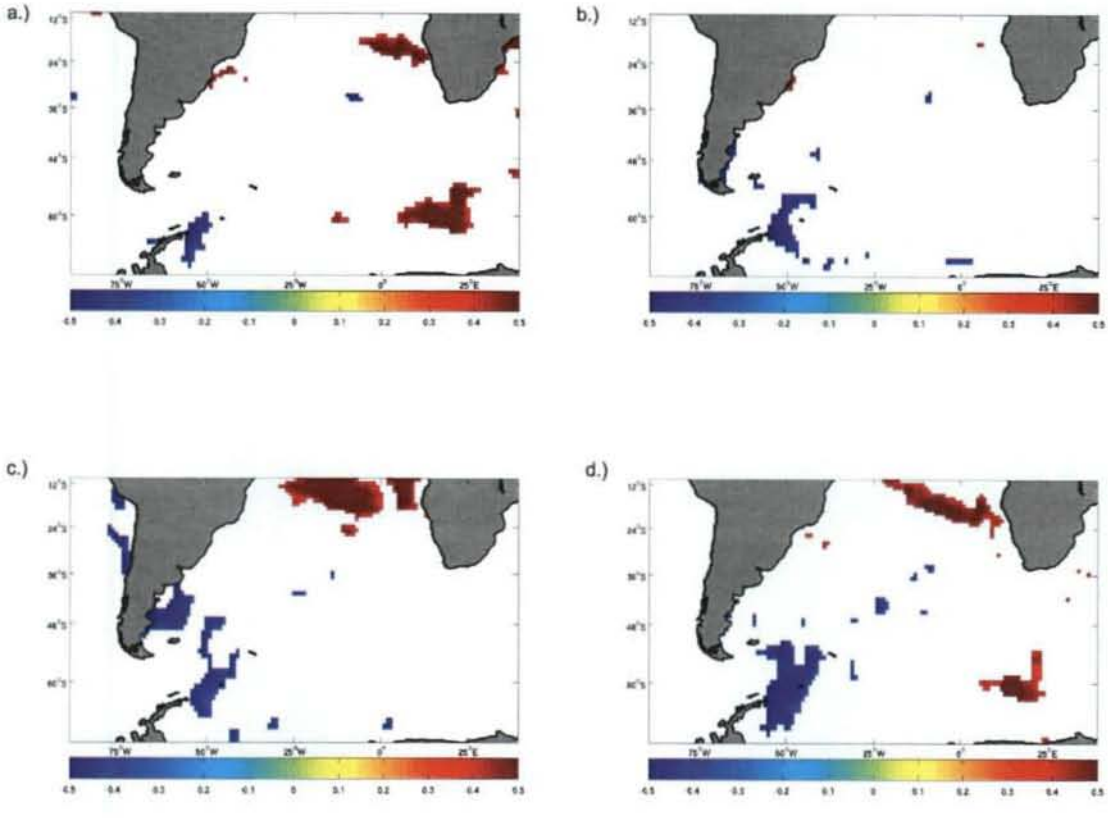

Figure 3.9: As for Figure 3.3 but for May sea surface temperature

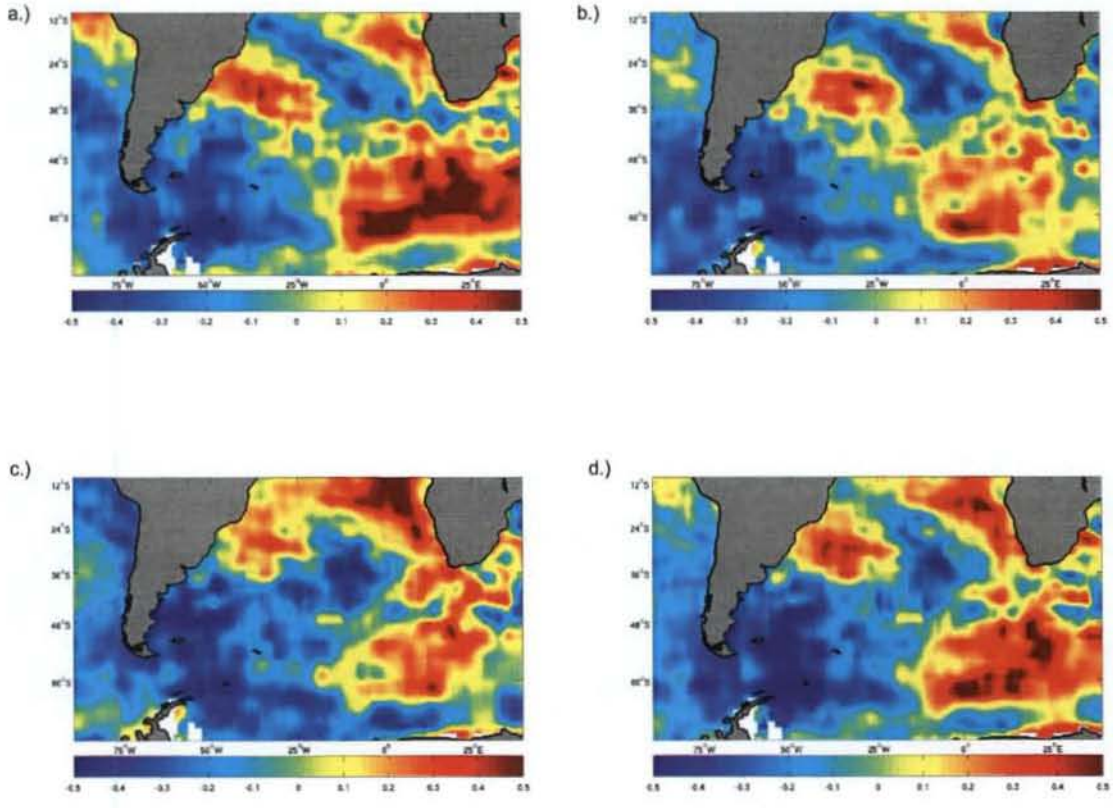

Figure 3.10: As for Figure 3.2 but for June sea surface temperature

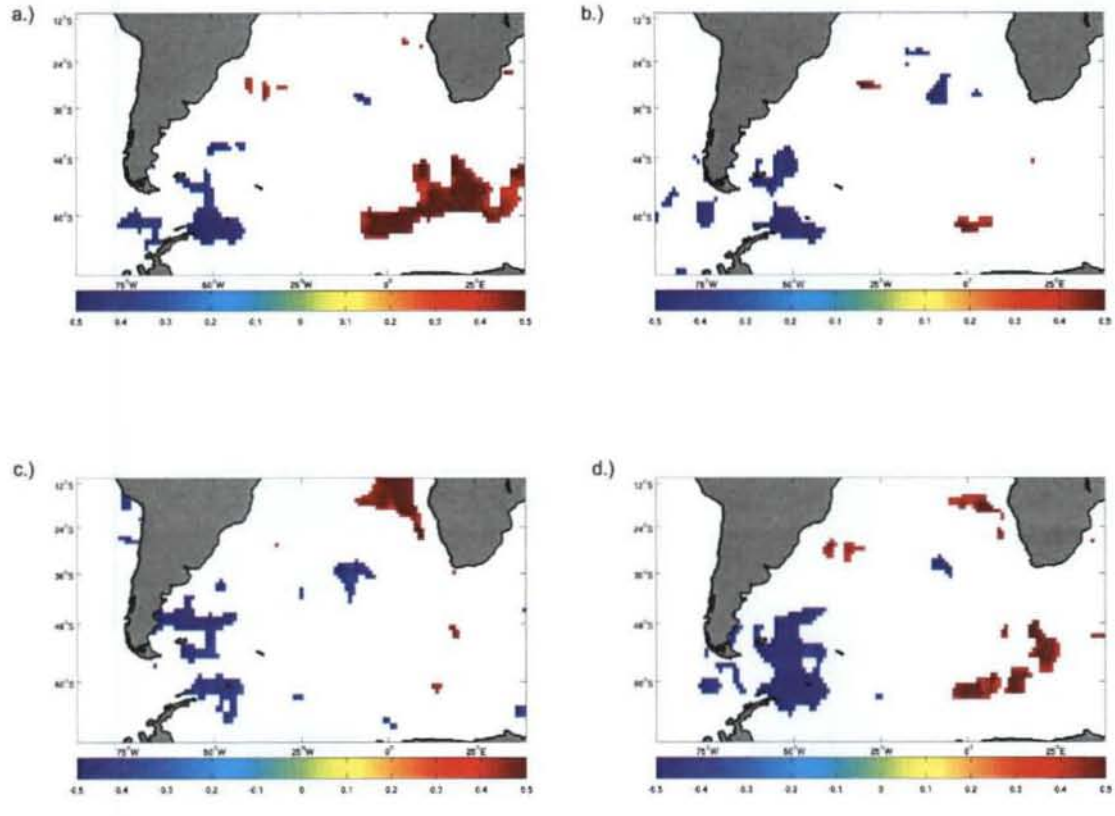

Figure 3.11: As for Figure 3.3 but for June sea surface temperature

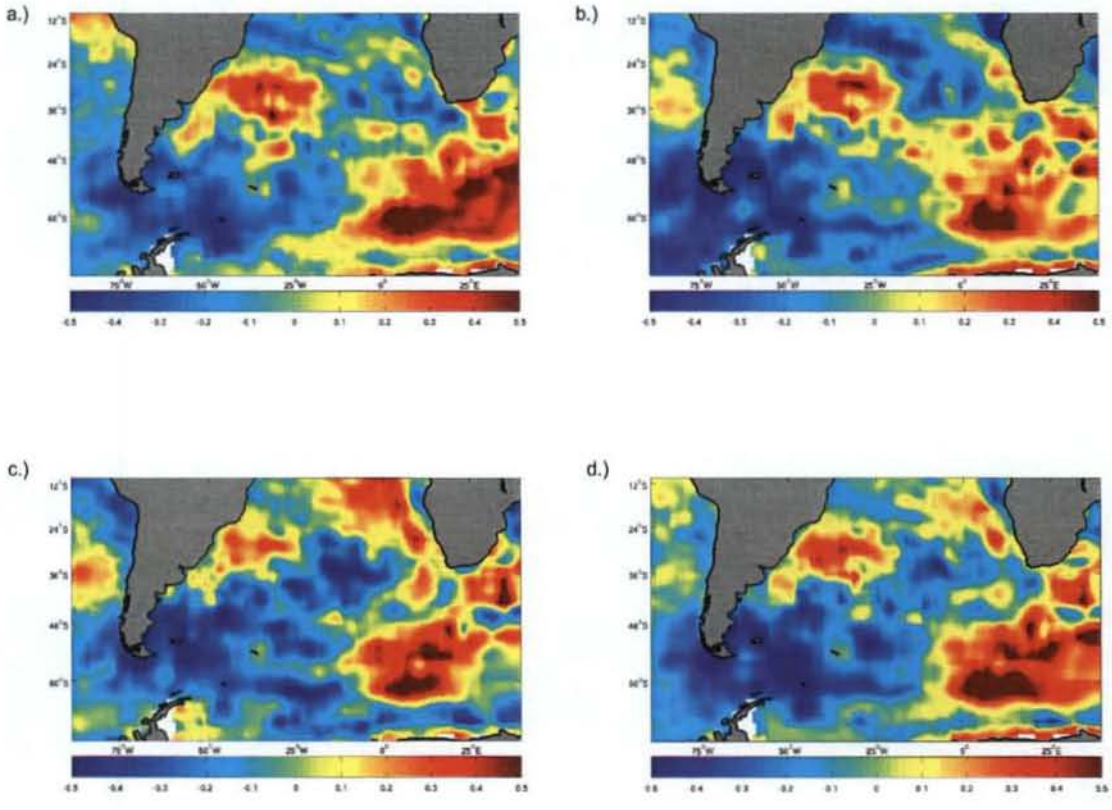

Figure 3.12: As for Figure 3.2 but for July sea surface temperature

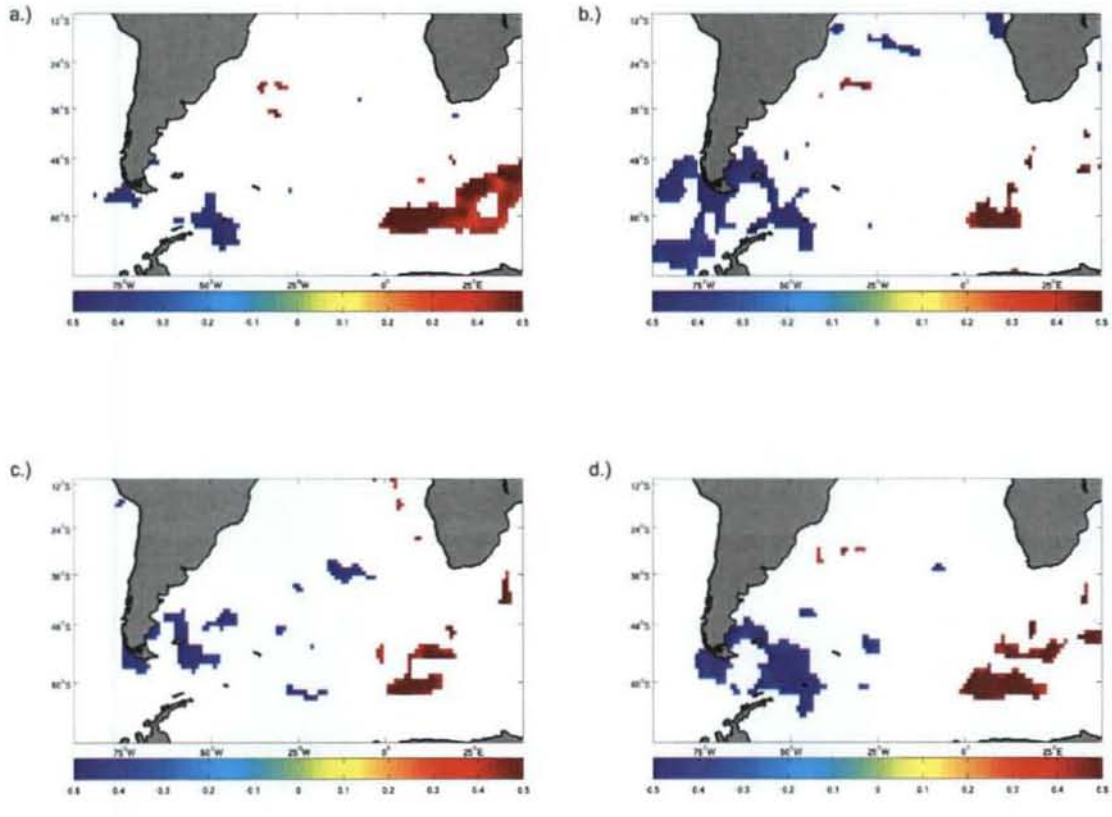

Figure 3.13: As for Figure 3.3 but for July sea surface temperature

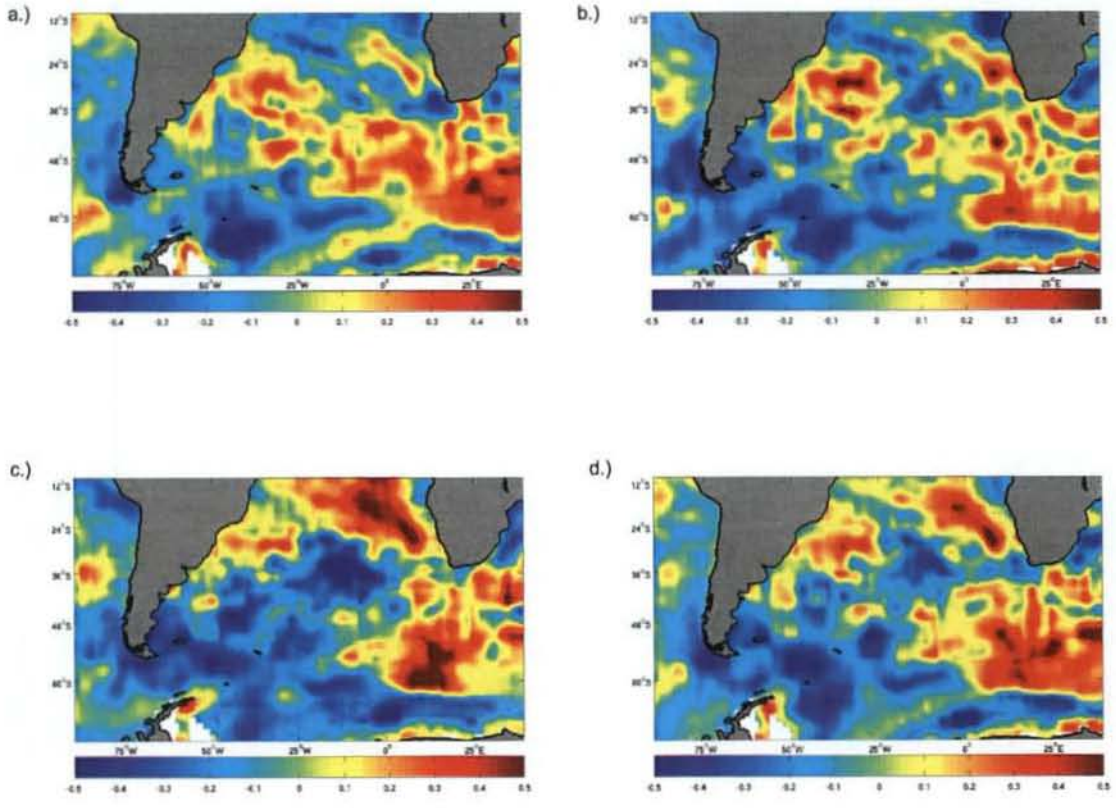

Figure 3.14: As for Figure 3.2 but for August sea surface temperature

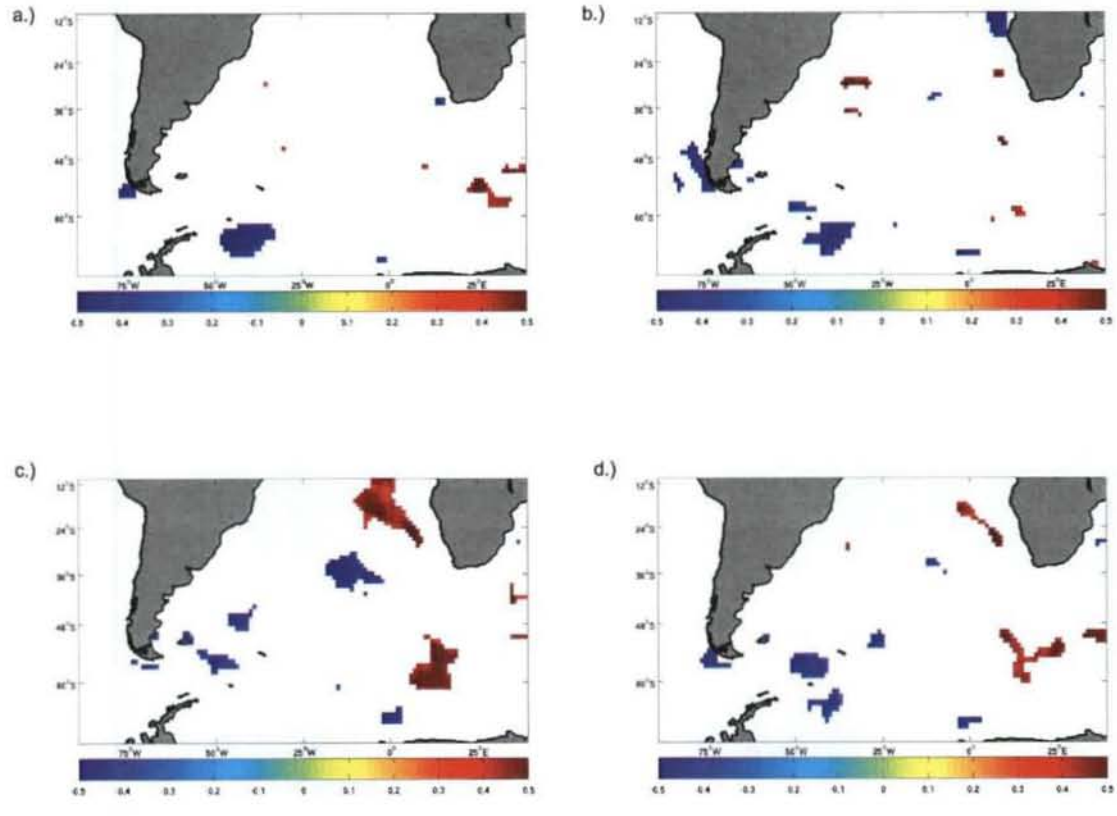

Figure 3.15: As for Figure 3.3 but for August sea surface temperature

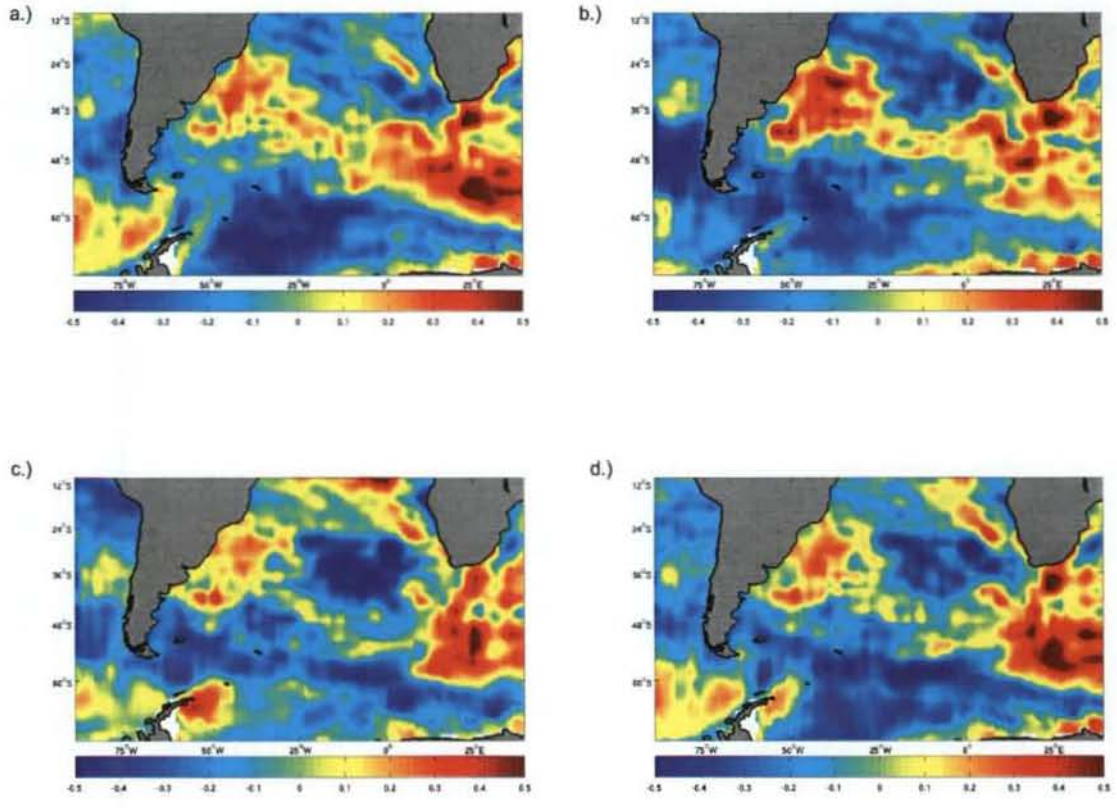

Figure 3.16: As for Figure 3.2 but for September sea surface temperature

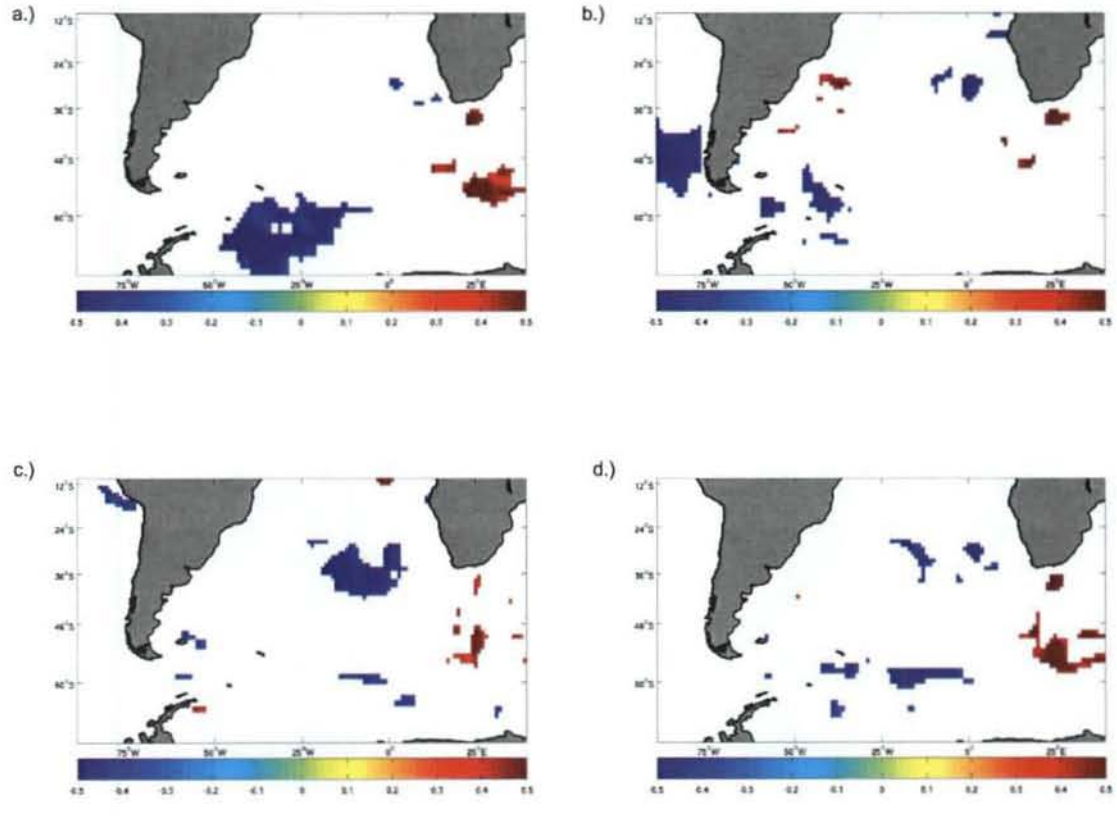

Figure 3.17: As for Figure 3.3 but for September sea surface temperature

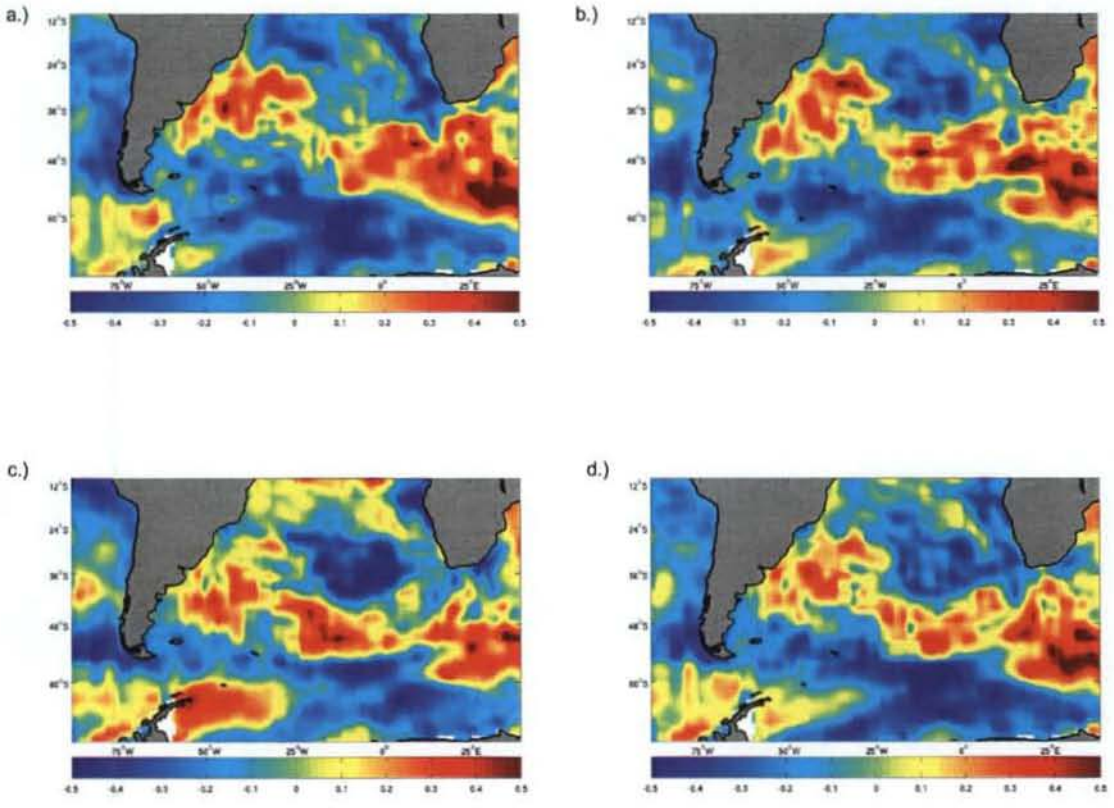

Figure 3.18: As for Figure 3.2 but for October sea surface temperature

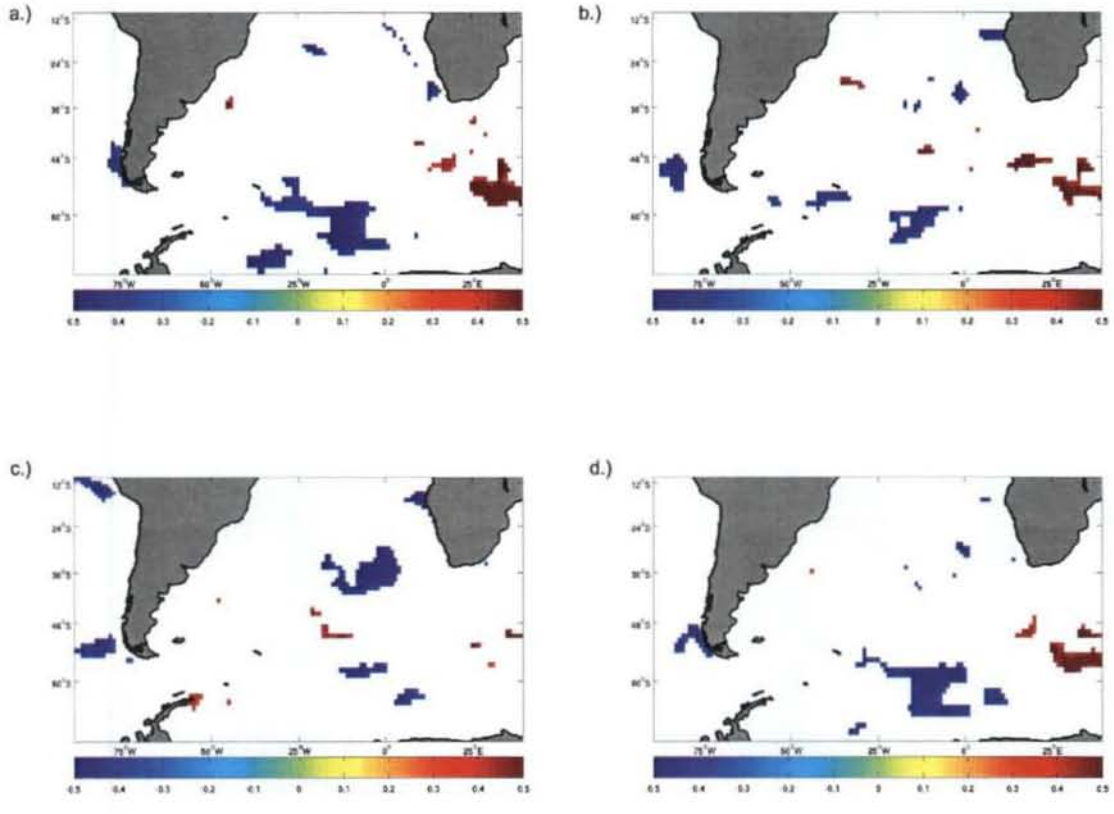

Figure 3.19: As for Figure 3.3 but for October sea surface temperature

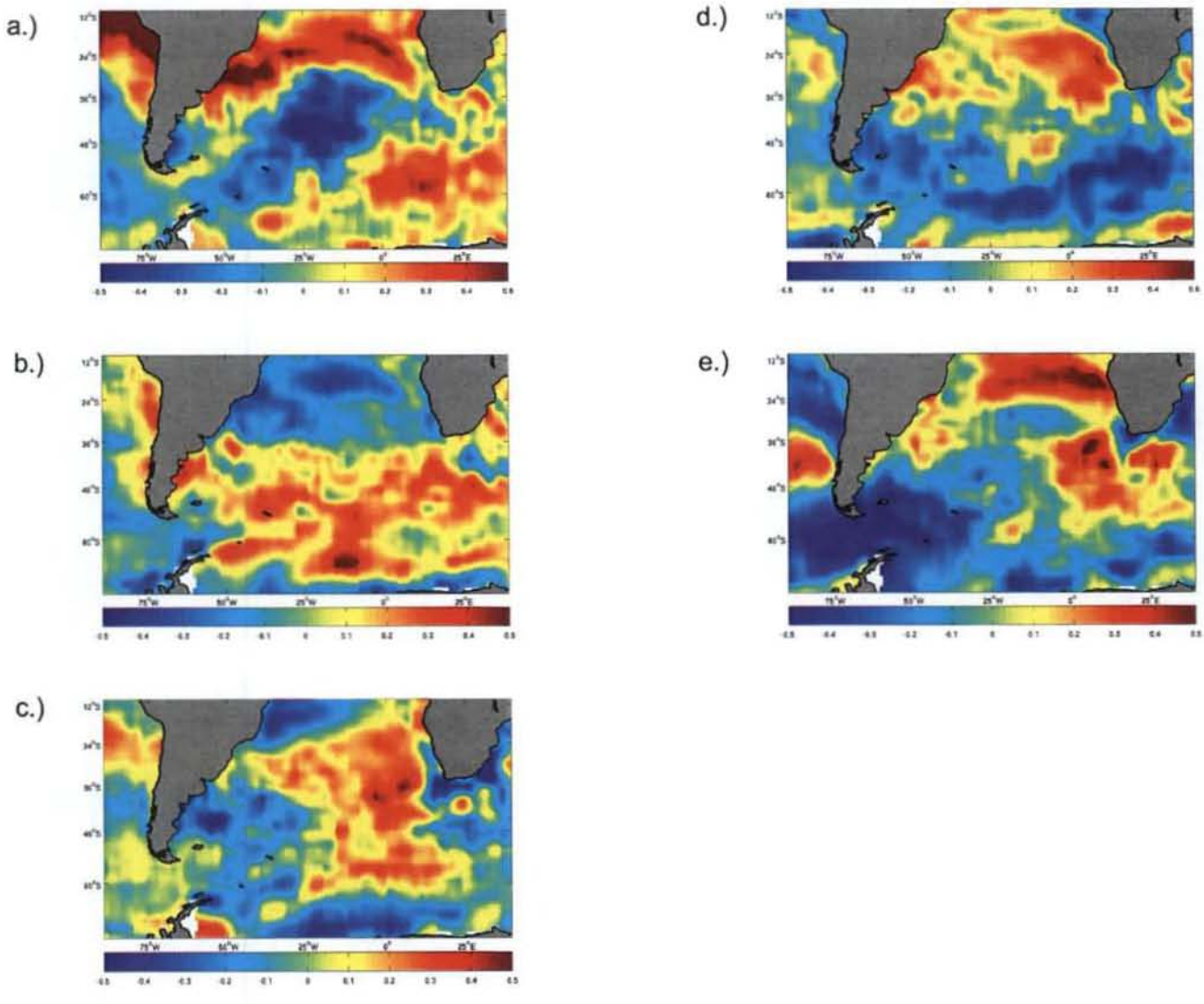

Figure 3.20: Spatial correlations between SWC rainfall in (a) May, (b) June, (c) July, (d) August, (e) September and sea surface temperature in January for the time period of 1982-2009. Correlation strength indicated by color shading ranging from -0.5 to 0.5.

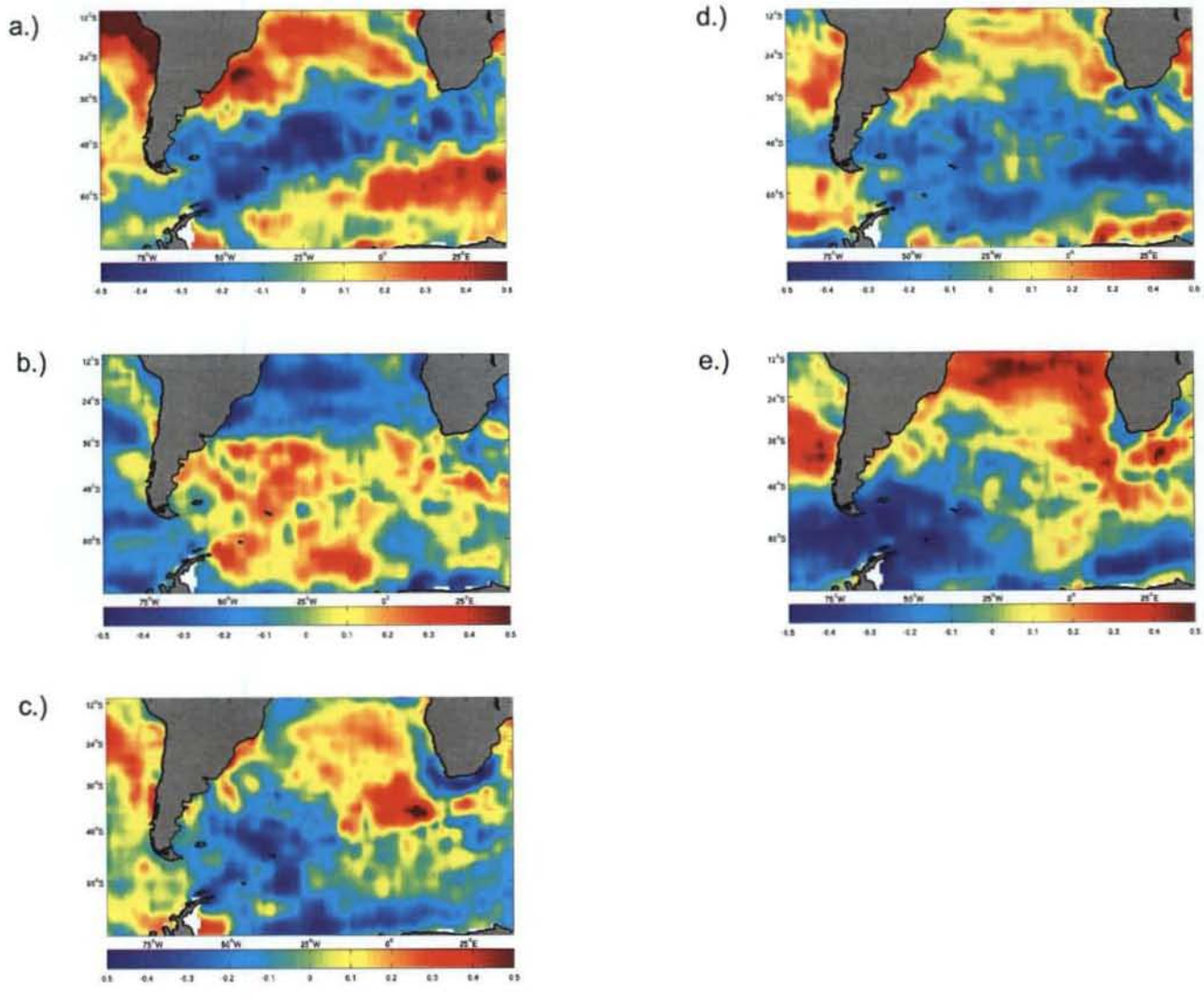

Figure 3.21: As for Figure 3.20 but with February sea surface temperature

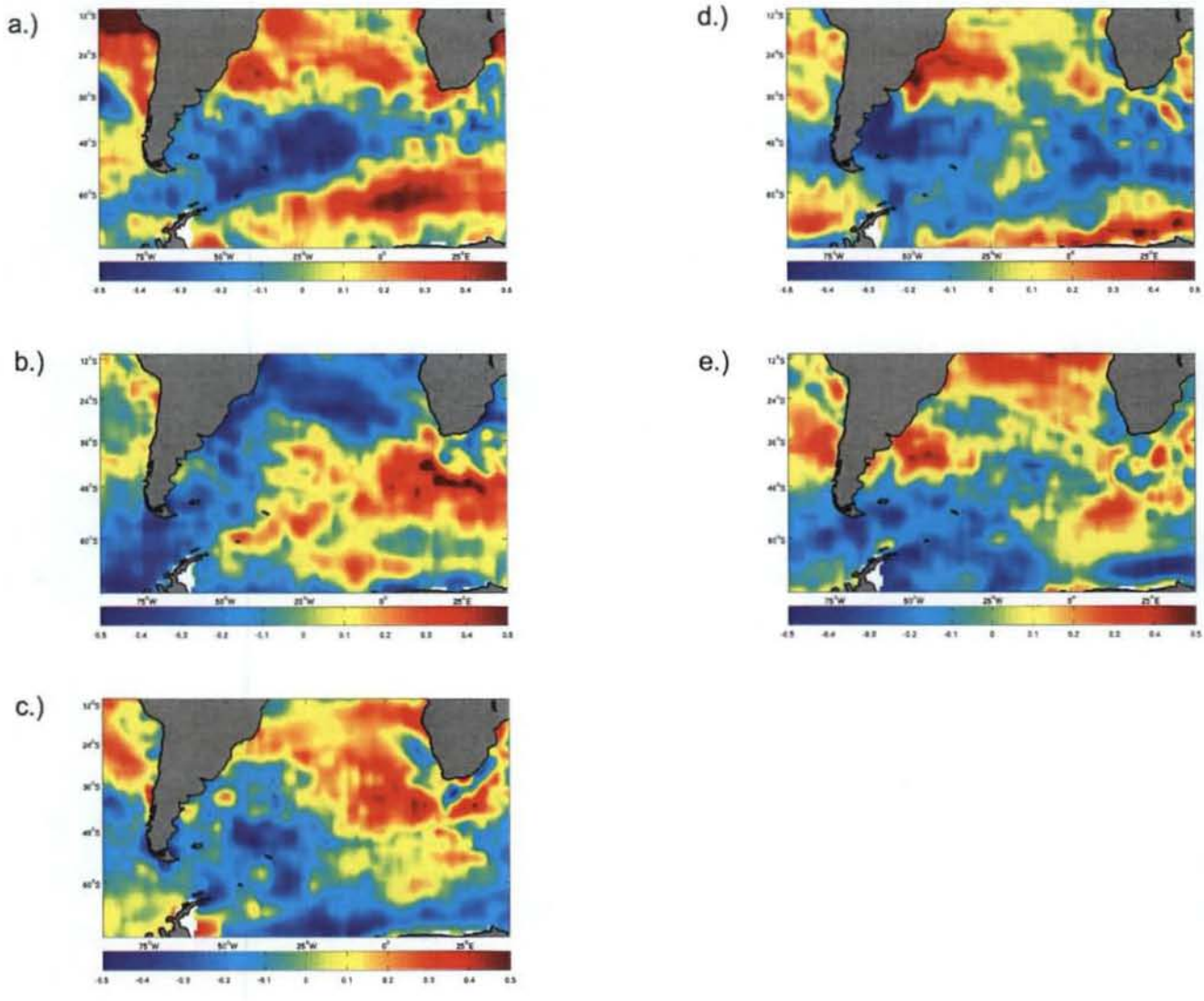

Figure 3.22: As for Figure 3.20 but with March sea surface temperature

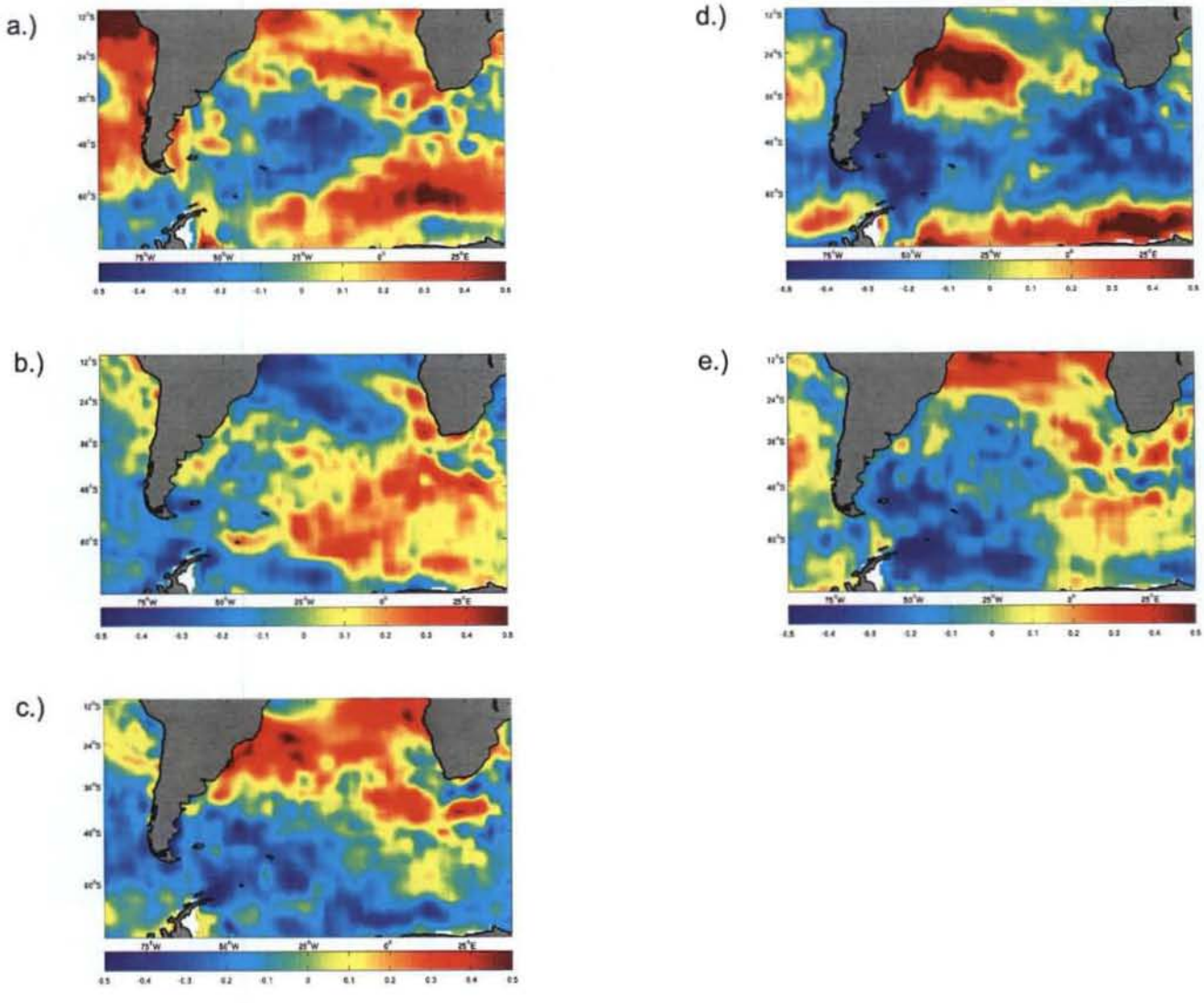

Figure 3.23: As for Figure 3.20 but with April sea surface temperature

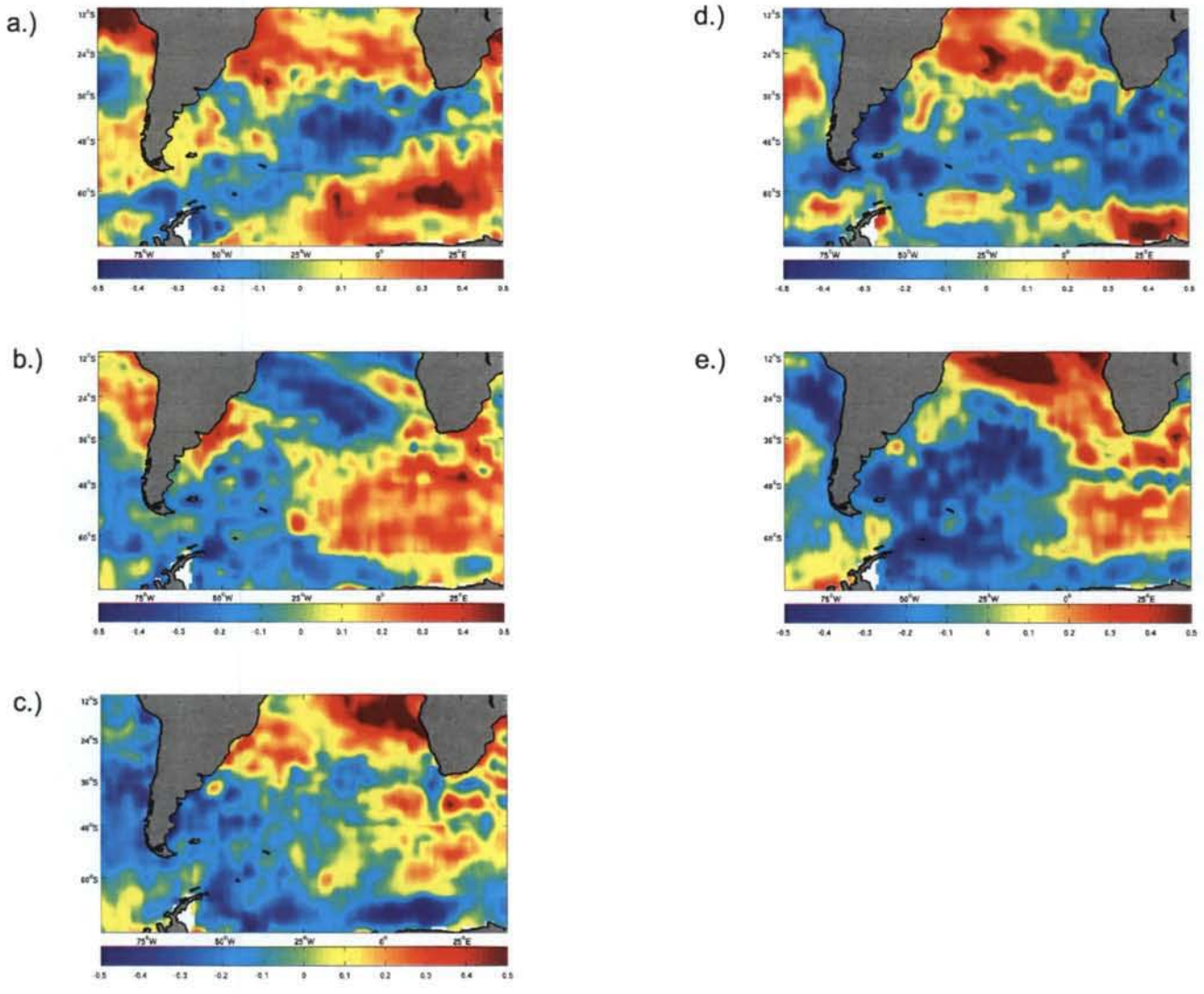

Figure 3.24: As for Figure 3.20 but with May sea surface temperature

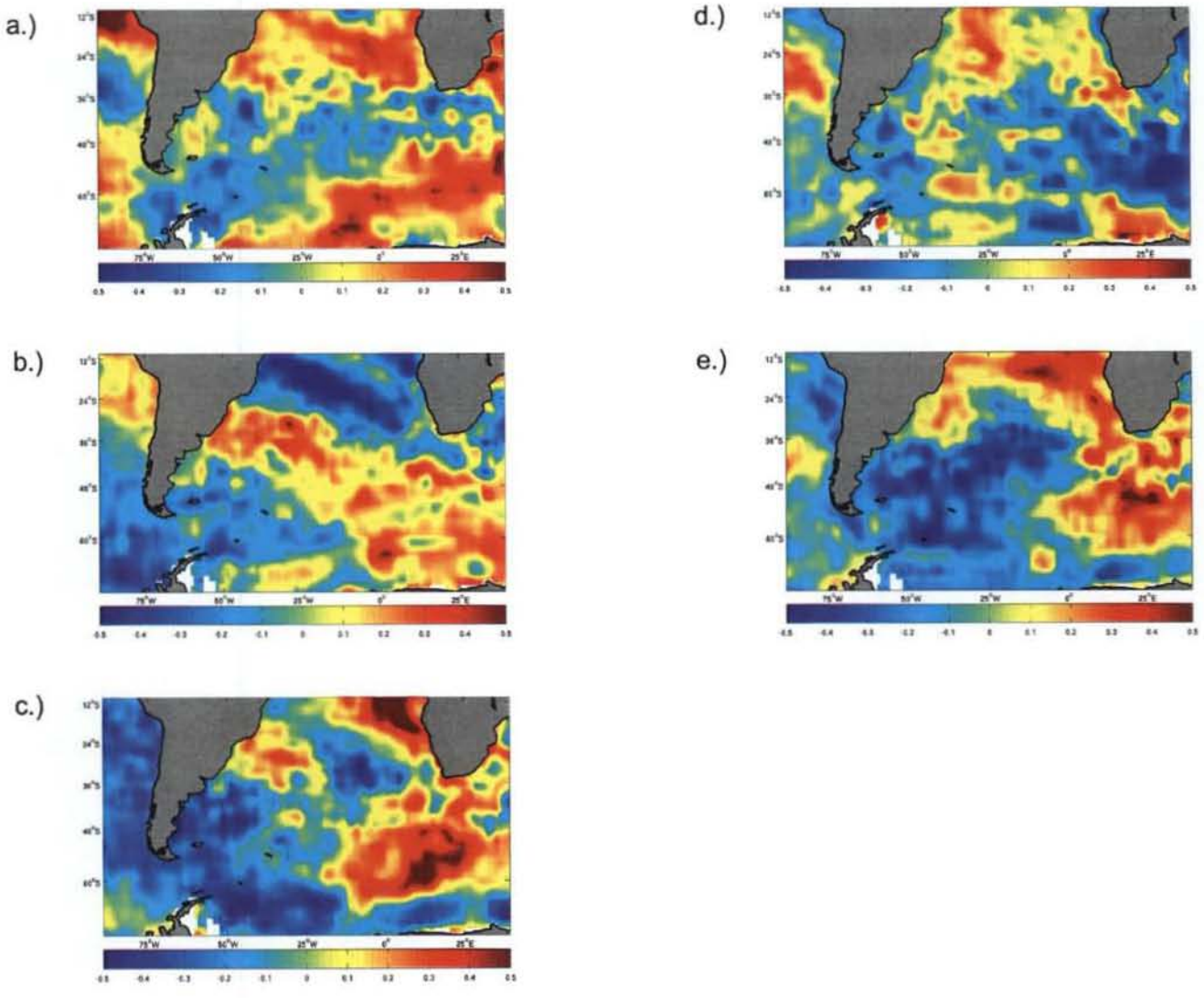

Figure 3.25: As for Figure 3.20 but with June sea surface temperature

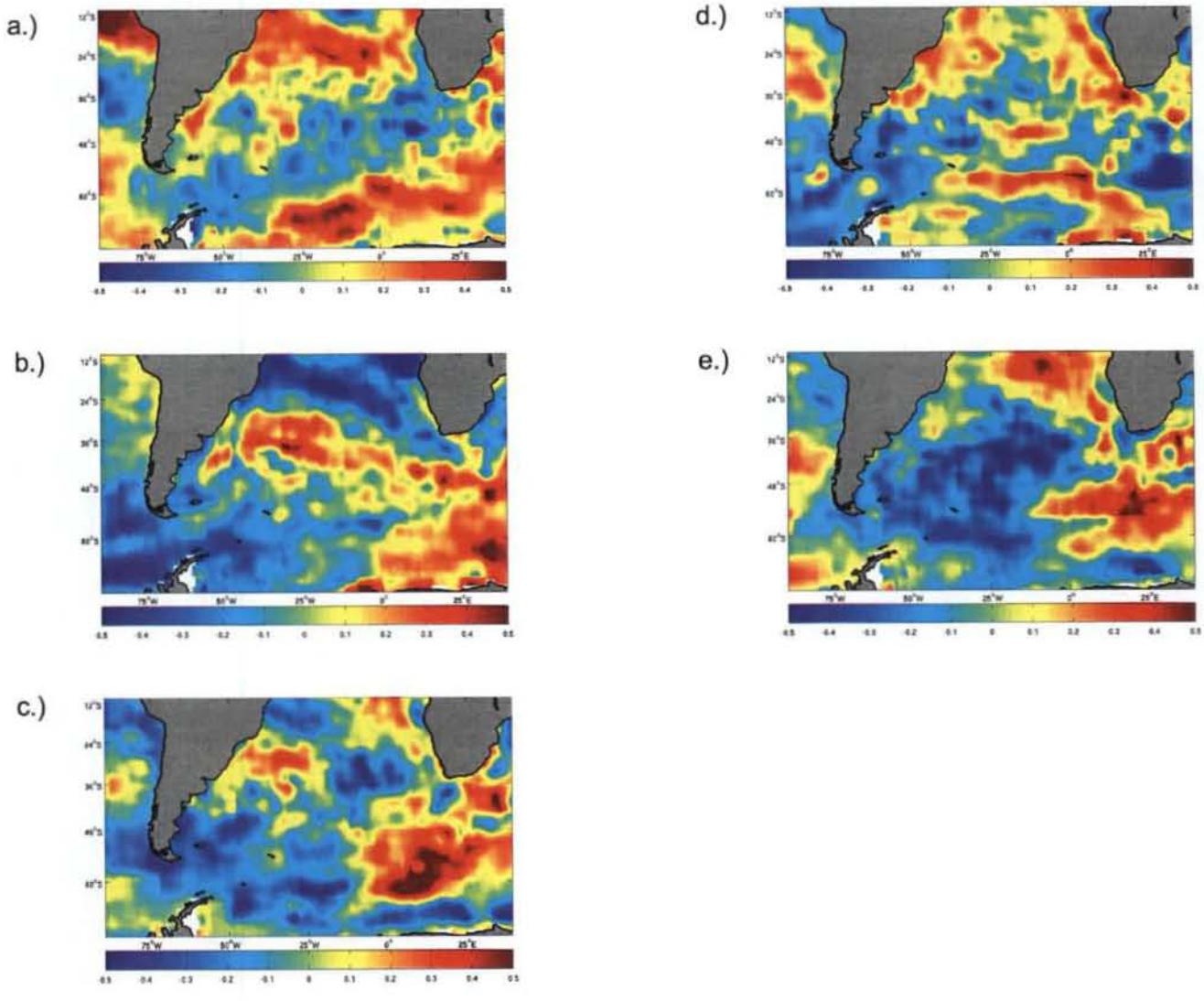

Figure 3.26: As for Figure 3.20 but with July sea surface temperature

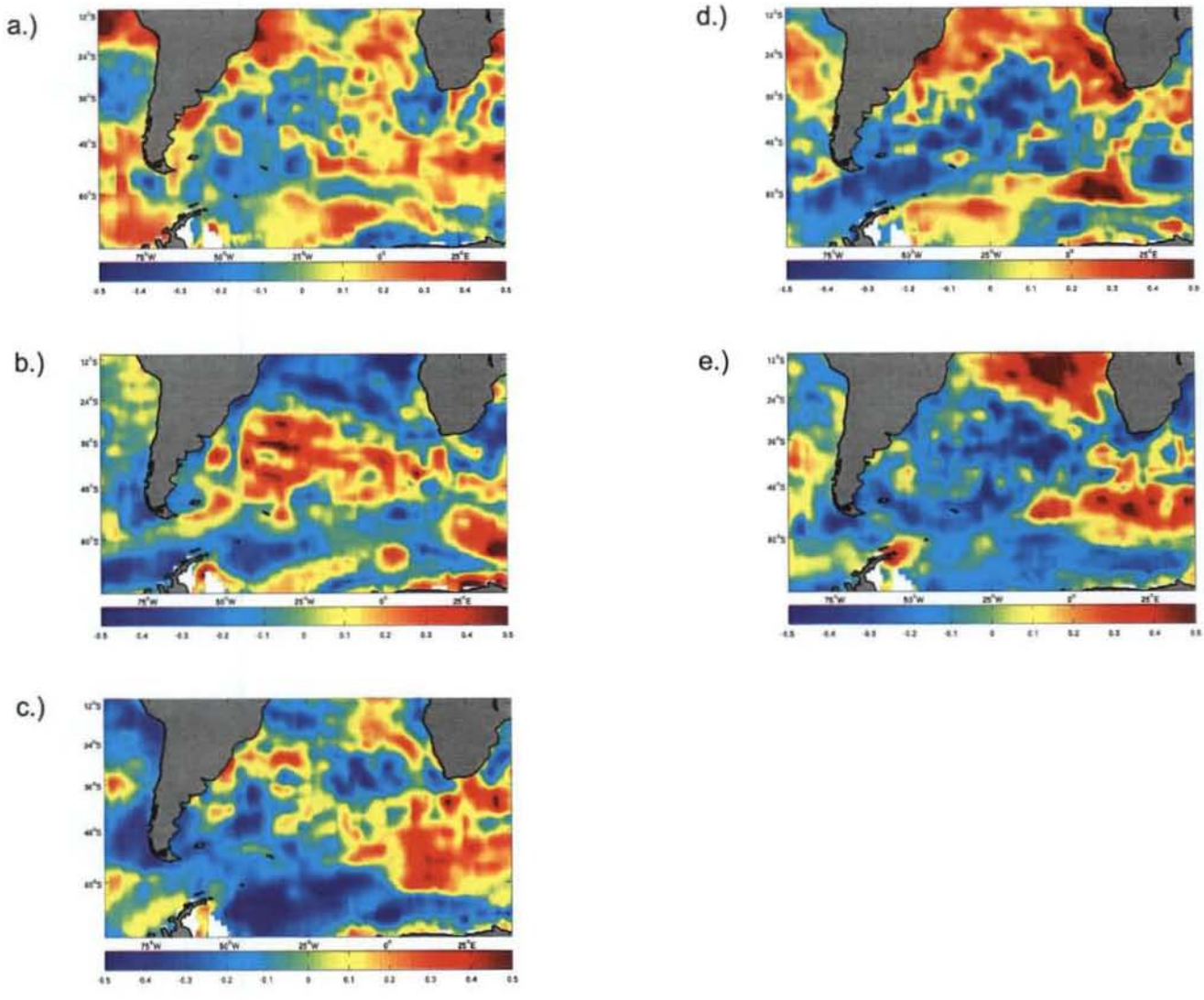

Figure 3.27: As for Figure 3.20 but with August sea surface temperature

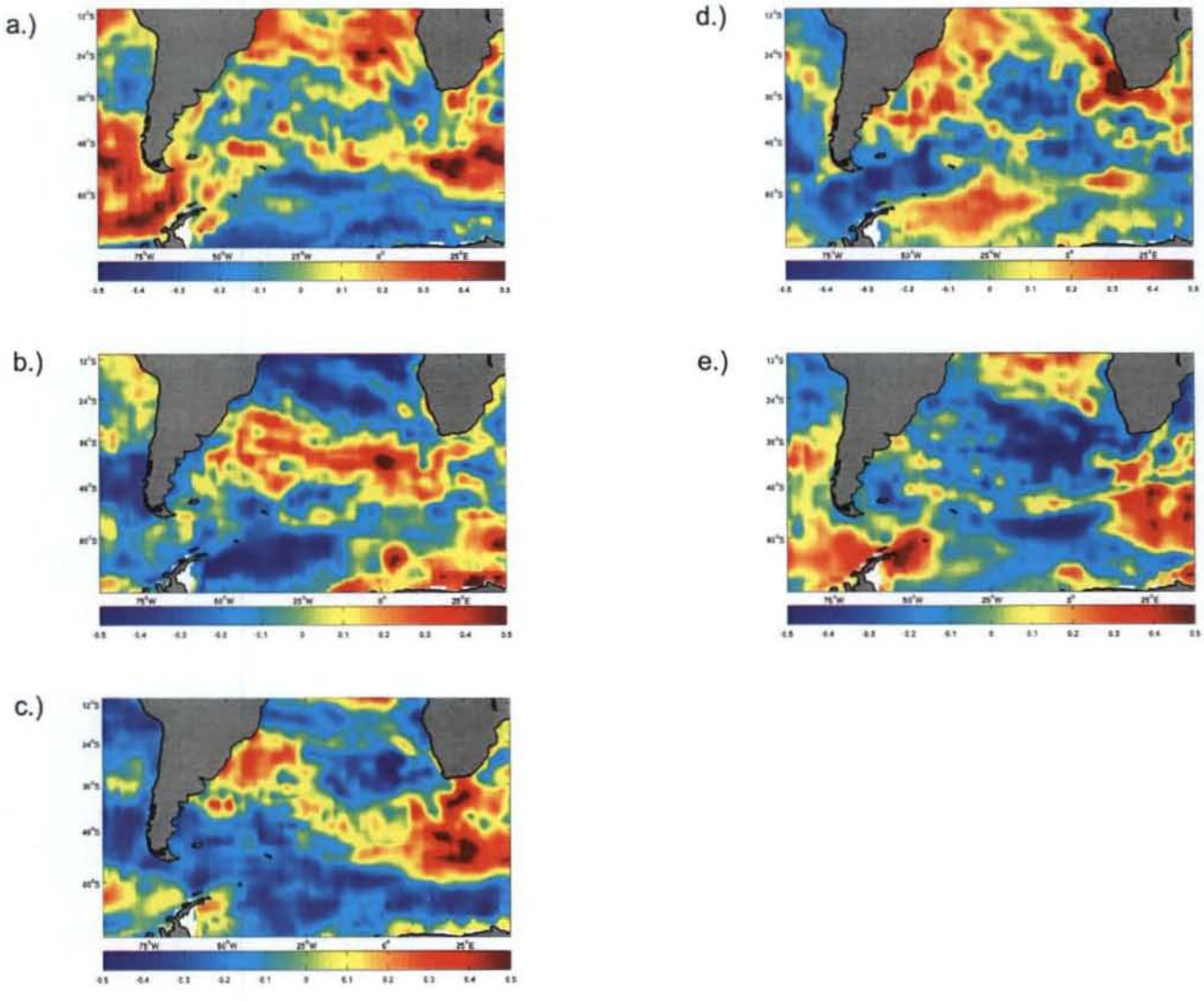

Figure 3.28: As for Figure 3.20 but with September sea surface temperature

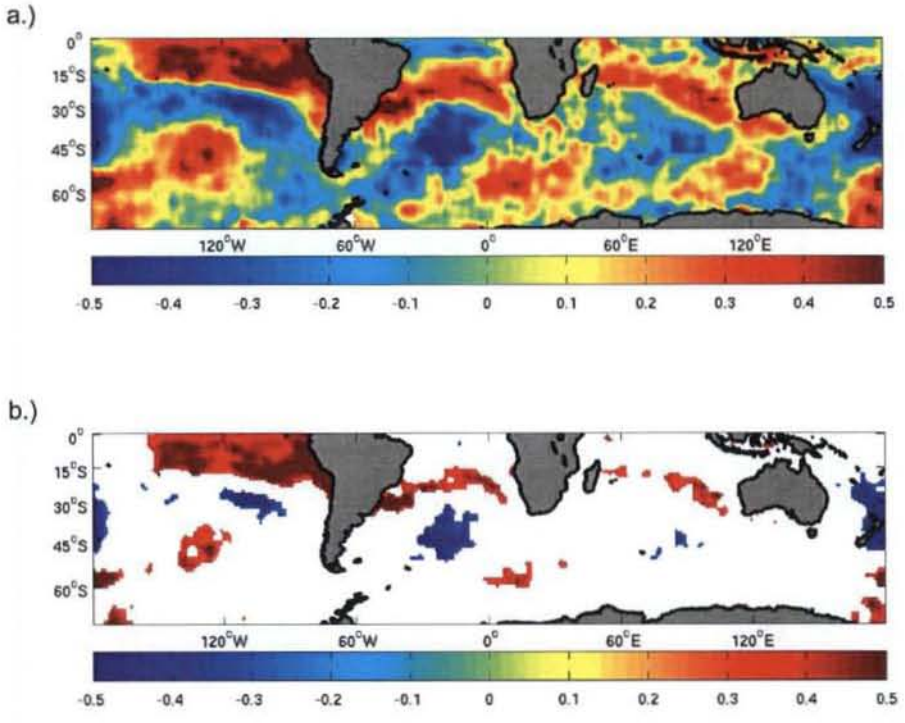

Figure 3.29: Spatial correlation (a) between May rainfall index for the SWC and sea surface temperature in January, and correlations statistically significant (b) above 95%

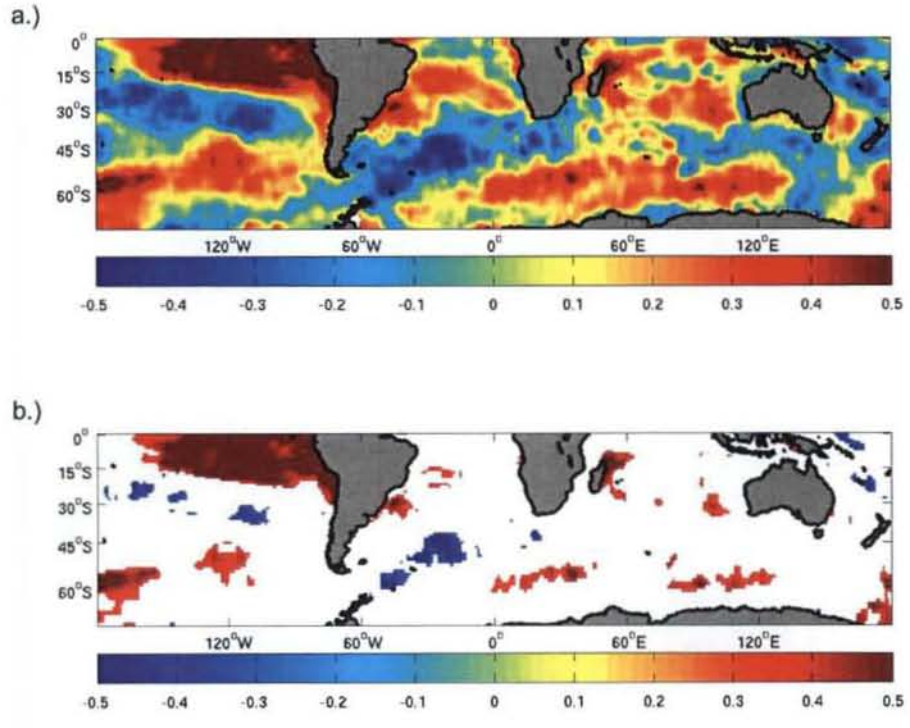

Figure 3.30: As for figure 3.29 but for February sea surface temperature

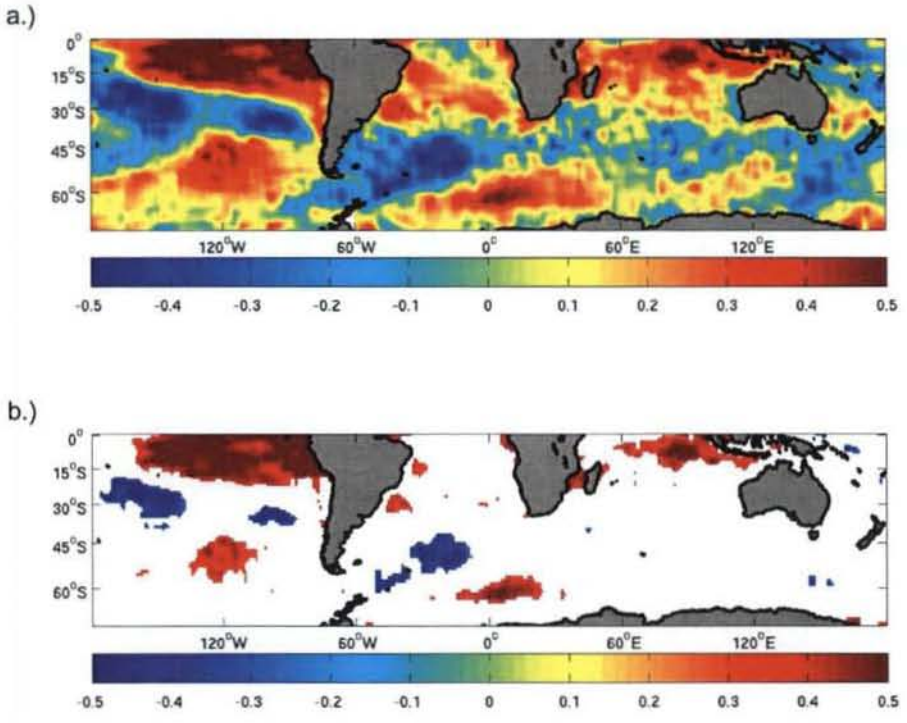

Figure 3.31: As for figure 3.29 but for March sea surface temperature

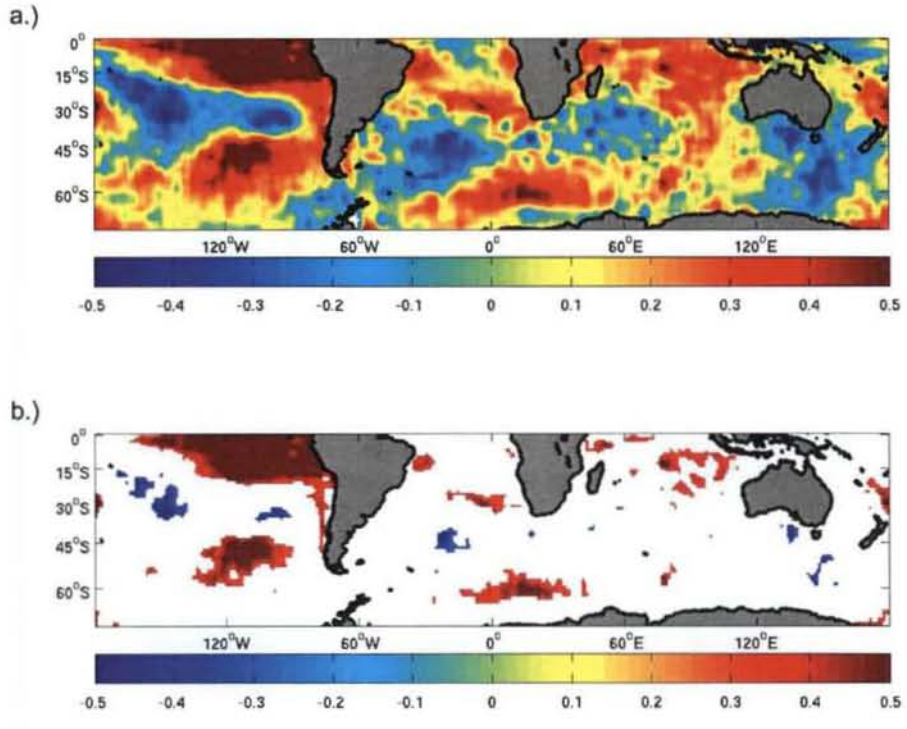

Figure 3.32: As for figure 3.29 but for April sea surface temperature

GM SAM Index(1982-2008)

a.) MJJ Rainfall

R Value

	No running mea	2 month	3 month	4 month
Jan	-0.16	-0.28	-0.36	-0.17
Feb	0.07	-0.03	-0.16	-0.26
Mar	-0.21	-0.08	-0.14	-0.23
Apr	**-0.38**	**-0.45**	-0.28	-0.31
May	-0.23	-0.40	**-0.44**	-0.33
Jun	0.11	-0.07	-0.25	-0.29
Jul	-0.32	-0.13	-0.20	-0.32

P Value

	No running mea	2 month	3 month	4 month
Jan	0.42	0.16	0.07	0.40
Feb	0.72	0.87	0.42	0.19
Mar	0.28	0.71	0.48	0.24
Apr	**0.05**	**0.02**	0.16	0.11
May	0.26	0.04	**0.02**	0.10
Jun	0.57	0.72	0.20	0.14
Jul	0.10	0.53	0.31	0.10

b.) JJA Rainfall

R Value

	No running mea	2 month	3 month	4 month
Jan	-0.18	-0.19	-0.25	-0.13
Feb	-0.13	-0.20	-0.21	-0.27
Mar	-0.17	-0.21	-0.26	-0.26
Apr	-0.31	-0.37	-0.36	**-0.39**
May	-0.31	**-0.42**	**-0.43**	**-0.43**
Jun	-0.07	-0.24	-0.37	-0.37
Jul	-0.31	-0.25	-0.33	**-0.41**
Aug	0.08	-0.16	-0.16	-0.27

P Value

	No running mea	2 month	3 month	4 month
Jan	0.38	0.34	0.20	0.52
Feb	0.52	0.31	0.29	0.18
Mar	0.39	0.30	0.19	0.19
Apr	0.12	0.06	0.07	**0.05**
May	0.11	**0.03**	**0.02**	**0.02**
Jun	0.73	0.23	0.06	0.06
Jul	0.11	0.22	0.09	**0.03**
Aug	0.69	0.44	0.41	0.17

c.) JAS Rainfall

R Value

	No running mea	2 month	3 month	4 month
Jan	-0.19	-0.10	-0.09	-0.12
Feb	**-0.39**	**-0.42**	-0.29	-0.25
Mar	-0.20	**-0.43**	**-0.45**	-0.34
Apr	-0.18	-0.28	**-0.48**	**-0.50**
May	-0.13	-0.20	-0.27	**-0.43**
Jun	0.17	0.02	-0.07	-0.13
Jul	-0.15	0.02	-0.05	-0.11
Aug	-0.13	-0.18	-0.05	-0.10
Sep	-0.04	-0.10	-0.16	-0.06

P Value

	No running mea	2 month	3 month	4 month
Jan	0.35	0.63	0.67	0.55
Feb	**0.04**	**0.03**	0.14	0.21
Mar	0.33	**0.03**	**0.02**	0.08
Apr	0.38	0.15	**0.01**	**0.01**
May	0.52	0.31	0.18	**0.02**
Jun	0.39	0.91	0.74	0.51
Jul	0.46	0.91	0.81	0.58
Aug	0.50	0.37	0.82	0.63
Sep	0.83	0.61	0.44	0.78

d.) MJJAS Rainfall

R Value

	No running mea	2 month	3 month	4 month
Jan	-0.23	-0.22	-0.28	-0.20
Feb	-0.19	-0.28	-0.27	-0.32
Mar	-0.25	-0.31	-0.37	-0.35
Apr	-0.35	**-0.46**	**-0.47**	**-0.50**
May	-0.21	-0.37	**-0.43**	**-0.46**
Jun	0.13	-0.05	-0.22	-0.28
Jul	-0.28	-0.09	-0.17	-0.28
Aug	-0.12	-0.26	-0.14	-0.20
Sep	-0.12	-0.15	-0.26	-0.16

P Value

	No running mea	2 month	3 month	4 month
Jan	0.25	0.27	0.16	0.33
Feb	0.34	0.15	0.17	0.11
Mar	0.21	0.12	0.06	0.08
Apr	0.07	**0.02**	**0.01**	**0.01**
May	0.29	0.06	**0.02**	**0.01**
Jun	0.52	0.80	0.27	0.16
Jul	0.15	0.65	0.40	0.15
Aug	0.54	0.19	0.50	0.31
Sep	0.55	0.47	0.20	0.43

700 EOF Index (1982-2008)

e.) MJJ Rainfall

R Value

	No running mea	2 month	3 month	4 month
Jan	-0.07	-0.23	-0.26	-0.14
Feb	-0.03	-0.07	-0.20	-0.23
Mar	-0.27	-0.18	-0.17	-0.26
Apr	-0.29	-0.37	-0.29	-0.27
May	-0.30	-0.37	**-0.38**	-0.35
Jun	-0.13	-0.26	-0.33	-0.34
Jul	-0.36	-0.29	-0.35	**-0.39**

P Value

	No running mea	2 month	3 month	4 month
Jan	0.74	0.24	0.19	0.50
Feb	0.87	0.74	0.32	0.25
Mar	0.18	0.38	0.40	0.19
Apr	0.14	0.06	0.14	0.17
May	0.13	0.06	**0.05**	0.07
Jun	0.52	0.18	0.10	0.08
Jul	0.07	0.14	0.08	**0.05**

f.) JJA Rainfall

R Value

	No running mea	2 month	3 month	4 month
Jan	-0.01	-0.04	-0.06	-0.02
Feb	-0.11	-0.08	-0.08	-0.09
Mar	-0.36	-0.29	-0.22	-0.18
Apr	-0.36	**-0.48**	**-0.42**	-0.35
May	-0.25	-0.36	**-0.41**	**-0.40**
Jun	-0.18	-0.26	-0.35	**-0.38**
Jul	**-0.42**	-0.36	**-0.37**	**-0.43**
Aug	0.14	-0.27	**-0.28**	-0.32

P Value

	No running mea	2 month	3 month	4 month
Jan	0.98	0.83	0.76	0.94
Feb	0.57	0.69	0.69	0.66
Mar	0.06	0.14	0.26	0.38
Apr	0.06	**0.01**	**0.03**	0.08
May	0.20	0.06	**0.03**	**0.04**
Jun	0.36	0.19	0.07	**0.05**
Jul	**0.03**	0.07	**0.05**	**0.03**
Aug	0.49	0.17	0.16	0.10

g.) JAS Rainfall

R Value

	No running mea	2 month	3 month	4 month
Jan	-0.09	0.04	-0.01	-0.04
Feb	-0.19	-0.19	-0.05	-0.07
Mar	-0.29	-0.31	-0.28	-0.13
Apr	-0.29	**-0.38**	**-0.40**	-0.36
May	-0.14	-0.24	-0.29	-0.33
Jun	0.22	0.03	-0.07	-0.13
Jul	-0.18	0.00	-0.06	-0.13
Aug	-0.08	-0.19	-0.03	-0.08
Sep	0.15	0.05	-0.09	0.03

P Value

	No running mea	2 month	3 month	4 month
Jan	0.67	0.85	0.97	0.83
Feb	0.33	0.34	0.81	0.74
Mar	0.14	0.12	0.16	0.53
Apr	0.14	**0.05**	**0.04**	0.06
May	0.49	0.22	0.15	0.10
Jun	0.27	0.88	0.73	0.51
Jul	0.37	0.99	0.76	0.53
Aug	0.70	0.34	0.90	0.69
Sep	0.46	0.79	0.67	0.88

h.) MJJAS Rainfall

R Value

	No running mea	2 month	3 month	4 month
Jan	-0.08	-0.11	-0.16	-0.10
Feb	-0.19	-0.18	-0.16	-0.19
Mar	-0.30	-0.31	-0.28	-0.23
Apr	-0.34	**-0.42**	**-0.43**	**-0.38**
May	-0.27	-0.36	**-0.39**	**-0.41**
Jun	-0.05	-0.20	-0.29	-0.32
Jul	-0.32	-0.23	-0.29	-0.35
Aug	0.03	-0.25	-0.20	-0.27
Sep	-0.04	0.00	-0.23	-0.19

P Value

	No running mea	2 month	3 month	4 month
Jan	0.69	0.60	0.42	0.60
Feb	0.35	0.37	0.43	0.33
Mar	0.12	0.12	0.16	0.25
Apr	0.08	**0.03**	**0.03**	**0.05**
May	0.18	0.06	**0.04**	**0.03**
Jun	0.79	0.32	0.14	0.11
Jul	0.10	0.25	0.15	0.08
Aug	0.86	0.21	0.32	0.18
Sep	0.86	0.99	0.26	0.35

GM SAM Index (1959-1981)

i.) MJJ Rainfall

R Value

	No running mea	2 month	3 month	4 month
Jan	-0.11	-0.19	-0.15	-0.03
Feb	0.25	0.10	0.00	0.00
Mar	-0.02	0.16	0.07	-0.01
Apr	0.11	0.04	0.17	0.09
May	-0.07	0.03	0.01	0.13
Jun	-0.39	-0.39	-0.26	-0.18
Jul	-0.13	-0.29	-0.31	-0.25

P Value

	No running mea	2 month	3 month	4 month
Jan	0.62	0.38	0.49	0.90
Feb	0.24	0.64	1.00	0.99
Mar	0.93	0.47	0.74	0.98
Apr	0.63	0.84	0.45	0.67
May	0.76	0.90	0.97	0.55
Jun	0.07	0.06	0.23	0.40
Jul	0.55	0.18	0.14	0.25

j.) JJA Rainfall

R Value

	No running mea	2 month	3 month	4 month
Jan	0.06	0.10	0.09	0.20
Feb	0.36	0.26	0.25	0.22
Mar	0.09	0.29	0.25	0.24
Apr	0.33	0.23	0.35	0.30
May	0.09	0.30	0.25	0.35
Jun	**-0.49**	-0.36	-0.09	-0.01
Jul	-0.19	-0.38	-0.33	-0.18
Aug	-0.29	-0.30	**-0.44**	**-0.41**

P Value

	No running mea	2 month	3 month	4 month
Jan	0.79	0.65	0.67	0.35
Feb	0.09	0.22	0.25	0.32
Mar	0.68	0.18	0.26	0.28
Apr	0.13	0.29	0.10	0.16
May	0.67	0.17	0.25	0.10
Jun	**0.02**	0.10	0.67	0.95
Jul	0.37	0.07	0.12	0.42
Aug	0.18	0.16	**0.04**	**0.05**

k.) JAS Rainfall

R Value

	No running mea	2 month	3 month	4 month
Jan	0.24	0.23	0.18	0.21
Feb	0.36	0.36	0.34	0.28
Mar	-0.03	0.22	0.27	0.27
Apr	0.12	0.04	0.22	0.27
May	0.02	0.10	0.05	0.21
Jun	**-0.42**	-0.35	-0.22	-0.16
Jul	-0.24	-0.37	-0.36	-0.29
Aug	-0.26	-0.31	**-0.42**	**-0.41**
Sep	0.11	-0.15	-0.25	-0.39

P Value

	No running mea	2 month	3 month	4 month
Jan	0.28	0.28	0.42	0.35
Feb	0.09	0.09	0.11	0.20
Mar	0.89	0.31	0.21	0.21
Apr	0.60	0.85	0.30	0.21
May	0.92	0.66	0.83	0.32
Jun	**0.05**	0.10	0.31	0.46
Jul	0.27	0.08	0.09	0.18
Aug	0.22	0.15	**0.05**	**0.05**
Sep	0.62	0.50	0.25	0.06

l.) MJJAS Rainfall

R Value

	No running mea	2 month	3 month	4 month
Jan	0.07	0.04	0.04	0.13
Feb	0.34	0.26	0.20	0.17
Mar	0.00	0.23	0.20	0.17
Apr	0.14	0.08	0.24	0.22
May	0.08	0.16	0.11	0.25
Jun	**-0.48**	-0.36	-0.21	-0.14
Jul	-0.23	-0.40	-0.35	-0.27
Aug	-0.29	-0.32	**-0.45**	**-0.42**
Sep	**0.42**	0.00	-0.13	-0.31

P Value

	No running mea	2 month	3 month	4 month
Jan	0.75	0.85	0.84	0.55
Feb	0.11	0.23	0.36	0.43
Mar	0.99	0.30	0.35	0.45
Apr	0.51	0.73	0.28	0.32
May	0.72	0.47	0.63	0.26
Jun	**0.02**	0.09	0.33	0.53
Jul	0.30	0.06	0.10	0.21
Aug	0.18	0.14	**0.03**	**0.04**
Sep	**0.05**	0.99	0.55	0.15

Table 3.2: Correlations between the GM SAM Index(1982-2008) (a-d), 700hPa EOF SAM Index(1982-2008) (e-h), GM SAM Index(1940-1981) (I-l) and SWC rainfall in early (a,e,I), mid (b,f,j), late (c,g,k), entire (d,h,l) winter rainfall. Values highlighted in bold indicate statistical significance at the 0.05 level.

GM SAM Index(1982-2008)

a.)

May Rainfall

R Value

	No running mea	2 month	3 month	4 month
Jan	-0.22	-0.31	-0.34	-0.27
Feb	0.00	-0.13	-0.23	-0.28
Mar	-0.26	-0.16	-0.24	-0.31
Apr	-0.02	-0.21	-0.15	-0.23
May	0.05	0.02	-0.11	-0.09

P Value

	No running mea	2 month	3 month	4 month
Jan	0.27	0.12	0.08	0.18
Feb	0.99	0.53	0.25	0.16
Mar	0.20	0.43	0.23	0.12
Apr	0.92	0.30	0.45	0.26
May	0.81	0.92	0.58	0.64

b.)

June Rainfall

R Value

	No running mea	2 month	3 month	4 month
Jan	0.04	0.00	-0.11	0.05
Feb	0.24	0.22	0.13	0.02
Mar	0.04	0.21	0.20	0.14
Apr	**-0.38**	-0.27	-0.03	-0.01
May	-0.25	**-0.42**	-0.32	-0.14
Jun	-0.28	-0.33	**-0.48**	-0.37

P Value

	No running mea	2 month	3 month	4 month
Jan	0.83	0.98	0.58	0.82
Feb	0.22	0.28	0.51	0.92
Mar	0.84	0.28	0.31	0.50
Apr	**0.05**	0.18	0.89	0.98
May	0.22	**0.03**	0.10	0.48
Jun	0.16	0.09	**0.01**	0.06

c.)

July Rainfall

R Value

	No running mea	2 month	3 month	4 month
Jan	-0.12	-0.18	-0.17	-0.09
Feb	-0.13	-0.17	-0.21	-0.20
Mar	-0.17	-0.21	-0.24	-0.26
Apr	-0.23	-0.30	-0.31	-0.32
May	-0.17	-0.26	-0.30	-0.33
Jun	0.21	0.02	-0.09	-0.14
Jul	-0.21	0.01	-0.08	-0.16

P Value

	No running mea	2 month	3 month	4 month
Jan	0.55	0.37	0.38	0.67
Feb	0.51	0.39	0.30	0.31
Mar	0.39	0.29	0.24	0.19
Apr	0.26	0.12	0.11	0.10
May	0.40	0.19	0.12	0.10
Jun	0.29	0.91	0.65	0.48
Jul	0.29	0.96	0.70	0.44

d.)

August Rainfall

R Value

	No running mea	2 month	3 month	4 month
Jan	-0.27	-0.15	-0.14	-0.21
Feb	**-0.43**	**-0.49**	-0.35	-0.31
Mar	-0.19	**-0.45**	**-0.51**	**-0.40**
Apr	0.17	-0.01	-0.30	**-0.38**
May	-0.09	0.05	-0.06	-0.28
Jun	-0.03	-0.08	0.02	-0.06
Jul	0.03	0.00	-0.05	0.03
Aug	0.15	0.11	0.07	0.02

P Value

	No running mea	2 month	3 month	4 month
Jan	0.18	0.44	0.48	0.28
Feb	**0.03**	**0.01**	0.07	0.11
Mar	0.34	**0.02**	**0.01**	**0.04**
Apr	0.39	0.97	0.13	**0.05**
May	0.66	0.82	0.77	0.16
Jun	0.88	0.71	0.92	0.77
Jul	0.89	0.99	0.82	0.89
Aug	0.46	0.58	0.72	0.94

e.)

September Rainfall

R Value

	No running mea	2 month	3 month	4 month
Jan	0.02	0.17	0.18	0.07
Feb	-0.23	-0.17	-0.01	0.04
Mar	0.00	-0.18	-0.15	-0.01
Apr	-0.26	-0.20	-0.31	-0.26
May	0.03	-0.14	-0.12	-0.23
Jun	0.12	0.09	-0.05	-0.04
Jul	-0.07	0.04	0.04	-0.06
Aug	-0.34	-0.26	-0.14	-0.10
Sep	**-0.42**	**-0.46**	**-0.41**	-0.29

P Value

	No running mea	2 month	3 month	4 month
Jan	0.91	0.39	0.37	0.74
Feb	0.24	0.38	0.97	0.85
Mar	0.99	0.36	0.46	0.97
Apr	0.20	0.31	0.12	0.19
May	0.89	0.48	0.55	0.26
Jun	0.55	0.65	0.82	0.85
Jul	0.73	0.85	0.84	0.75
Aug	0.08	0.20	0.50	0.64
Sep	**0.03**	**0.02**	**0.03**	0.14

700 EOF Index (1982-2008)

f.)

May Rainfall

R Value

	No running mea	2 month	3 month	4 month
Jan	-0.32	**-0.39**	**-0.42**	-0.32
Feb	-0.06	-0.25	-0.33	-0.36
Mar	-0.11	-0.11	-0.25	-0.33
Apr	0.04	-0.04	-0.07	-0.20
May	-0.11	-0.07	-0.09	-0.10

P Value

	No running mea	2 month	3 month	4 month
Jan	0.10	**0.05**	**0.03**	0.10
Feb	0.77	0.21	0.09	0.06
Mar	0.59	0.60	0.22	0.09
Apr	0.86	0.83	0.74	0.32
May	0.59	0.74	0.66	0.62

g.)

June Rainfall

R Value

	No running mea	2 month	3 month	4 month
Jan	0.26	0.08	0.06	0.15
Feb	-0.01	0.16	0.06	0.05
Mar	-0.04	-0.03	0.11	0.04
Apr	-0.24	-0.19	-0.15	-0.01
May	-0.20	-0.27	-0.23	-0.21
Jun	**-0.54**	**-0.43**	**-0.45**	**-0.39**

P Value

	No running mea	2 month	3 month	4 month
Jan	0.19	0.71	0.76	0.47
Feb	0.97	0.41	0.78	0.81
Mar	0.84	0.88	0.58	0.84
Apr	0.22	0.33	0.46	0.98
May	0.31	0.17	0.25	0.30
Jun	**0.00**	**0.03**	**0.02**	**0.05**

h.)

July Rainfall

R Value

	No running mea	2 month	3 month	4 month
Jan	-0.09	-0.12	-0.13	-0.09
Feb	0.01	-0.06	-0.09	-0.10
Mar	-0.31	-0.18	-0.18	-0.18
Apr	-0.28	**-0.39**	-0.29	-0.27
May	-0.20	-0.28	-0.33	-0.29
Jun	0.26	0.01	-0.08	-0.15
Jul	-0.25	-0.02	-0.10	-0.16

P Value

	No running mea	2 month	3 month	4 month
Jan	0.64	0.55	0.53	0.65
Feb	0.97	0.78	0.64	0.61
Mar	0.11	0.38	0.37	0.38
Apr	0.16	**0.05**	0.15	0.17
May	0.32	0.15	0.10	0.15
Jun	0.19	0.95	0.68	0.46
Jul	0.21	0.92	0.61	0.42

i.)

August Rainfall

R Value

	No running mea	2 month	3 month	4 month
Jan	-0.25	-0.04	-0.05	-0.12
Feb	-0.23	-0.32	-0.12	-0.12
Mar	-0.29	-0.33	**-0.38**	-0.19
Apr	-0.06	-0.22	-0.30	-0.35
May	0.01	-0.02	-0.11	-0.18
Jun	0.04	0.03	0.01	-0.07
Jul	-0.07	-0.02	-0.01	-0.02
Aug	0.04	-0.03	-0.01	0.00

P Value

	No running mea	2 month	3 month	4 month
Jan	0.21	0.85	0.80	0.57
Feb	0.25	0.10	0.55	0.57
Mar	0.14	0.09	**0.05**	0.33
Apr	0.78	0.27	0.13	0.07
May	0.95	0.93	0.59	0.37
Jun	0.85	0.89	0.98	0.74
Jul	0.74	0.91	0.96	0.91
Aug	0.85	0.87	0.98	1.00

j.)

September Rainfall

R Value

	No running mea	2 month	3 month	4 month
Jan	0.18	0.26	0.19	0.13
Feb	-0.18	-0.01	0.13	0.10
Mar	0.07	-0.09	0.02	0.14
Apr	-0.20	-0.09	-0.18	-0.06
May	-0.05	-0.14	-0.08	-0.14
Jun	0.10	0.02	-0.05	-0.02
Jul	0.00	0.05	0.01	-0.04
Aug	-0.20	-0.11	-0.03	-0.04
Sep	-0.27	-0.30	-0.23	-0.12

P Value

	No running mea	2 month	3 month	4 month
Jan	0.37	0.19	0.34	0.51
Feb	0.36	0.96	0.50	0.62
Mar	0.71	0.66	0.91	0.47
Apr	0.31	0.64	0.38	0.75
May	0.79	0.50	0.68	0.48
Jun	0.61	0.92	0.80	0.91
Jul	0.99	0.80	0.95	0.85
Aug	0.33	0.59	0.90	0.83
Sep	0.18	0.12	0.26	0.55

GM SAM Index (1959-1981)

k.)

May Rainfall

R Value

	No running mea	2 month	3 month	4 month
Jan	-0.05	-0.21	-0.21	-0.20
Feb	0.01	-0.02	-0.14	-0.15
Mar	-0.09	-0.04	-0.05	-0.14
Apr	-0.22	-0.18	-0.11	-0.11
May	-0.24	-0.33	-0.27	-0.18

P Value

	No running mea	2 month	3 month	4 month
Jan	0.82	0.33	0.33	0.35
Feb	0.97	0.92	0.54	0.51
Mar	0.68	0.85	0.81	0.52
Apr	0.31	0.42	0.61	0.62
May	0.26	0.13	0.21	0.40

l.)

June Rainfall

R Value

	No running mea	2 month	3 month	4 month
Jan	-0.11	0.00	0.07	0.19
Feb	0.18	0.06	0.09	0.12
Mar	0.12	0.19	0.10	0.12
Apr	0.33	0.25	0.27	0.18
May	0.34	**0.47**	0.38	0.36
Jun	-0.33	-0.04	0.17	0.18

P Value

	No running mea	2 month	3 month	4 month
Jan	0.63	0.99	0.77	0.40
Feb	0.40	0.78	0.68	0.58
Mar	0.58	0.39	0.66	0.60
Apr	0.13	0.25	0.22	0.42
May	0.11	**0.02**	0.07	0.09
Jun	0.12	0.87	0.43	0.42

m.)

July Rainfall

R Value

	No running mea	2 month	3 month	4 month
Jan	-0.02	-0.13	-0.14	-0.06
Feb	0.26	0.16	0.05	0.01
Mar	-0.10	0.12	0.09	0.01
Apr	0.05	-0.04	0.12	0.09
May	-0.31	-0.18	-0.17	0.01
Jun	-0.31	**-0.50**	-0.39	-0.31
Jul	-0.10	-0.23	-0.36	-0.32

P Value

	No running mea	2 month	3 month	4 month
Jan	0.93	0.57	0.52	0.79
Feb	0.23	0.47	0.83	0.97
Mar	0.67	0.58	0.69	0.97
Apr	0.81	0.87	0.59	0.68
May	0.15	0.41	0.43	0.96
Jun	0.15	**0.01**	0.07	0.16
Jul	0.65	0.30	0.09	0.14

n.)

August Rainfall

R Value

	No running mea	2 month	3 month	4 month
Jan	0.29	0.35	0.25	0.24
Feb	0.28	0.34	0.37	0.29
Mar	0.12	0.25	0.31	0.35
Apr	0.21	0.19	0.28	0.33
May	0.03	0.17	0.19	0.27
Jun	-0.30	-0.24	-0.07	0.02
Jul	-0.33	-0.37	-0.35	-0.24
Aug	**-0.49**	**-0.51**	**-0.53**	**-0.52**

P Value

	No running mea	2 month	3 month	4 month
Jan	0.18	0.11	0.25	0.27
Feb	0.20	0.12	0.08	0.18
Mar	0.57	0.25	0.14	0.11
Apr	0.34	0.38	0.20	0.12
May	0.87	0.44	0.40	0.22
Jun	0.17	0.28	0.76	0.93
Jul	0.12	0.08	0.10	0.26
Aug	**0.02**	**0.01**	**0.01**	**0.01**

o.)

September Rainfall

R Value

	No running mea	2 month	3 month	4 month
Jan	0.20	0.28	0.31	0.26
Feb	0.10	0.17	0.23	0.26
Mar	-0.14	-0.01	0.08	0.15
Apr	-0.12	-0.16	-0.05	0.03
May	**0.53**	0.29	0.11	0.12
Jun	-0.15	0.27	0.15	0.03
Jul	0.08	-0.03	0.21	0.15
Aug	0.22	0.19	0.09	0.27
Sep	-0.03	0.16	0.16	0.08

P Value

	No running mea	2 month	3 month	4 month
Jan	0.37	0.20	0.15	0.23
Feb	0.66	0.44	0.28	0.23
Mar	0.52	0.96	0.73	0.51
Apr	0.57	0.47	0.81	0.89
May	**0.01**	0.18	0.62	0.57
Jun	0.51	0.21	0.49	0.91
Jul	0.72	0.90	0.34	0.50
Aug	0.32	0.40	0.68	0.21
Sep	0.89	0.48	0.45	0.71

Table 3.3: Correlations between the GM SAM Index(1982-2008) (a-e), 700hPa EOF SAM Index(1982-2008) (f-j), GM SAM Index(1940-1981) (k-o) and SWC rainfall in May (a,f,k), June (b,g,l), July (c,h,m), June (d,i,n), September (e,j,o) winter rainfall. Values highlighted in bold indicate statistical significance at the 0.05 level.

Nino3 Correlations - 0 Year Lag

a.)

		MJJ Rain						
		Jan	Feb	Mar	Apr	May	Jun	Jul
1940-1981	R Value	-0.07	-0.08	0.12	-0.07	0.01	0.12	0.17
	P Value	0.67	0.62	0.44	0.66	0.94	0.43	0.29
1982-2009	R Value	0.24	0.30	0.31	**0.41**	**0.43**	0.36	0.20
	P Value	0.22	0.12	0.10	**0.03**	**0.02**	0.06	0.31

b.)

		JJA Rain							
		Jan	Feb	Mar	Apr	May	Jun	Jul	Aug
1940-1981	R Value	-0.19	-0.19	-0.10	-0.25	-0.15	-0.01	0.08	0.00
	P Value	0.22	0.23	0.54	0.11	0.33	0.95	0.59	1.00
1982-2009	R Value	-0.03	-0.04	-0.04	0.03	0.07	0.23	0.16	0.04
	P Value	0.87	0.84	0.84	0.90	0.71	0.24	0.43	0.84

c.)

		JAS Rain								
		Jan	Feb	Mar	Apr	May	Jun	Jul	Aug	Sep
1940-1981	R Value	-0.16	-0.15	-0.07	-0.23	-0.24	-0.23	-0.19	-0.15	-0.17
	P Value	0.31	0.35	0.68	0.15	0.13	0.14	0.23	0.35	0.29
1982-2009	R Value	-0.22	-0.20	-0.15	-0.16	-0.21	-0.12	-0.04	-0.12	-0.20
	P Value	0.26	0.32	0.45	0.41	0.28	0.55	0.84	0.55	0.31

d.)

		MJJAS Rain								
		Jan	Feb	Mar	Apr	May	Jun	Jul	Aug	Sep
1940-1981	R Value	-0.10	-0.06	0.10	-0.07	0.03	0.09	0.12	0.03	0.02
	P Value	0.54	0.71	0.51	0.65	0.85	0.59	0.44	0.87	0.89
1982-2009	R Value	0.06	0.10	0.15	0.18	0.19	0.21	0.18	0.03	-0.12
	P Value	0.76	0.60	0.46	0.35	0.34	0.28	0.37	0.90	0.54

Table 3.4: Correlations between the Nino3 index and SWC early (a), mid (b), late (c), entire (d) winter rainfall for time periods of 1940-1981(above), 1982-2009(below). Values in bold and underlined indicate statistical significange at the 0.05 level

Nino3 Correlations - 1 Year Lag

a.)

		MJJ Rain								
		Jan	**Feb**	**Mar**	**Apr**	**May**	**Jun**	**Jul**	**Aug**	**Sep**
1941-1981	**R Value**	-0.16	-0.07	-0.08	0.15	0.06	0.02	-0.11	0.02	0.03
	P Value	0.32	0.67	0.64	0.36	0.71	0.92	0.50	0.89	0.84
1982-2009	**R Value**	-0.21	-0.17	-0.29	-0.01	0.09	0.12	0.10	0.11	0.13
	P Value	0.29	0.38	0.13	0.97	0.66	0.54	0.63	0.58	0.52

b.)

		JJA Rain								
		Jan	**Feb**	**Mar**	**Apr**	**May**	**Jun**	**Jul**	**Aug**	**Sep**
1941-1981	**R Value**	-0.13	-0.06	-0.15	0.00	-0.04	-0.08	-0.19	-0.09	-0.10
	P Value	0.43	0.71	0.36	0.98	0.79	0.62	0.24	0.59	0.52
1982-2009	**R Value**	**-0.43**	**-0.46**	**-0.59**	**-0.43**	**-0.45**	**-0.42**	**-0.39**	-0.34	-0.22
	P Value	**0.02**	**0.01**	**0.00**	**0.02**	**0.02**	**0.03**	**0.04**	0.07	0.26

c.)

		JAS Rain								
		Jan	**Feb**	**Mar**	**Apr**	**May**	**Jun**	**Jul**	**Aug**	**Sep**
1941-1981	**R Value**	-0.10	-0.04	-0.08	-0.04	-0.02	0.03	-0.02	0.04	0.03
	P Value	0.54	0.81	0.61	0.80	0.90	0.86	0.92	0.78	0.83
1982-2009	**R Value**	-0.24	-0.29	**-0.39**	-0.35	**-0.43**	**-0.41**	**-0.38**	-0.35	-0.30
	P Value	0.22	0.14	**0.04**	0.06	**0.02**	**0.03**	**0.05**	0.07	0.12

d.)

		MJJAS Rain								
		Jan	**Feb**	**Mar**	**Apr**	**May**	**Jun**	**Jul**	**Aug**	**Sep**
1941-1981	**R Value**	-0.05	0.03	0.01	0.13	0.05	0.04	-0.08	0.06	0.05
	P Value	0.77	0.86	0.95	0.42	0.77	0.79	0.61	0.72	0.76
1982-2009	**R Value**	-0.22	-0.24	**-0.38**	-0.19	-0.18	-0.12	-0.12	-0.09	-0.06
	P Value	0.26	0.22	**0.05**	0.32	0.37	0.55	0.54	0.63	0.77

Table 3.5: Correlations between the Nino3 index at 1-year lead and SWC early (a), mid (b), late (c), enti
time periods of 1941-1981(above), 1982-2009(below). Values in bold and underlined indicate statistical s

Nino3 Correlations - 0 Year Lag

a.)

		May Rain				
		Jan	**Feb**	**Mar**	**Apr**	**May**
1940-1981	**R Value**	0.12	0.15	**0.30**	0.21	0.22
	P Value	0.45	0.36	**0.05**	0.18	0.17
1982-2009	**R Value**	**0.37**	**0.49**	**0.52**	**0.53**	**0.44**
	P Value	**0.05**	**0.01**	**0.00**	**0.00**	**0.02**

b.)

		June Rain					
		Jan	**Feb**	**Mar**	**Apr**	**May**	**Jun**
1940-1981	**R Value**	-0.09	-0.06	0.02	-0.03	0.15	0.29
	P Value	0.56	0.73	0.91	0.83	0.35	0.06
1982-2009	**R Value**	0.14	0.09	0.08	0.15	0.30	**0.39**
	P Value	0.48	0.64	0.68	0.44	0.12	**0.04**

c.)

		July Rain						
		Jan	**Feb**	**Mar**	**Apr**	**May**	**Jun**	**Jul**
1940-1981	**R Value**	-0.15	-0.24	-0.10	**-0.31**	**-0.40**	**-0.30**	-0.23
	P Value	0.35	0.12	0.54	**0.05**	**0.01**	**0.05**	0.14
1982-2009	**R Value**	-0.08	-0.02	-0.02	0.05	0.00	-0.01	-0.09
	P Value	0.69	0.92	0.93	0.81	0.98	0.97	0.65

d.)

		August Rain							
		Jan	**Feb**	**Mar**	**Apr**	**May**	**Jun**	**Jul**	**Aug**
1940-1981	**R Value**	-0.12	-0.05	-0.12	-0.13	-0.09	-0.09	-0.01	-0.07
	P Value	0.46	0.75	0.44	0.39	0.59	0.56	0.95	0.67
1982-2009	**R Value**	-0.16	-0.18	-0.17	-0.21	-0.26	-0.05	0.11	0.13
	P Value	0.43	0.36	0.39	0.28	0.18	0.80	0.56	0.50

e.)

		September Rain								
		Jan	**Feb**	**Mar**	**Apr**	**May**	**Jun**	**Jul**	**Aug**	**Sep**
1940-1981	**R Value**	0.01	0.09	0.14	0.12	0.16	0.04	-0.06	-0.01	0.06
	P Value	0.96	0.57	0.36	0.44	0.30	0.80	0.70	0.96	0.73
1982-2009	**R Value**	-0.21	-0.21	-0.12	-0.19	-0.19	-0.19	-0.08	-0.13	-0.25
	P Value	0.29	0.30	0.54	0.34	0.34	0.34	0.68	0.50	0.20

Table 3.6: Correlations between the Nino3 index at 0-year lead and SWC rainfall in May (a), June (b), July (c), August (d), September(e) for time periods of 1940-1981(above), 1982-2009(below). Values in bold and underlined indicate statistical significange at the 0.05 level

Nino3 Correlations - 1 Year Lag

a.)

		May Rain											
		Jan	Feb	Mar	Apr	May	Jun	Jul	Aug	Sep	Oct	Nov	Dec
1940-1981	R Value	0.06	0.11	0.17	0.16	0.11	0.13	0.06	0.11	0.17	0.13	0.11	0.08
	P Value	0.70	0.50	0.28	0.30	0.48	0.42	0.69	0.48	0.30	0.42	0.48	0.63
1982-2009	R Value	0.10	0.14	0.15	0.32	**0.45**	**0.51**	**0.49**	**0.51**	**0.43**	**0.37**	0.33	0.32
	P Value	0.62	0.48	0.46	0.10	**0.02**	**0.01**	**0.01**	**0.01**	**0.02**	**0.05**	0.09	0.10

b.)

		June Rain											
		Jan	Feb	Mar	Apr	May	Jun	Jul	Aug	Sep	Oct	Nov	Dec
1941-1981	R Value	-0.02	0.00	-0.04	0.14	0.01	-0.07	-0.19	-0.05	-0.10	-0.08	-0.06	-0.08
	P Value	0.88	0.98	0.81	0.38	0.96	0.67	0.24	0.78	0.55	0.64	0.70	0.63
1982-2009	R Value	-0.14	-0.13	-0.24	-0.10	-0.06	-0.03	-0.07	-0.08	-0.02	0.08	0.12	0.11
	P Value	0.49	0.51	0.21	0.63	0.78	0.88	0.74	0.69	0.93	0.69	0.56	0.58

c.)

		July Rain											
		Jan	Feb	Mar	Apr	May	Jun	Jul	Aug	Sep	Oct	Nov	Dec
1941-1981	R Value	-0.35	-0.26	-0.29	-0.06	-0.02	-0.03	-0.05	-0.02	0.00	-0.07	-0.06	-0.09
	P Value	0.02	0.10	0.06	0.69	0.91	0.87	0.75	0.88	0.99	0.68	0.69	0.57
1982-2009	R Value	-0.30	-0.29	**-0.38**	-0.21	-0.21	-0.24	-0.22	-0.21	-0.17	-0.16	-0.16	-0.13
	P Value	0.12	0.13	**0.05**	0.29	0.28	0.22	0.26	0.28	0.40	0.42	0.40	0.50

d.)

		August Rain											
		Jan	Feb	Mar	Apr	May	Jun	Jul	Aug	Sep	Oct	Nov	Dec
1941-1981	R Value	0.18	0.18	0.08	-0.12	-0.09	-0.04	-0.08	-0.10	-0.09	-0.12	-0.10	-0.14
	P Value	0.27	0.26	0.60	0.45	0.59	0.80	0.64	0.55	0.58	0.46	0.54	0.37
1982-2009	R Value	-0.30	**-0.38**	**-0.39**	**-0.48**	**-0.57**	**-0.50**	**-0.42**	-0.32	-0.21	-0.16	-0.13	-0.13
	P Value	0.12	**0.05**	**0.04**	**0.01**	**0.00**	**0.01**	**0.03**	0.10	0.28	0.40	0.52	0.50

e.)

		September Rain											
		Jan	Feb	Mar	Apr	May	Jun	Jul	Aug	Sep	Oct	Nov	Dec
1940-1981	R Value	0.09	0.08	0.14	0.15	0.08	0.15	0.13	0.24	0.17	0.15	0.13	0.22
	P Value	0.60	0.61	0.37	0.35	0.60	0.37	0.43	0.13	0.28	0.34	0.43	0.16
1982-2009	R Value	0.17	0.14	0.03	-0.01	-0.08	-0.06	-0.10	-0.16	-0.21	-0.25	-0.25	-0.21
	P Value	0.40	0.48	0.87	0.95	0.70	0.75	0.61	0.43	0.28	0.19	0.20	0.29

Table 3.7: Correlations between the Nino3 index at 1-year lead and SWC rainfall in May (a), June (b), July (c), August (d), September(e) for time periods of 1940-1981(above), 1982-2009(below). Values in bold and underlined indicate statistical significange at the 0.05 level

Chapter 4

Exploring the Potential for Statistical Seasonal Forecasting

4.1 Introduction

This chapter attempts to assess the potential for statistical seasonal forecasting of SWC rainfall. This is accomplished by using forward stepwise linear regression to create statistical forecast models of late winter rainfall in the SWC. Late winter rainfall exhibits strong relationships at considerable leads with SST, SIC, the Nino3 index, and SAM indices, making it suitable for an initial forecasting attempt. Three statistical models were created, using different pools of potential predictor variables to highlight relevant characteristics of late winter rainfall predictability. Model 1 uses a black box approach, allowing the forward stepwise regression procedure to select variables it determines to be optimal for inclusion into the regression model. Model 2 uses a similar approach but allows the subjective creation of combined predictor indices to represent perceived interactions between regions of SST. Model 3 attempts to use knowledge of the relationships between SWC rainfall and variables, as discussed in Chapter 3, to limit potential predictor variables for a comparison of forecast performance.

4.2 Data and Methods

4.2.1 Selecting potential predictor variables

Due to the limited availability of sea ice data, and to the apparent instability of the relationship between SWC rainfall and various climate variables, the initial investigation

of SWC rainfall predictability was limited to the period of 1982-2009. Model 1 used regions where SST/SIC was previously identified as exhibiting strong, persistent correlations with SWC rainfall at substantial lead times, and that suggested physically reasonable connections, as potential predictor variables. Monthly averaged values of SST/SIC within these areas were spatially averaged, detrended and normalized to create a time series of each. At each region, every month, from the time that correlations begin to develop to the time of rainfall, was included as a potential predictor variable. Detrended time series were constructed of periods where SAM indices exhibited strong correlations with late winter rainfall and included as potential predictor variables. A detrended time series were constructed of the period where the Nino3 index exhibited the strongest correlation with late winter rainfall at 1-year lag and was included as a potential predictor variable. A description of these variables is included in Table 4.1.

Model 2 used combined predictor indices (CPI) that were created as the sum of, or difference between the detrended, normalized predictor variables used in Model 1 for each month. Each CPI was detrended and normalized, creating a time series of each. Correlations between the CPI and late winter rainfall (Table 4.2) were used to determine which were most appropriate for inclusion as potential predictor variables. The CPI from each month that showed the strongest correlation with JAS rainfall, while including the fewest predictor variables, was included as a potential predictor variable in Model 2. These CPI were included with all the potential predictor variables used in Model 1 to create a pool of potential predictor variables for use in Model 2. Model 3 used only CPI-6 and SIC-1 as potential predictor variables.

Potential Predictor	Latitude	Longitude	Description	Correlation (r-value)
SST-1a	46°S - 54°S	67°W - 42°W	Spatially averaged April SST within subset of area A1	-0.62
SST-1b	46°S - 54°S	67°W - 42°W	Spatially averaged May SST within subset of area A1	-0.45
SST-1c	46°S - 54°S	67°W - 42°W	Spatially averaged June SST within subset of area A1	-0.53
SST-2a	21°S - 28°S	41°W - 25°W	Spatially averaged April SST within subset of area A2	0.52
SST-2b	21°S - 28°S	41°W - 25°W	Spatially averaged May SST within subset of area A2	0.28
SST-2c	21°S - 28°S	41°W - 25°W	Spatially averaged June SST within subset of area A2	0.22
SST-4a	12°S - 19°S	0° - 9°E	Spatially averaged May SST within subset of area A4	0.49
SST-4b	12°S - 19°S	0° - 9°E	Spatially averaged June SST within subset of area A4	0.54
SST-5a	34°S - 38°S	15°W - 8°W	Spatially averaged May SST within subset of area A5	-0.32
SST-5b	34°S - 38°S	15°W - 8°W	Spatially averaged June SST within subset of area A5	-0.50
SST-6a	48°S - 52°S	5°E - 25°E	Spatially averaged June SST within subset of area A6	0.26
SIC-1	61°S - 65°S	57°W - 52°W	Spatially averaged April SIC near the tip of the AAP	0.65
SAM-3	N/A	N/A	3 month running mean April GM SAM index values	-0.47
SAM-4	N/A	N/A	4 month running mean April GM SAM index values	-0.48
Nino-1	N/A	N/A	May Nino3 index values leading rainfall by 1 year	-0.43

Table 4.1: Potential predictor variables included in Model 1, with their spatial dimensions, description, and correlation with late winter SWC rainfall.

Combined Predictor Index	Month	Description	Correlation (r-value)
CPI-1	April	(SST-2a) - (SST-1a)	0.69
CPI-2	May	(SST-4b) - (SST-1b)	0.58
CPI-3	May	(SST-4b) - (SST-1b) - (SST-5b)	0.57
CPI-4	May	(SST-2b) + (SST-4b) - (SST-1b)	0.58
CPI-5	June	(SST-4c) - (SST-1c)	0.65
CPI-6	June	(SST-4c) - (SST-1c) - (SST-5c)	0.70
CPI-7	June	(SST-2c) + (SST-4c) - (SST-1c) - (SST-5c)	0.63
CPI-8	June	(SST-4c) + (SST-6c) - (SST-1c) - (SST-5c)	0.65
CPI-9	June	(SST-2c) + (SST-4c) + (SST-6c) - (SST-1c) - (SST-5c)	0.63

Table 4.2: Combined predictor indices of SST, the month to which they apply, a description of the combination of predictor indices from which they were calculated, and the correlation of each combined predictor index with late winter SWC rainfall. Combined predictor indicies highlighted in bold were selected for inclusion in Model 2. Details of the predictor indices from which the combined predictor indices were calculated can be found in Table 4.1

4.2.2 Stepwise regression model

The forward stepwise regression procedure, as described in Draper and Smith (1998), was chosen as the method for selecting the best regression equation. This procedure is used in order to avoid the inclusion of too many predictor variables in the forecast equation. A general introduction to forward stepwise regression and the necessary statistical framework can be found in Wilks (2006), but a brief introduction will be given here.

In the multiple regression setting there are often more potential predictor variables available than are practical, or advisable to use. Determining if the inclusion of another predictor variable is worthwhile is typically accomplished by comparing its additional contribution to the regression sum of squares, were it included in the model, to the sample variance. If this contribution is substantial, then the additional predictor term

should be included in the regression. The partial F-test is typically used to determine whether this contribution is in fact substantial. The F statistic is a measure of the mean squared regression (MSR) relative to the mean squared error (MSE), and in multiple regression analysis it serves as a qualitative measure of the strength of a regression. Put simply, it is a measure of how much variability in the predictand is described by the regression equation relative to the variability unaccounted for. In the partial F-test, the F statistic is calculated using only the additional MSR contributed by the inclusion of the additional predictor variable. When using the partial F-test to assess the contribution of a single additional variable, the F-statistic is exactly interchangeable with the square of the t-statistic and its corresponding p-values (Draper and Smith, 1998).

To begin the forward stepwise regression procedure, the predictor variable most correlated with the predictand is selected from the pool of all potential predictor variables. This variable is checked for significance using the partial F-test, with the significance level to enter the regression equation, F-to-enter, set to the corresponding p-value of 0.05. If the variable is not significant the regression equation $Y = \overline{Y}$ is chosen. If the variable is significant, it is then adopted into the regression equation. Next, the predictor variable with the highest partial F-value is chosen from the pool of remaining potential predictor variables and tested for significance against the F-to-enter value. If significant, this variable is included in the regression equation, and then the partial F-value of both variables in the equation is compared to a chosen significance level, F-to-remove, set to the corresponding p-value of 0.10. If either of the variables currently in the equation has become insignificant it is removed from the equation. This procedure of selecting the most significant predictor variable and testing it against the F-to-enter value,

then testing the usefulness of each predictor in the regression equation against the F-to-remove value, is repeated until no new variable can be included into the regression equation and no variables in the current equation can be removed.

4.2.3 Forecast verification and assessment

An accuracy measure commonly used for forecast assessment is the Mean Square Error (MSE), the average squared difference between forecast and observation pairs. It is calculated as:

$$MSE = \frac{1}{n}\sum_{k=1}^{n}(y_k - o_k)^2 \qquad (3.2)$$

Where: (y_k, o_k) is the k^{th} of n pairs of forecasts and observations respectively.

As the MSE is squared function, it is particularly sensitive to large errors (i.e. outliers). A perfect forecast, whereby $y_k = o_k$ for every forecast-observation pair, will have a MSE of zero, which will quickly increase as discrepancies between forecasts and observations increase. A more recognizable form of this is the square root of the MSE, or RMSE, which can be thought of as the typical magnitude of forecast error and has the same physical dimensions as the forecasts and observations (Wilks, 2006).

Typically the scalar accuracy of a model is assessed using data withheld during the development of the model, allowing an estimation of the difference between the MSE observed in the model itself and the MSE that could be expected of a model forecast using independent data. Due to the small size of the data set available in this study, the reservation of an independent data set was not practical. Instead, two separate methods of

cross validation, Leave-One-Out (LOT) cross validation and K-fold cross validation, were used to estimate prediction MSE.

Using the LOT cross validation method (Elsner and Schmertmann, 1994), a model is developed based on (n-1) data points, where n is equal to the total number of data points available. This model was then used to forecast the remaining datum point that was withheld from the training set. This procedure was repeated for each of the n data points, gathering n estimations of n independent data. At each step the entire forward stepwise regression process was repeated, allowing the potential selection of different predictors when developing the models. In this sense it was the fitting algorithm that was successively repeated, not the specific statistical model derived from the entire data set (Wilks, 2006).

In order to insure the datum point "left out" at each stage was truly independent and did not contain significant "information" about data points nearby, the rainfall data was checked for serial correlation. The autocorrelation was computed using the Pearson's correlation, where the rainfall data set was correlated with itself at 1-year lag.

K-fold cross validation (Kohavi, 1995 and Wilks, 2006), a more general form of LOT cross validation, was used as a second estimate of prediction MSE. The data set was randomly partitioned in 10 sub-samples, whereby 1 sub-sample was used for validation and the remaining 9 sub-samples were used for model training. This procedure was repeated 10 times, with each of the 10 sub-samples used for validation exactly once. In order to gain a better estimate of the prediction MSE suggested by this method, 1000 Monte-Carlo repetitions were performed, whereby the K-fold method was repeated 1000 times and the mean of the MSE values across all Monte-Carlo repetitions was taken.

The Mean Error (ME), a measure of forecast bias, was determined by subtracting the mean of the observed values from the mean of the predicted values. When ME > 0 it indicates that forecasts are, on average, too high and when ME < 0 forecasts are, on average, too low. As no historical forecast for SWC rainfall could be found, reference forecasts based on persistence and climatological values were used to calculate the relative accuracy, or Skill Score (SS), of the model forecast. The skill scores were constructed based on MSE measures, where:

$$MSE_{C\,\mathrm{lim}} = \frac{1}{n}\sum_{k=1}^{n}(\bar{o} - o_k)^2 \qquad (3.3)$$

$$MSE_{Pers} = \frac{1}{n}\sum_{k=1}^{n}(o_{k-1} - o_k)^2 \qquad (3.4)$$

$$SS_{C\,\mathrm{lim}} = \frac{MSE - MSE_{C\,\mathrm{lim}}}{0 - MSE_{C\,\mathrm{lim}}} = 1 - \frac{MSE}{MSE_{C\,\mathrm{lim}}} \qquad (3.5)$$

$$SS_{Pers} = \frac{MSE - MSE_{Pers}}{0 - MSE_{Pers}} = 1 - \frac{MSE}{MSE_{Pers}} \qquad (3.6)$$

Where: o is observation; n is number of observations; MSE is the MSE calculated by either the LOT or K-fold cross validation methods

As the quotient being subtracted from 1 in equation 3.5 is the average squared error divided by the climatological variance, SS_{Clim} can be thought of as a measure of the reduction of variance (Wilks, 2006).

4.3 Results

4.3.1 Scatterplots

The relationship of each predictor variable to rainfall is illustrated in Figures 4.1 to 4.5. The paucity of data available is apparent, and in several cases influential outliers are present. In most cases modest linear relationships are apparent, and corresponding correlations between these potential predictor variables and JAS rainfall are strong and significant. Potential predictor variables SST-2b (Fig. 4.2b), SST-2c (Fig 4.2c), SST-5a (Fig. 4.3b) and SST-6a (Fig. 4.3d) display weak relationships both in their scatterplots and in correlations (Table 4.1). Potential predictor variables SST-1c (Fig. 4.1d), SST-4a (Fig. 4.2d) and CPI-6 (Fig. 4.5c) display particularly influential outliers.

4.3.2 Model 1

Initially all potential predictor variables except SST-2b, SST-2c, SST-5a, and SST-6a described a significant portion of the variability in the rainfall data (Table 4.3a). Of these, SIC-1 had the largest t-statistic and was the first predictor added to the regression equation. This significantly reduced the MSE and increased the R^2 value (Table 4.3b). The associated p-value of the Nino-1 predictor increased the most with the inclusion of the SIC-1 predictor. The next predictor variable added to the regression equation was SST-1a, reducing the MSE from 0.61 to 0.48 and increasing the R^2 value from 0.42 to 0.56 (Table 4.3c) but reducing the F-statistic slightly. The associated p-value of several variables increased dramatically (Table 4.3c) and only SST-4b remained significant, making it the final variable to be added to the regression equation. This further reduced the MSE to 0.36 and increased the R^2 value to 0.68 (Table 4.3d). The

two most significant remaining variables were SST-2a and Nino-1, with Nino-1 nearly being significant enough for inclusion into the regression equation. The co-efficients of the predictor variables included in the regression equation are all relatively close. The standard error for each, and the final regression equation are included in Table 4.3.

The ME was approximately zero, indicating little bias in the forecast values. Cross validation methods produced MSE estimates substantially higher than the in-model estimate (Table 4.4). Lag-1 auto-correlation of JAS rainfall produced an r-value of 0.088 with associated p-value of 0.66, indicating no significant correlations between JAS rainfall and its preceding or following values. This suggests that both the LOT cross validation and K-fold cross validation methods appropriately isolate the left out data point(s) from information pertaining to the system being regressed. Using climatological average values provided a reference forecast with lower MSE than the forecast based on persistence values (Table 4.4). Model 1, assessed with LOT cross validation, had a skill score of 0.18 and 0.55 when measured relative to the climatological average and persistence forecasts respectively. When assessed with K-fold cross validation these scores were 0.21 and 0.57 respectively.

The minimum and maximum observed JAS rainfall values were -1.72 and 2.37 respectively, while the predicted values only ranged from -1.32 to 1.91. The minimum and maximum residuals were -1.23 and 0.92 respectively. Residual analysis indicates that variance is approximately constant (Fig. 4.6a), residuals are approximately normally distributed (Fig. 4.6b), and that residuals follow a roughly Gaussian distribution (Fig. 4.6c). A scatterplot of residuals versus observed values (Fig. 4.6d) indicates that the forecast tends to under predict large positive and negative observations. Scatterplots of

residuals versus predictor variables included in the regression equation (Fig. 4.7a, b, c) show no obvious signs of non-constant variance, missing predictor variables or influential outliers. A scatterplot of predicted values versus observed values (Fig 4.7d) illustrates the approximately linear relationship with no obvious influential outliers, and also highlights to tendency for the forecast to under predict large anomalous observed values. The standard deviation for Model 1 was 0.82.

4.3.3 Model 2

Initially all potential predictor variables except SST-2b, SST-2c, SST-5a, and SST-6a described a significant portion of the variability in the rainfall data (Table 4.5a). Of these, CPI-3 had the largest t-statistic and was the first predictor added to the regression equation. This significantly reduced the MSE and increased the R^2 value (Table 4.5b). The associated p-value of many of the predictors increased substantially with the inclusion of CPI-6 in the regression equation. In contrast, Nino-1 remained unaffected and became the next variable included in the regression equation, reducing the MSE from 0.53 to 0.37 and increasing the R^2 value from 0.49 to 0.66 (Table 4.5c) but reducing the F-statistic slightly. Only CPI-1, CPI-2 and SIC-1 remained significant (Table 4.5c), with SIC-1 having the larger t-statistic and being selected next to enter the regression equation. This further reduced the MSE only slightly to 0.31 and increased the R^2 value to 0.72 (Table 4.3d), and also reduced the F-statistic again. The significance of CPI-1 and CPI-2 remained relatively unaffected, and CPI-2 was selected next for inclusion into the regression equation. No other predictors remained significant enough to be added to the regression equation, though CPI-1 and SST-1a were both very close.

The co-efficients of the CPI predictor variables included in the regression equation are significantly larger than those of the Nino-1 and SIC-1 variables. The standard error for each, and the final regression equation are included in Table 4.5.

The ME was approximately zero, indicating little bias in the forecast values. Cross validation methods produced MSE estimates substantially higher than the in-model estimate (Table 4.6). Model 2, assessed with LOT cross validation, had a skill score of 0.29 and 0.61 when measured relative to the climatological average and persistence forecasts respectively. When assessed with K-fold cross validation these scores were 0.36 and 0.65 respectively.

The minimum and maximum observed JAS rainfall values were -1.72 and 2.37 respectively, while the predicted values only ranged from -1.60 to 1.93. The minimum and maximum residuals were -0.88 and 0.90 respectively. Residual analysis indicates that variance is approximately constant (Fig. 4.8a), residuals are approximately normally distributed (Fig. 4.8b), and that residuals follow a roughly Gaussian distribution (Fig. 4.8c). A scatterplot of residuals versus observed values (Fig. 4.8d) indicates that the forecast tends to under predict large positive and negative observations. Scatterplots of residuals versus predictor variables included in the regression equation (Fig. 4.9a, b, c, d) show no obvious signs of non-constant variance, missing predictor variables or influential outliers. A scatterplot of predicted values versus observed values (Fig 4.10a) illustrates the approximately linear relationship with no obvious influential outliers, and also highlights to tendency for the forecast to under predict large anomalous observed values. The standard deviation for Model 2 was 0.88.

4.3.4 Model 3

Initially both potential predictor variables described a significant portion of the variability in the rainfall data (Table 4.7a). Of these, CPI-6 had the largest t-statistic and was the first predictor added to the regression equation. This significantly reduced the MSE and increased the R^2 value (Table 4.7b). The t-statistic of SIC-1 decreased slightly with the inclusion of CPI-6 in the regression equation, but remained significant enough to be included in the regression equation. This reduced the MSE from 0.53 to 0.37 and increasing the R^2 value from 0.49 to 0.65 (Table 4.7c) but also reduced the F-statistic slightly. The co-efficients of both predictor variables were close in magnitude. The standard error for each, and the final regression equation are included in Table 4.7.

The ME was approximately zero, indicating little bias in the forecast values. Cross validation methods produced MSE estimates very close to the in-model estimate (Table 4.8). Model 3, assessed with LOT cross validation, had a skill score of 0.60 and 0.78 when measured relative to the climatological average and persistence forecasts respectively. When assessed with K-fold cross validation these scores were also 0.60 and 0.78 respectively.

The minimum and maximum observed JAS rainfall values were -1.72 and 2.37 respectively, while the predicted values only ranged from -1.57 to 1.54. The minimum and maximum residuals were -1.21 and 1.04 respectively. Residual analysis indicates that variance is approximately constant (Fig. 4.10b), residuals are approximately normally distributed (Fig. 4.10c), and that residuals follow a roughly Gaussian distribution (Fig. 4.10d). A scatterplot of residuals versus observed values (Fig. 4.11a) indicates that the forecast tends to under predict large positive and negative observations.

Scatterplots of residuals versus predictor variables included in the regression equation (Fig. 4.11b, c) show no obvious signs of non-constant variance, missing predictor variables or influential outliers. A scatterplot of predicted values versus observed values (Fig 4.11d) illustrates the approximately linear relationship with no obvious influential outliers, and also highlights to tendency for the forecast to under predict large anomalous observed values. The standard deviation for Model 3 was 0.81.

4.4 Discussion

4.4.1 The use of three models

While the selection of potential predictor variables for Model 1, as outlined in section 4.3.1, was rather straightforward, the use of CPI variables in Model 2 merits further discussion. Superficially, the choice to combine two variables that are already individually available for selection may seem arbitrary, or even to circumvent the limitations set by the forward stepwise regression procedure to avoid overfitting. However, if the underlying physical mechanism(s) which relates these variables to SWC rainfall is not a function of just one of these variables, but instead several, then the stepwise regression model could be led to discard variables which still contain valuable information relating to the underlying physical phenomenon.

For example, imagine that potential predictor variables in the SST-1 and SST-2 regions did not independently influence SWC rainfall, but that instead the underlying physical mechanism connecting both was the meridional temperature gradient created by the two. Further suppose that variability in SST-2 was slightly larger than that of SST-1, so that SST-2 would then be selected first into the regression equation. Since SST-1

describes a part of rainfall variability similar to SST-2, it may no longer be significant enough to be included in the regression equation, while still describing substantial variability of the underlying phenomenon. To capture this variability by creating a single variable of the meridional temperature gradient would only improve the forecast.

The inherent danger in using CPI variables when the underlying physical influence variables have on SWC rainfall is not confidently known is that the forecast will produce a false representation of the MSE. The robustness of the SST pattern, as discussed in Chapter 3, gives confidence that attempts with CPI are not misguided. Furthermore, the CPI variables included in Model 2 and Model 3 show substantially stronger correlations with JAS rainfall than any of their constituent variables (Table 4.2). Model 2 exhibited a similar increase of MSE from in-model estimation to cross validation estimates to Model 1. Model 3, which used a CPI predictor variable in its regression equation, showed almost no increase from in-model to out-of-model estimation of MSE, suggesting the use of the CPI variable did not lead to the overfitting of the model. Taken together, this suggests that CPI variables were not a roundabout way of overfitting the regression, but instead may represent a real physical interconnectivity among the SST potential predictor variables.

The more subjective approach in selecting the pool of potential predictor variables for Model 3 was chosen to act as an assessment of the forward stepwise regression approach in selecting an "optimum" regression equation. Forward stepwise regression is a tool used to help select regression equations of the most value and avoid the problems associated with overfitting while circumventing the inefficiency of testing every possible regression equation. This does not guarantee that the stepwise regression procedure will

pick the "best" possible equation, and in this study it is evident that having a large pool of potential predictor variables originating from small data sets that includes influential outliers magnifies weaknesses in the forward stepwise regression procedure. To simply include a mass of potential predictor variables without a critical examination based on knowledge of the physical system in question is to trust the black box approach of the stepwise regression procedure to find physically meaningful relationships from variability within the data. With so few data points this is inevitably a dangerous approach. This is apparent in the large discrepancies between in-model and out-of-model MSE estimates observed for Model 1 and Model 2.

Though certainly not conclusive, results from Chapter 3 provide valuable insight to the physical relationship between SWC rainfall and potential predictor variables that can be used to critically filter variables from the regression procedure. It appears that there is a certain SST pattern that may work in concert to influence SWC rainfall. SAM events occurring more than a month prior, and ENSO events occurring the previous year are unlikely to influence SWC rainfall directly through modifications in atmospheric circulation, but do contribute to variability of SST within the influential regions. Hence the influence of the SAM and ENSO predictors on SWC rainfall should be included with the CPI predictors. SST anomalies present the month before rainfall should be more likely to persist until the time of rainfall than anomalies present several months before, so the CPI-6 variable, representing June SST's, was selected to represent the influence of SST anomalies. It is unclear if SIC near the Antarctic Peninsula has a direct physical influence on SWC rainfall, or only acts as indicator of the combined state of larger modes

of variability. This led to the choice of SIC in April, when correlations were strongest, to act as the second potential predictor variable.

The results of Model 3 support these speculative relationships. Model 3 was still subjected to the stepwise regression procedure, as was still allowed the freedom to adjust predictors and associated co-efficients within each step of the cross-validation process. Similar in-model and out-of model estimates of MSE indicate the relationship between the predictor variables and SWC rainfall is stable and not subject to wild fluctuations with the removal of a single or group of data points. The small change in the t-statistic of SIC-1 after the inclusion of CPI-6 in the regression equation suggests these variables describe a substantially different portion of SWC rainfall variability.

4.4.2 Interpretation of results and shortcomings of the regression approach

Regression analysis attempts to summarize the relationship between a predictand and independent variables in a way that produces the least "error". In this study, "error" is defined as the averaged squared error in predictions of Y given the values of independent variables, and as such, the regression will adjust itself significantly to avoid large discrepancies. Influential outliers were present in predictor variables, such as CPI-6, that became part of the regression equation. For other predictor variables, such as SST-1b, influential outliers may have weakened otherwise strong relationships and prevented them from becoming part of the regression equation. Either way, influential outliers affected the development of the models and a further examination of these influential outliers, and the conditions present during the corresponding time periods is warranted, but beyond the scope of this study.

During the development of the forecast models, one concern was that the bias in the pdf of SWC rainfall events, related to changes in predictor variables, might not be significant in comparison to the inherent variability of the mid-latitudes. Model results indicate that changes in the physical mechanisms that connect the predictor variables to SWC rainfall have the ability to create significant bias's. Model 3 performed the best, and its skill score referenced to a climatological average forecast corresponds to a 60% reduction of variance when based on both K-fold and LOT cross validation MSE estimates. Using the same assessment references, Model 1 and Model 2 posted substantially poorer skill scores. Residual analysis identified no foundational flaws with any of the models, though none re-create the extreme values or the variance present in the observed values.

4.4.3 Functional relevance and real world use

Underlying any investigation into climate predictability is the idea of its potential real world application. Further discussion of this is curtailed in light of the potentially unstable predictor-predictand relationships outlined in Chapter 3. Any potential benefit received that could be received from the reduction of variance provided by the statistical forecast could only be accrued through its application over a substantial period of time, during which another substantial shift in the predictor-predictand relationships could occur. Evidence of any shift in the predictor-predictand relationships post-1982 is not observed in the residual analysis from Model 1 or Model 2. The assumption that a given residual is equally likely to occur at any part of the regression line, central to making statistical inferences in the regression setting, appears to be justified.

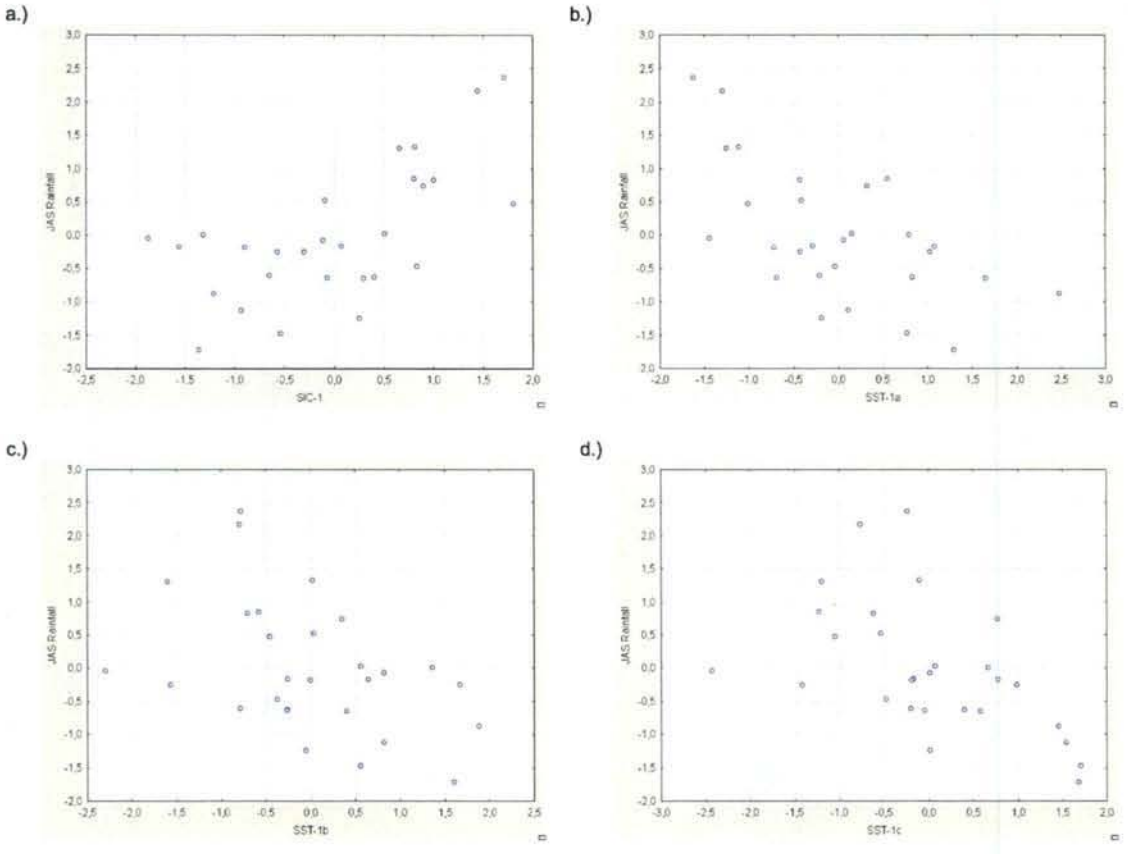

Figure 4.1: Scatterplot of potential predictor variable (a) SIC-1, (b) SST-1a, (c) SST-1b, (d) SST-1c versus JAS rainfall, plotted on the X and Y-axis respectively. All values are normalized.

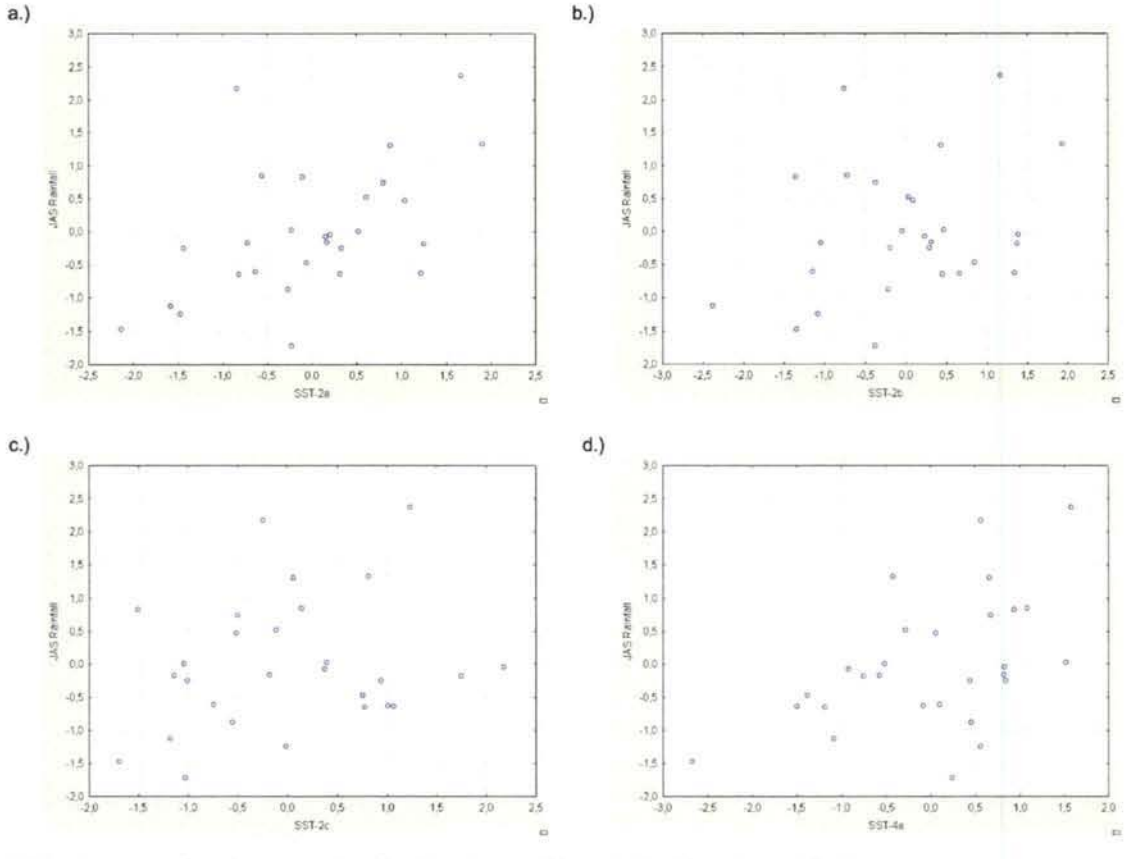

Figure 4.2: As for Figure 4.1, but for (a) SST-2a, (b) SST-2b, (c) SST-2c, (d) SST-4a

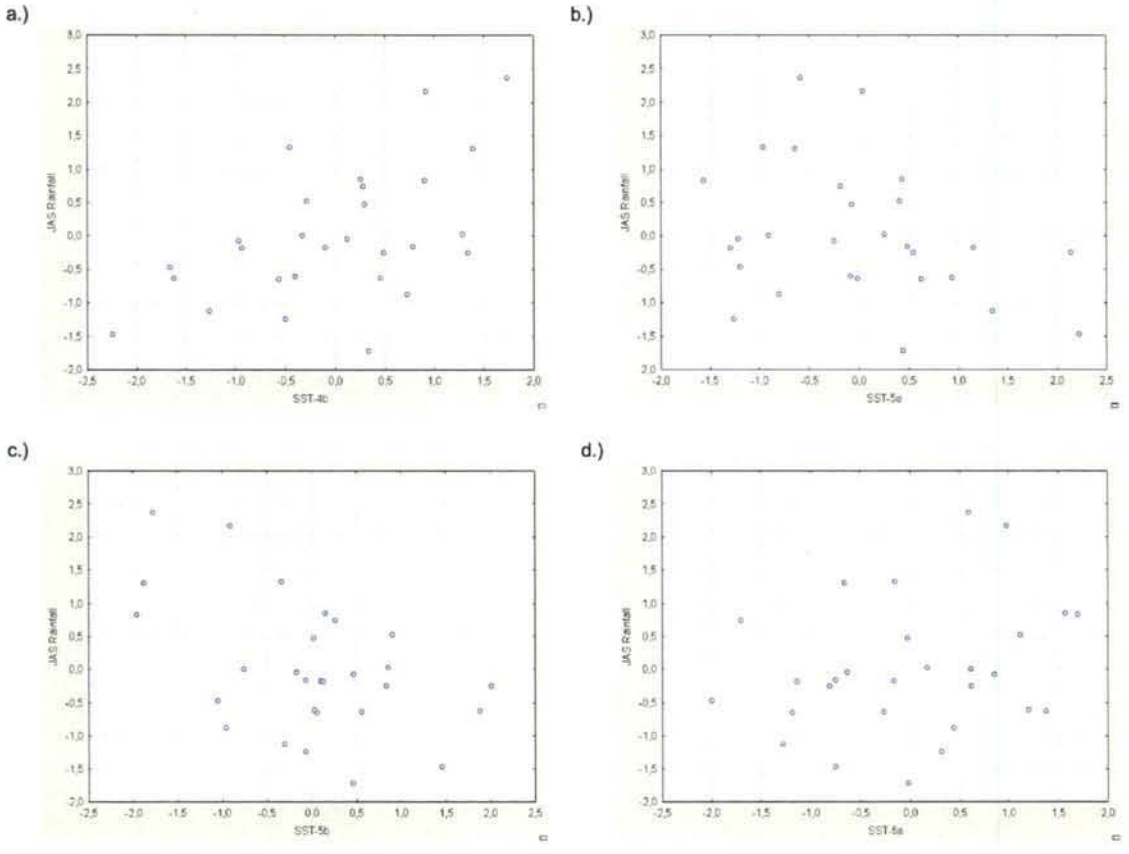

Figure 4.3: As for Figure 4.1, but for (a) SST-4b, (b) SST-5a, (c) SST-5b, (d) SST-6a

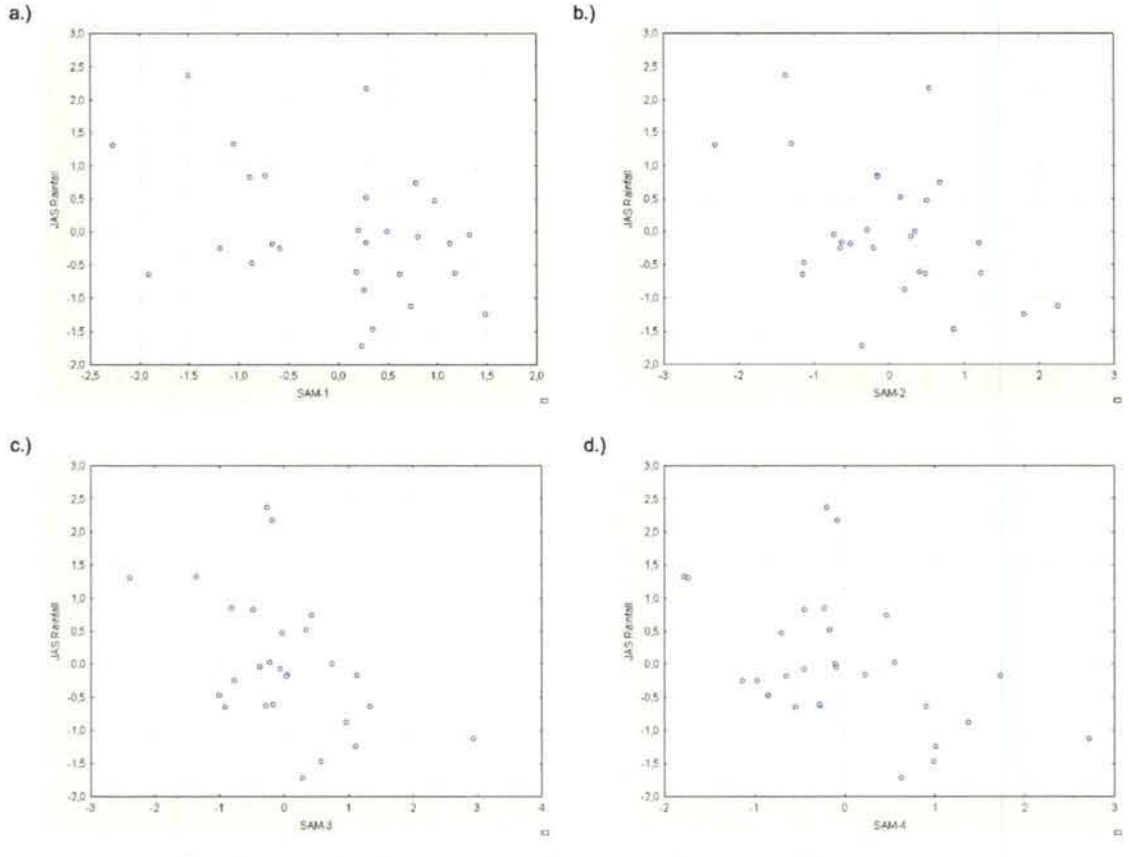

Figure 4.4: As for Figure 4.1, but for (a) SAM-1, (b) SAM-2, (c) SAM-3, (d) SAM-4

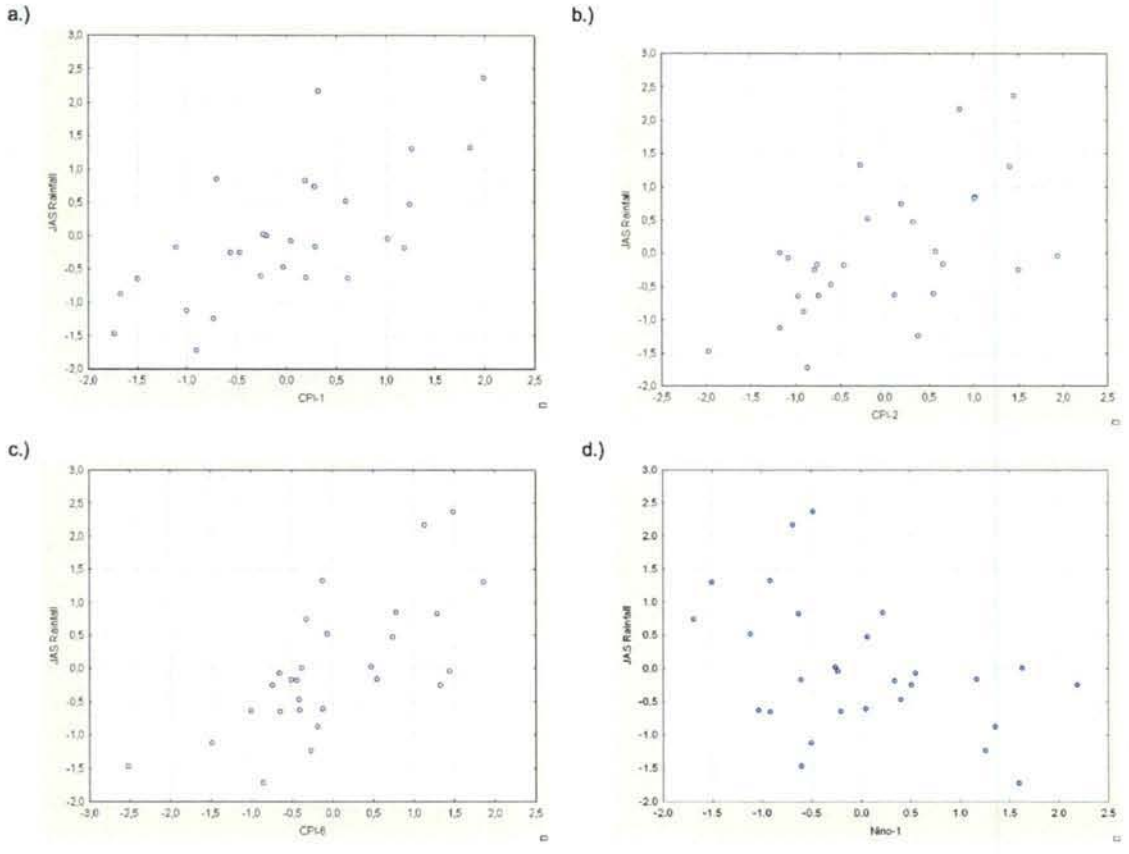

Figure 4.5: As for Figure 4.1, but for (a) CPI-1, (b) CPI-2, (c) CPI-6, (d) Nino-1

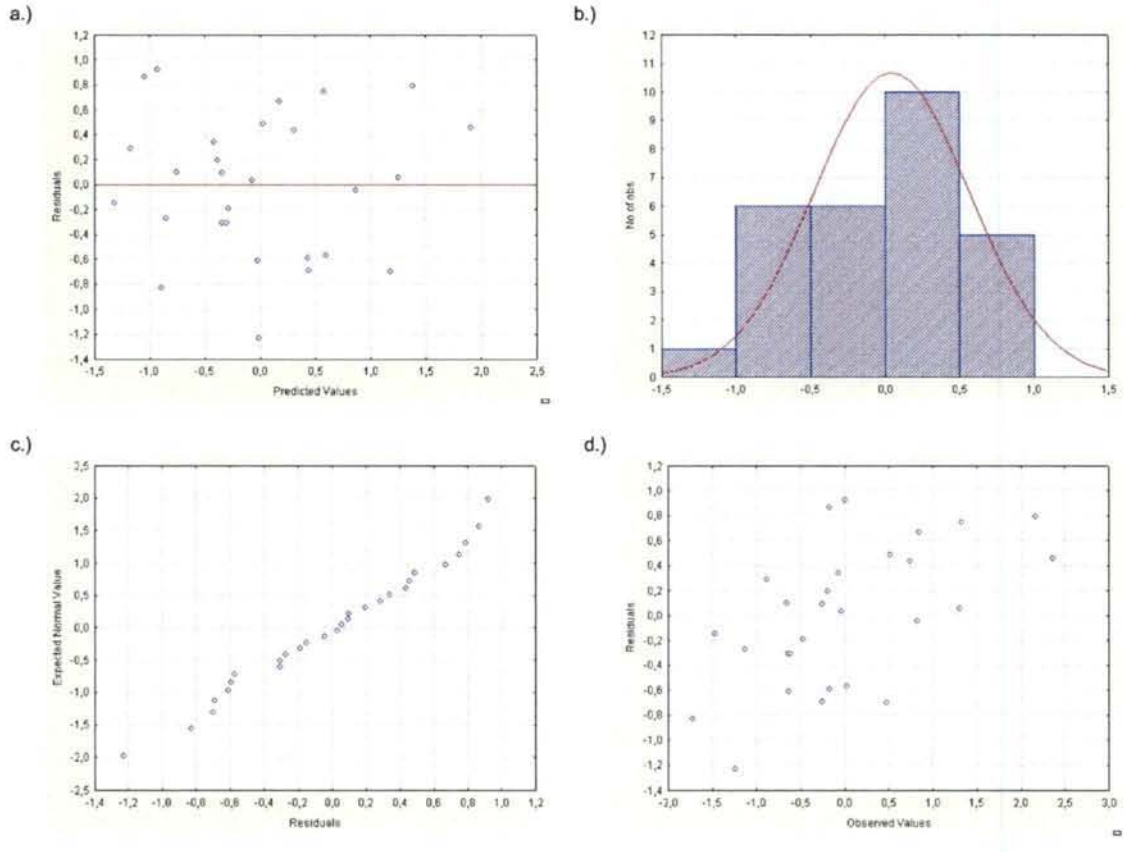

Figure 4.6: Residual analysis of Model 1 showing (a) predicted vs. residual scatterplot, (b) histogram of residuals with expected normal value line in red, (c) normal probability plot and (d) observed values vs. residual scatterplot

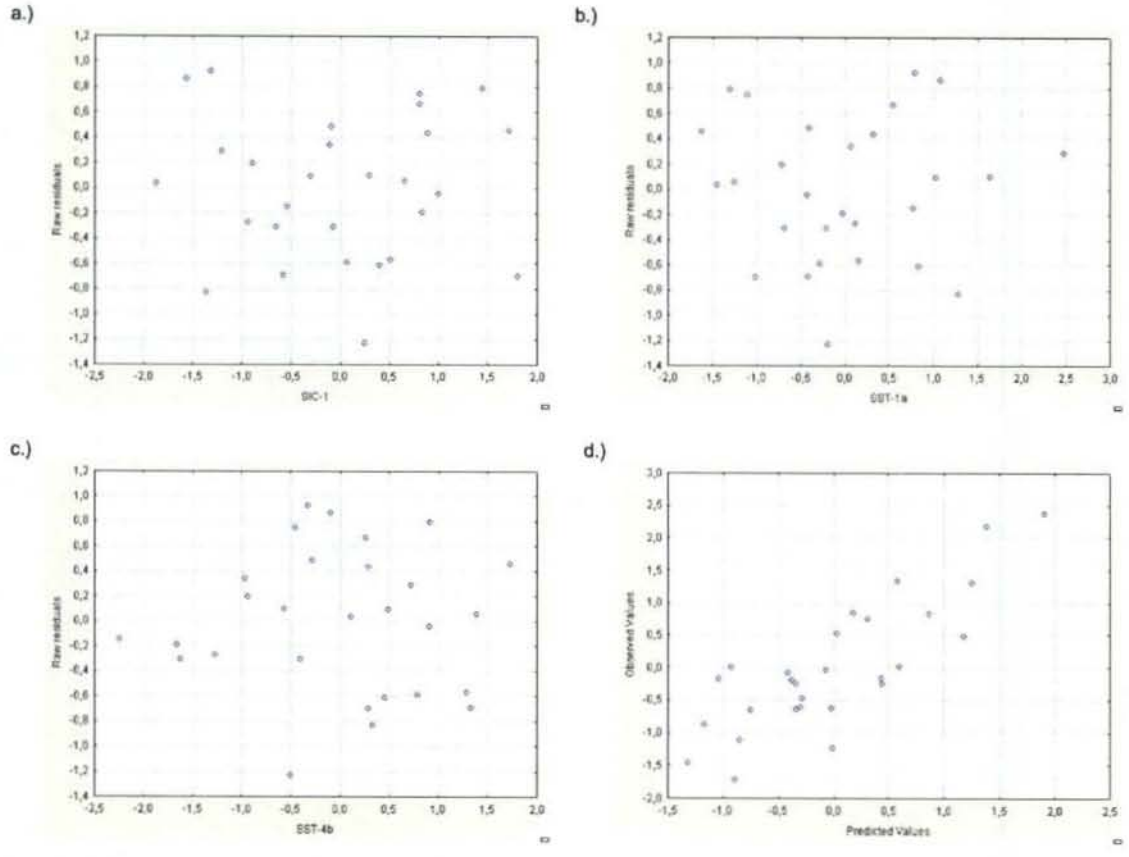

Figure 4.7: Residual analysis of Model 1 showing (a) predictor variable SIC-1 vs. residual scatterplot, (b) predictor variable SST-1a vs. residual scatterplot, (c) predictor variable SIC-1 vs. residual scatterplot and (d) predicted value vs. observed value scatterplot

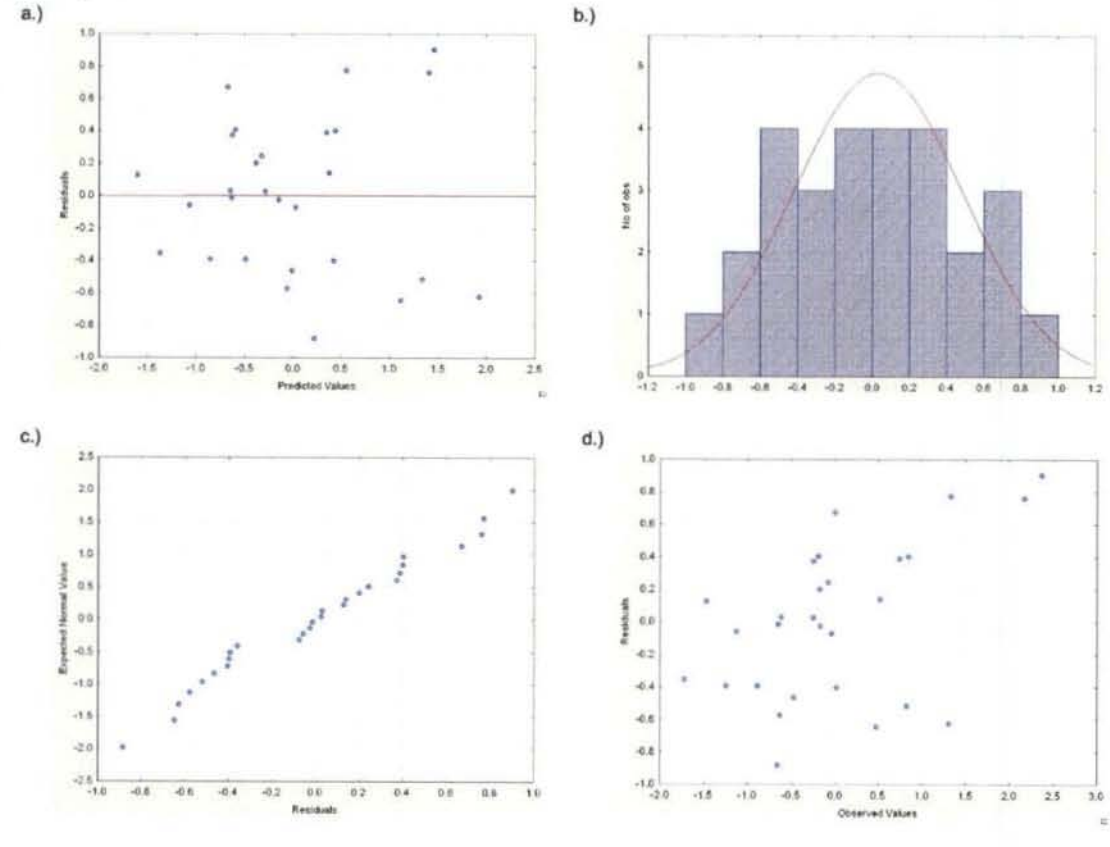

Figure 4.8: As for Figure 4.6, but for Model 2

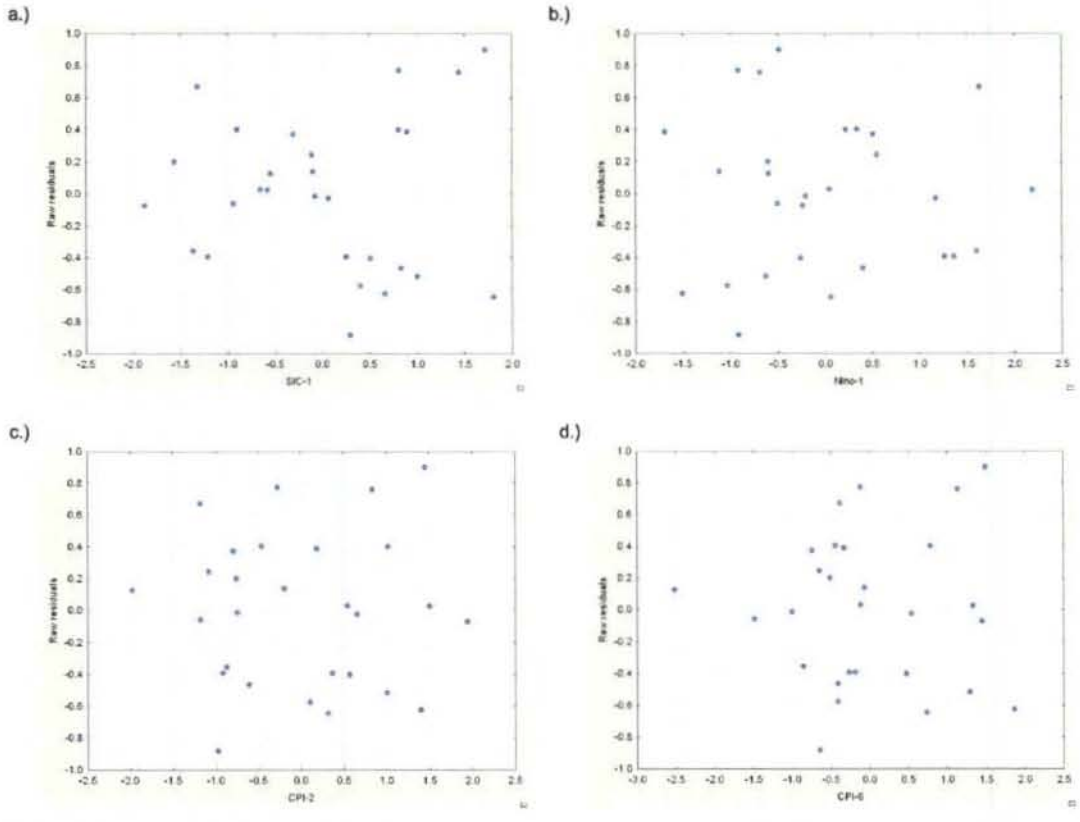

Figure 4.9: Residual analysis of Model 2 showing (a) predictor variable SIC-1 vs. residual scatterplot, (b) predictor variable Nino-1 vs. residual scatterplot, (c) predictor variable CPI-2 vs. residual scatterplot and (d) predictor variable CPI-6 vs. residual scatterplot

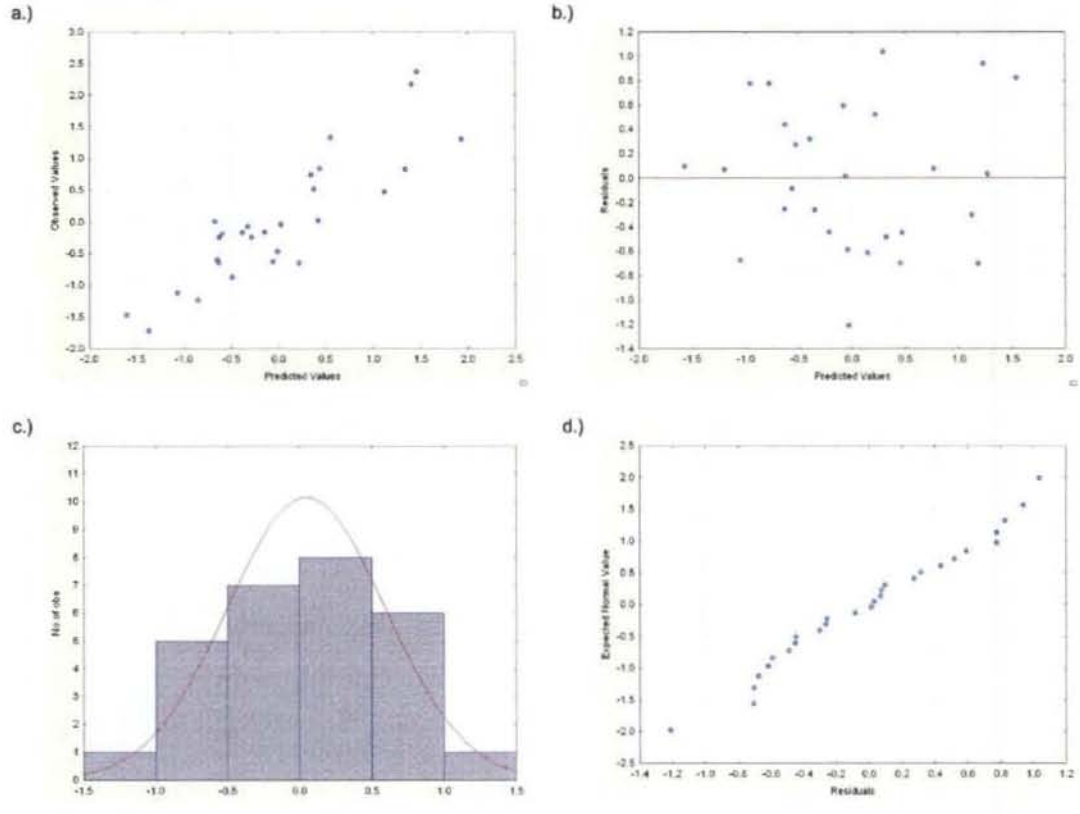

Figure 4.10: Residual analysis of (a) Model 2 predicted value vs. observed value scatterplot, (b) Model 3 predicted vs. residual scatterplot, (c) Model 3 histogram of residuals with expected normal value line in red, (d) Model 3 normal probability plot

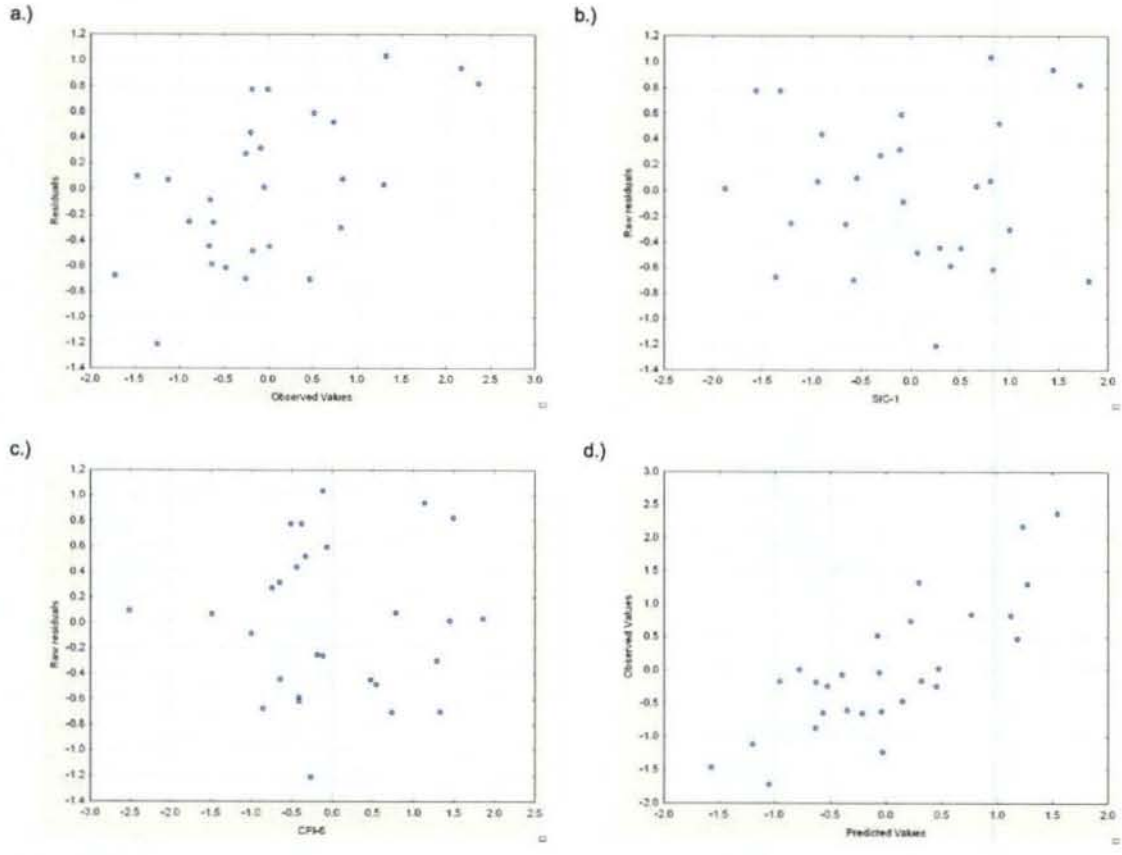

Figure 4.11: Residual analysis of Model 3 showing (a) observed value vs. residual scatterplot, (b) predictor variable SIC-1 vs. residual scatterplot, (c) predictor variable CPI-6 vs. residual scatterplot and (d) predicted value vs. observed value

a.) Initial

Variable	Beta	s.e	t-stat	p-value
SIC-1	0.65	0.15	4.31	0.00
SST-1a	-0.62	0.15	-4.00	0.00
SST-1b	-0.45	0.18	-2.54	0.02
SST-1c	-0.53	0.17	-3.17	0.00
SST-2a	0.52	0.17	3.13	0.00
SST-2b	0.28	0.19	1.52	0.14
SST-2c	0.22	0.19	1.15	0.26
SST-4a	0.49	0.17	2.86	0.01
SST-4b	0.54	0.17	3.23	0.00
SST-5a	-0.32	0.19	-1.71	0.10
SST-5b	-0.50	0.17	-2.92	0.01
SST-6a	0.26	0.19	1.36	0.19
SAM-3	-0.47	0.17	-2.72	0.01
SAM-4	-0.48	0.17	-2.82	0.01
Nino-1	-0.43	0.18	-2.45	0.02

MSE	RMSE
1	1
R^2	**Adjusted R^2**
0	0
f-stat	**p-value**
N/A	N/A

b.) Stage 1

Variable	Beta	s.e	t-stat	p-value
SIC-1	**0.65**	**0.15**	**4.31**	**0.00**
SST-1a	-0.42	0.15	-2.82	0.01
SST-1b	-0.27	0.15	-1.79	0.09
SST-1c	-0.36	0.14	-2.53	0.02
SST-2a	0.35	0.15	2.40	0.02
SST-2b	0.19	0.15	1.26	0.22
SST-2c	0.15	0.15	1.01	0.32
SST-4a	0.34	0.14	2.34	0.03
SST-4b	0.38	0.14	2.70	0.01
SST-5a	-0.22	0.15	-1.47	0.15
SST-5b	-0.35	0.14	-2.43	0.02
SST-6a	0.17	0.15	1.16	0.26
SAM-3	-0.24	0.16	-1.51	0.14
SAM-4	-0.26	0.16	-1.63	0.12
Nino-1	-0.20	0.16	-1.26	0.22

MSE	RMSE
0.61	0.78
R^2	**Adjusted R^2**
0.42	0.39
f-stat	**p-value**
18.61	0.00

c.) Stage 2

Variable	Beta	s.e	t-stat	p-value
SIC-1	**0.47**	**0.15**	**3.17**	**0.00**
SST-1a	**-0.42**	**0.15**	**-2.82**	**0.01**
SST-1b	0.04	0.21	0.19	0.85
SST-1c	-0.17	0.19	-0.91	0.37
SST-2a	0.26	0.14	1.91	0.07
SST-2b	0.09	0.14	0.62	0.54
SST-2c	-0.02	0.15	-0.12	0.91
SST-4a	0.29	0.13	2.19	0.04
SST-4b	0.36	0.12	3.00	0.01
SST-5a	-0.08	0.15	-0.57	0.58
SST-5b	-0.26	0.14	-1.90	0.07
SST-6a	0.18	0.13	1.34	0.19
SAM-3	-0.20	0.14	-1.36	0.19
SAM-4	-0.16	0.15	-1.09	0.29
Nino-1	-0.16	0.15	-1.10	0.28

MSE	RMSE
0.48	0.69
R^2	**Adjusted R^2**
0.56	0.52
f-stat	**p-value**
15.78	0.00

d.) Final

Variable	Beta	s.e	t-stat	p-value
SIC-1	**0.37**	**0.13**	**2.78**	**0.01**
SST-1a	**-0.40**	**0.13**	**-3.11**	**0.00**
SST-1b	0.16	0.18	0.88	0.39
SST-1c	-0.02	0.18	-0.11	0.91
SST-2a	0.20	0.13	1.59	0.13
SST-2b	0.05	0.13	0.40	0.69
SST-2c	-0.03	0.13	-0.19	0.85
SST-4a	-0.23	0.28	-0.82	0.42
SST-4b	**0.36**	**0.12**	**3.00**	**0.01**
SST-5a	-0.06	0.13	-0.45	0.66
SST-5b	-0.19	0.12	-1.55	0.14
SST-6a	0.06	0.13	0.46	0.65
SAM-3	-0.08	0.14	-0.61	0.55
SAM-4	-0.10	0.13	-0.75	0.46
Nino-1	-0.24	0.12	-1.98	0.06

MSE	RMSE
0.36	0.60
R^2	**Adjusted R^2**
0.68	0.64
f-stat	**p-value**
16.87	0.00

Final Prediction Equation

$$\hat{y} = 0.37SIC1 - 0.40SST1a + 0.36SST4b$$

Table 4.3: (a.) initial stage, (b.) stage 1, (c.) stage 2, (d.) final statistics of the Model 1 forward stepwise regression. Variables included in the model at each stage are highlighted in bold along with their statistics.

	Reference Forecast		Cross Validation	
	Climatological Average	Persistence	Leave-One-Out	K-fold
RMSE	0.98	1.33	0.89	0.87
MSE	0.96	1.77	0.79	0.76
SS_{clim}	N/A	N/A	0.18	0.21
SS_{pers}	N/A	N/A	0.55	0.57

Table 4.4: Forecast assesment values for two reference forecasts as well as Model 1 forecast assesment values, including associated skill scores, using two methods of cross validation.

a.) Initial

Variable	Beta	s.e	t-stat	p-value
SIC-1	0.65	0.15	4.31	0.00
SST-1a	-0.62	0.15	-4.00	0.00
SST-1b	-0.45	0.18	-2.54	0.02
SST-1c	-0.53	0.17	-3.17	0.00
SST-2a	0.52	0.17	3.13	0.00
SST-2b	0.28	0.19	1.52	0.14
SST-2c	0.22	0.19	1.15	0.26
SST-4a	0.49	0.17	2.86	0.01
SST-4b	0.54	0.17	3.23	0.00
SST-5a	-0.32	0.19	-1.71	0.10
SST-5b	-0.50	0.17	-2.92	0.01
SST-6a	0.26	0.19	1.36	0.19
SAM-3	-0.47	0.17	-2.72	0.01
SAM-4	-0.48	0.17	-2.82	0.01
Nino-1	-0.43	0.18	-2.45	0.02
CPI-1	0.69	0.14	4.85	0.00
CPI-2	0.58	0.16	3.61	0.00
CPI-6	0.70	0.14	5.01	0.00

MSE	RMSE
1	1
R^2	Adjusted R^2
0	0
f-stat	p-value
N/A	N/A

b.) Stage 1

Variable	Beta	s.e	t-stat	p-value
SIC-1	0.44	0.13	3.41	0.00
SST-1a	-0.32	0.16	-2.00	0.06
SST-1b	0.08	0.20	0.38	0.70
SST-1c	0.08	0.24	0.36	0.72
SST-2a	0.33	0.14	2.46	0.02
SST-2b	0.09	0.15	0.59	0.56
SST-2c	-0.03	0.15	-0.21	0.84
SST-4a	-0.19	0.23	-0.80	0.43
SST-4b	-0.05	0.23	-0.24	0.82
SST-5a	0.03	0.16	0.18	0.86
SST-5b	-0.17	0.17	-1.04	0.31
SST-6a	0.01	0.15	0.09	0.93
SAM-3	-0.12	0.17	-0.70	0.49
SAM-4	-0.19	0.16	-1.22	0.23
Nino-1	-0.41	0.12	-3.51	0.00
CPI-1	0.44	0.15	3.01	0.01
CPI-2	-0.43	0.35	-1.22	0.23
CPI-6	**0.70**	**0.14**	**5.01**	**0.00**

MSE	RMSE
0.53	0.73
R^2	Adjusted R^2
0.49	0.47
f-stat	p-value
25.14	0.00

c.) Stage 2

Variable	Beta	s.e	t-stat	p-value
SIC-1	0.30	0.13	2.33	0.03
SST-1a	-0.19	0.15	-1.28	0.21
SST-1b	0.29	0.16	1.74	0.10
SST-1c	0.14	0.20	0.70	0.49
SST-2a	0.23	0.12	1.88	0.07
SST-2b	0.07	0.12	0.54	0.60
SST-2c	-0.05	0.13	-0.39	0.70
SST-4a	-0.03	0.20	-0.17	0.87
SST-4b	0.02	0.20	0.12	0.91
SST-5a	-0.03	0.14	-0.24	0.81
SST-5b	-0.14	0.14	-1.00	0.33
SST-6a	0.08	0.13	0.64	0.53
SAM-3	-0.03	0.15	-0.23	0.82
SAM-4	-0.16	0.13	-1.22	0.24
Nino-1	**-0.41**	**0.12**	**-3.51**	**0.00**
CPI-1	0.30	0.14	2.16	0.04
CPI-2	-0.60	0.28	-2.14	0.04
CPI-6	**0.69**	**0.12**	**5.88**	**0.00**

MSE	RMSE
0.37	0.61
R^2	Adjusted R^2
0.66	0.63
f-stat	p-value
24.19	0.00

d.) Stage 3

Variable	Beta	s.e	t-stat	p-value
SIC-1	**0.30**	**0.13**	**2.33**	**0.03**
SST-1a	-0.14	0.14	-1.00	0.33
SST-1b	0.25	0.15	1.67	0.11
SST-1c	0.12	0.18	0.65	0.52
SST-2a	0.20	0.11	1.73	0.10
SST-2b	0.06	0.11	0.52	0.61
SST-2c	-0.03	0.12	-0.29	0.78
SST-4a	-0.05	0.19	-0.26	0.80
SST-4b	0.02	0.18	0.10	0.92
SST-5a	-0.03	0.13	-0.21	0.84
SST-5b	-0.12	0.13	-0.95	0.35
SST-6a	0.06	0.12	0.54	0.59
SAM-3	0.03	0.14	0.23	0.82
SAM-4	-0.09	0.13	-0.67	0.51
Nino-1	**-0.29**	**0.12**	**-2.44**	**0.02**
CPI-1	0.25	0.13	1.86	0.08
CPI-2	-0.56	0.26	-2.18	0.04
CPI-6	**0.57**	**0.12**	**4.83**	**0.00**

MSE	RMSE
0.31	0.56
R^2	Adjusted R^2
0.72	0.69
f-stat	p-value
20.81	0.00

e.) Final

Variable	Beta	s.e	t-stat	p-value
SIC-1	**0.28**	**0.12**	**2.36**	**0.03**
SST-1a	-0.25	0.13	-1.96	0.06
SST-1b	0.09	0.19	0.49	0.63
SST-1c	0.00	0.18	0.02	0.99
SST-2a	0.14	0.11	1.23	0.23
SST-2b	0.04	0.11	0.36	0.73
SST-2c	0.02	0.11	0.19	0.85
SST-4a	0.09	0.18	0.49	0.63
SST-4b	0.00	0.17	-0.03	0.98
SST-5a	0.02	0.12	0.13	0.89
SST-5b	-0.01	0.13	-0.08	0.94
SST-6a	0.07	0.11	0.63	0.54
SAM-3	0.07	0.13	0.53	0.60
SAM-4	-0.04	0.12	-0.32	0.75
Nino-1	**-0.33**	**0.11**	**-2.95**	**0.01**
CPI-1	0.25	0.12	2.04	0.05
CPI-2	**-0.56**	**0.26**	**-2.18**	**0.04**
CPI-6	**1.09**	**0.26**	**4.15**	**0.00**

MSE	RMSE
0.27	0.52
R^2	Adjusted R^2
0.77	0.73
f-stat	p-value
19.23	0.00

Final Prediction Equation

$$\hat{y} = 0.28SIC + 1.09CPI - 0.33Nino - 0.56CPI$$

Table 4.5: (a.) initial stage, (b.) stage 1, (c.) stage 2, (d.) stage 3, (e.) final statistics of the Model 2 forward stepwise regression. Variables included in the model at each stage are highlighted in bold along with their statistics.

	Reference Forecast		Cross Validation	
	Climatological Average	Persistence	Leave-One-Out	K-fold
RMSE	0.98	1.33	0.83	0.79
MSE	0.96	1.77	0.69	0.62
SS_{clim}	N/A	N/A	0.29	0.36
SS_{pers}	N/A	N/A	0.61	0.65

Table 4.6: Forecast assesment values for two reference forecasts as well as Model 2 forecast assesment values, including associated skill scores, using two methods of cross validation.

a.) Initial

Variable	Beta	s.e	t-stat	p-value	MSE	RMSE
SIC-1	0.65	0.15	4.31	0.00	1	1
CPI-6	0.70	0.14	5.01	0.00		

R^2	Adjusted R^2
0	0

f-stat	p-value
N/A	N/A

b.) Stage 1

Variable	Beta	s.e	t-stat	p-value	MSE	RMSE
SIC-1	0.44	0.13	3.41	0.00	0.53	0.73
CPI-6	**0.70**	**0.14**	**5.01**	**0.00**		

R^2	Adjusted R^2
0.49	0.47

f-stat	p-value
25.14	0.00

c.) Final

Variable	Beta	s.e	t-stat	p-value	MSE	RMSE
SIC-1	**0.44**	**0.13**	**3.41**	**0.00**	0.37	0.61
CPI-6	**0.53**	**0.13**	**4.13**	**0.00**		

R^2	Adjusted R^2
0.65	0.63

f-stat	p-value
23.55	0.00

Final Prediction Equation

$$\hat{y} = 0.44\ SIC\ 1 + 0.53\ CPI\ 3$$

Table 4.7: (a.) initial stage, (b.) stage 1, (c.) final statistics of the Model 3 forward stepwise regression. Variables included in the model at each stage are highlighted in bold along with their statistics.

	Reference Forecast		Cross Validation	
	Climatological Average	Persistence	Leave-One-Out	K-fold
RMSE	0.98	1.33	0.62	0.62
MSE	0.96	1.77	0.38	0.39
SS_{clim}	N/A	N/A	0.60	0.60
SS_{pers}	N/A	N/A	0.78	0.78

Table 4.8: Forecast assesment values for two reference forecasts as well as Model 3 forecast assesment values, including associated skill scores, using two methods of cross validation.

Chapter 5

Conclusion

5.1 Conclusion

Winter rainfall in the Southwestern Cape is received primarily from temperate disturbances in the westerlies, and is characterized by significant inter-annual and inter-decadal variability. Previous studies identified relationships between SWC rainfall and the Southern Annular Mode, South Atlantic sea surface temperature, Antarctic sea ice concentration, and the El Nino-Southern Oscillation. This study used spatial and temporal correlations to further explore the development of these relationships and gain an understanding of their underlying physical connections. However, correlation analysis is a rough mathematical tool, and a more in-depth study would be required to make conclusive statements regarding these relationships. Insight gained from the correlation analysis was used to develop statistical forecast models for SWC seasonal rainfall. These models served as an initial assessment of the potential for statistical seasonal forecasting of SWC rainfall. The following summarizes the findings of this study.

SST in several regions of the South Atlantic appears to influence rainfall primarily on seasonal timescales. In some of these regions SST anomalies appear to develop several months prior to, and persist until the time of rainfall. Preliminary investigation indicates that SST anomalies within these regions work in concert to

influence rainfall. This is also supported by a robust pattern of correlation that is observed during each month of rainfall for early, mid and late-winter periods. Both the SAM and ENSO contribute to the variability of SST within these regions.

The SAM appears to influence SWC rainfall directly through its affects on atmospheric circulation, and indirectly through its persisting affects on SST. SST responses to the SAM are greatest at ~1-month lag and have the ability to persist for several months, re-imprinting themselves on surface air temperatures (Sen Gupta and England, 2006). The SAM appears to influence rainfall of both monthly and seasonal timescales, as would be expected with its dual nature of influence.

ENSO appears to influence SWC rainfall directly through its affects on atmospheric circulation during the year of onset, and indirectly through lagged affects on SST during its mature phase. SWC rainfall in the early-winter exhibits a positive relationship to ENSO in the mature phase, while rainfall in the late-winter exhibits a negative relationship. This dual characteristic this relationship merits further study.

Anomalies in zonal wind and geopotential height appear to strongly influence SWC rainfall, though this relationship is regionally restricted to the area over, and slightly upstream of South Africa. Anomalies in zonal wind and geopotential height that influence SWC rainfall do not appear to be persistent, and are not observed in the months preceding or following rainfall.

Antarctic sea ice concentration also has a strong relationship with SWC rainfall, though it remains unclear if rainfall is directly influenced by SIC or the two are related through larger modes of variability. The SIC-dipole relationship observed by Blamey and Reason (2007) is related to rainfall at monthly timescales, but appears to be much

more robust at seasonal timescales. SIC anomalies appear to develop near the Antarctic Peninsula several months before rainfall, while anomalies near 0-30°E appear to develop only at the time of rainfall. Both regions of anomalous SIC persist and propagate downstream.

A statistical forecast model of SWC late-winter rainfall was developed, which used April SIC near the Antarctic Peninsula and a combined index of South Atlantic SST as predictor variables. This forecast was able to produce an estimated 60% reduction of variance from a forecast based on climatological average values, as estimated with cross-validation techniques. The potential practical application of this forecast is overshadowed by the instability of the predictor-predictand relationship. This instability is observed in the relationships between SWC rainfall and South Atlantic SST, SAM indices, and ENSO. This appears to be a result of decadal variability in Southern Hemisphere circulation, and in particular a major shift in Southern Hemisphere circulation that occurred after 1976 (Van loon et. al. 1993).

Prediction is, in its very essence, the identification and appraisal of influence. This study has, using coarse mathematical tools, attempted to identify and assess the influence several variables have on SWC rainfall. It appears that the influence these variables possess is significant in comparison to the substantial variability of the mid-latitudes. Understanding this influence allows us to insulate ourselves to some degree from the capricious nature of the mid-latitudes. Yet variability on longer timescales puts us once again in the dark. How did SWC rainfall before 1976 differ from SWC rainfall today? How did this shift in circulation affect the relationships between SWC rainfall

and the variables discussed? What future shifts in circulation can be expected and how will this affect SWC rainfall and its relationships with these variables?

Bibliography

Arblaster JM, Meehl GA (2006) Contributions of external forcing to southern annular mode trends. *Journal of Climate* **19**: 2896-2905

Blamey R, Reason CJC (2007) Relationship between Antarctic sea-ice and South African winter rainfall. *Climate Research* **33**: 183-193

Broccoli AJ, Manabe S (1992) as cited in Hall A, Visbeck M (2002) Synchronous variability in the Southern Hemisphere atmosphere, sea ice, and ocean resulting from the annular mode. *Journal of Climate* **15**: 3043-3057

Colberg F, Reason CJC, Rodgers K (2004) South Atlantic response to El Nino-Southern Oscilation induced climate variability in an ocean general circulation model. *Journal of Geophysical Research* **109**: C12015, doi:10.1029/2004JC002301

Draper NR, Smith H (1998) *Applied Regression Analysis*. Wiley pp. 706

Elsner JB, Schmertmann (1994) Assessing forecast skill through cross-validation. *Journal of Climate* **9**: 619-624

Fogt RL, Bromwich DH (2006) Decadal variability of ENSO teleconnection to high-latitude South Pacific governed by coupling with the Southern Annular Mode. *Journal of Climate* **19**: 979-997

Gallego D, Ribera P, Garcia-Herrera R, Hernandez E, Gilmeno L (2005) A new look for the Southern Hemisphere jetstream. *Climate Dynamics* **24**: 607-621

Goddard L, Mason SJ, Zebiak SE, Ropelewski CF, Basher R, Cane MA (2001) Current Approaches to seasonal and interannual climate prediction. *International Journal of Climatology* **21**: 1111-1152

Godfred-Spenning CR, Simmonds I (1996) An analysis of Antarctic sea ice and extra-tropical cyclone associations. International *Journal of Climatology* **16**: 1315-1332

Gong D, Wang S (1999) Definition of Antarctic oscillation index. *Geophysical Research Letters* **26**(4): 459-462

Hall A, Visbeck M (2002) Synchronous variability in the Southern Hemisphere atmosphere, sea ice, and ocean resulting from the annular mode. *Journal of Climate* **15**: 3043-3057

Hartmann DL, Lo F (1998) Wave driven flow vacillation in the Southern Hemisphere. *Journal of the Atmospheric Sciences* **55**: 1303-1315

Hastenrath S, Greischar L, van Heerden J (1995) Prediction of summer rainfall over South Africa. *Journal of Climate* **8**: 1511-1518

Kalnay E, Kanamitsu M, Kistler R, Collins W and 18 others (1996) The NCEP/NCAR 40 year reanalysis project. *Bulletin of the American Meteorological Society* **77**: 437-471

Karoly DJ (1990) The role of transient eddies in low-frequency zonal variations of the southern hemisphere zonal circulation. *Tellus* **42A**: 41-50

Kidson JW, Sinclair MR (1995) The influence of persistent anomalies on Southern Hemisphere storm tracks. *Journal of Climate* **8**: 1938-1950

Kohavi R (1995) A study of cross-validation and bootstrap for accuracy estimation and model selection. Appears in the International Joint Conference on Artificial Intelligence (IJCAI)

Lefebvre W, Goosse H, Timmermann R, Fichefet T (2004) Influence of the Southern Annular mode on the sea ice-ocean system. *Journal of Geophysical Research* **109**: C09005, doi:101029/2004Jc002403

Lefebvre W, Goosse H (2005) Influence of the Southern Annular Mode on the sea ice-ocean system: the role of thermal and mechanical forcing. *Ocean Science* **1**: 145-157

Lefebvre W, Goosse H (2008) An analysis of atmospheric processes driving large-scale winter sea ice variability in the Southern Ocean. *Journal of Geophysical Research* **113**: C02004, doi:10.1029/2006JC004032

Limpasuvan V, Hartmann DL (2000) Wave-maintained annular modes of climate variability. *Journal of Climate* **13**: 4414-4429

Liu J, Yuan X, Rind D, Martinson D (2002) Mechanism study of the ENSO and southern high latitude climate teleconnections. Geophysical Research Letters 29, doi:10.1029/2002GL015143

Marshall GJ (2003) Trends in the southern annular mode from observations and reanalyses. *Journal of Climate* **16**: 4134-4143

Mo KC (2000) Relationships between low-frequency variability in the Southern Hemisphere and sea surface temperature anomalies. *Journal of Climate* **13**: 3599-3610

Mo KC, Peagle JN (2001) The Pacific-South America modes and their downstream effects. *International Journal of Climatology* **21**: 1211-1229

Palmer TN (1993) Extended range weather prediction and the Lorenz model. *Bulletin of the American Meteorological Society* **74**: 49-65

Palmer TN, Anderson DLT (1994) The prospects for seasonal forecasting-A review paper. *Quarterly Journal of the Royal Meteorological Society* **120**: 755-793

Rashid HA, Simmonds I (2005) Southern Hemisphere annular mode variability and the role of optimal nonmodal growth. *Journal of the Atmospheric Sciences* **62**: 1947-1961

Rayner NA, Parker DE, Horton EB, Folland CK, Alexander LV, Rowell DP (2003) Global analysis of sea surface temperature, sea ice, and night marine air temperature since the late nineteenth century. *Journal of Geophysical Research* **108**: D14 4407 doi: 10.1029/2002JD002670

Reason CJC, Murray RJ (2001) Modelling low-frequency variability in Southern Hemisphere extra-tropical cyclone characteristics and its sensitivity to sea-surface temperature. *International Journal of Climatology* **21**: 249-267

Reason CJC, Rouault M (2002) ENSO-like decadal patterns and South African rainfall. *Geophysical Research Letters* **29**(13):1638, doi:10.1029/2002GL014663

Reason CJC, Rouault M, Melice JL, Jagadheesha D (2002) Interannual winter rainfall variability in SW South Africa and large scale ocean atmosphere interactions. *Meteorology and Atmospheric Physics* **80**: 19-29

Reason CJC, Jagadheesa D, Tadross M (2003) A model investigation of inter-annual winter rainfall variability over southwestern South Africa and associated ocean-atmosphere interactions. *South African Journal of Science* **99**: 75-80

Reason CJC, Jagadheesha D (2005) Relationships between South Atlantic SST variability and atmospheric circulation over the South Africa region during austral winter. *Journal of Climate* **18**: 3059-3075

Reason CJC, Rouault M (2005) Links between the Antarctic Oscillation and winter rainfall over western South Africa. *Geophysical Research Letters* **32**:L07705, doi:10.1029/2005GL022419

Reynolds RW, Rayner NW, Smith TM, Stokes DC, Wang W (2002) An improved in-situ and satellite SST analysis for climate. *Journal of Climate* **15**: 1609-1625

Rind D, Chandler M, Lerner J, Martinson DJ, Yuan X (2001) The climate response to basin-specific changes in latitudinal temperature gradients and the implications for sea ice variability. *Journal of Geophysical Research* **106**(20): 161- 173

Rogers JC, Van Loon H (1982) Spatial variability of sea level pressure and 500-mb height anomalies over the southern hemisphere. *Monthly weather review* **110**: 1375-1392

Sen Gupta A, England MH (2006) Coupled ocean-atmosphere-ice response to variation in the southern annular mode. *Journal of Climate* **19**: 4457-4486

Shiotani M (1990) Low frequency variations of the zonal mean state of the southern hemisphere troposphere. *Journal of the Meteorological Society of Japan* **68**: 461-471

Shukla J (1998) Predictability in the midst of chaos: a scientific basis for climate forecasting. *Science* **282**: 728-731

Simmonds I, Budd WF (1991) Sensitivity of the Southern Hemisphere circulation to leads in Antarctic pack ice. *Quarterly Journal of the Royal Meteorological Society* **117**: 1003-1024

Simmonds I, Keay K (2000) Mean Southern Hemisphere extra-tropical cyclone behavior in the 40-year NCEP-NCAR re-analysis. *Journal of Climate* **13**: 873-885

Singleton AT, Reason CJC (2006) Numerical simulations of a severe rainfall event over the Eastern Cape coast of South Africa: sensitivity to sea surface temperature and topography. *Tellus* **53A**:355-367

Smith RC, Stammerjohn SE (2001) Variations of surface air temperature and sea ice extent in the western Antarctic Peninsula region. *Annals of Glaciology* **33**: 493-500

Stammerjohn SE, Drinkwater MR, Smith RC, Liu X (2003) Ice-atmosphere interactions during sea-ice advance and retreat in the western Antarctic Peninsula region. *Journal of Geophysical Research **108*** (C10): 3329, doi: 10.1029/2002JC001543

Stammerjohn SE, Martinson DG, Smith RC, Yuan X, Rind D (2008) Trends in Antarctic annual sea ice retreat and advance and their relationship to El Nino-Southern Oscillation and Southern Annular Mode variability. *Journal of Geophysical Research* **113**: C03S90

Stockdale TN (2000) An overview of techniques for seasonal forecasting. *Stochastic Environmental Research and Risk Assessment* **14**: 305-318

Thompson DWJ, Wallace JM (2000) Annular modes in extratropical circulation. Part I: month-to-month variability. *Journal of Climate* **13**: 1000-1016

Thompson DWJ, Wallace JM, Hegerl GC (2000) Annular modes in extratropical circulation. Part II: Trends. *Journal of Climate* **13**: 1018-1036

Thompson DWJ, Solomon S (2002) Interpretation of recent Southern Hemisphere climate change. *Science* **296**: 895-899

Trenberth KE (1991) Storm tracks in the southern hemisphere. *Journal of Atmospheric Sciences* **48**: 2159-2178

Tyson PD, Preston-Whyte RA (2000) *The Weather and Climate of Southern Africa.* Oxford University Press, Cape Town pp. 396

Van Loon HJ, Kidson W, Mullan AN (1993) Decadal variation of the annual cycle in the Australian dataset. *Journal of Climate* **6**: 1227-1231

Watkins AB, Simmonds I (1995) Sensitivity of numerical prognosis to Antarctic sea ice distribution. *Journal of Geophysical Research* **100**: 22681-22696

Wilks DS (2006) *Statistical Methods in the Atmospheric Sciences*. Elsevier pp. 627

Yoden SM, Shiotani M, Hirota I (1987) Multiple planetary flow regimes in the southern hemisphere. *Journal of the Meteorological Society of Japan* **65**: 571-586

Yuan X, Martinson DG (2000) Antarctic sea ice extent variability and its global connectivity. *Journal of Climate* **13**: 1697-1717

Yuan X, Martinson DG (2001) The Antarctic Dipole and its predictability. *Journal of Geophysical Research* **28**: 3609-3612

Yuan X (2004) ENSO-related impacts on Antarctic sea ice: a synthesis of phenomenon and mechanisms. *Antarctic Science* **16**(4): 416-425

Yuan X, Li C (2008) Climate modes in southern high latitudes and their impacts on Antarctic sea ice. *Journal of Geophysical Research* **113**: C06S91